Symmetry Analysis and Analytic Solutions for Unsteady Flows on a Stretching Surface in the Presence of Magnetic Field, Internal Heat Source and Thermocapillary Effects

Ghani Khan

Reg No # 362122

Supervisor

Dr. Muhammad Safdar

Department of Mechanical Engineering

School of Mechanical and Manufacturing Engineering (SMME)

National University of Sciences and Technology (NUST)

Islamabad, Pakistan

May 2023

Symmetry Analysis and Analytic Solutions for Unsteady Flows on a Stretching Surface in the Presence of Magnetic Field, Internal Heat Source and Thermocapillary Effects

Author

Ghani Khan

Reg No # 362122

A thesis submitted in partial fulfillment of the requirements for the degree of *Master of Science* in Mechanical Engineering

Supervisor
Dr. Muhammad Safdar

Thesis Supervisor Signature:_____

Department of Mechanical Engineering
School of Mechanical and Manufacturing Engineering (SMME)
National University of Sciences and Technology (NUST)
Islamabad, Pakistan

May 2023

Declaration

I Ghani Khan certify that this research work titled “Symmetry Analysis and Analytic Solutions for Unsteady Flows on a Stretching Surface in the Presence of Magnetic Field, Internal Heat Source and Thermocapillary Effects” is my own work. The work has not been presented elsewhere for assessment. The material that has been used from other sources has been properly acknowledged/referred.

_____

Ghani Khan,

Reg No # 362122

Date: _____

Copyright Notice

Dedicated to my parents

Abstract

This study employs Lie point symmetry analysis to investigate the unsteady flow on a stretching surface. Such flows are common in various manufacturing processes such as extrusion, melt-spinning, and coating. Three cases have been discussed i.e. unsteady flow on a stretching surface in the presence of a variable magnetic field, its 1-dimensional optimal system, and unsteady flow on a stretching surface in the presence of thermocapillarity, an internal source or sink, and a variable magnetic field.

For unsteady flow on a stretching surface in the presence of a variable magnetic field, a general linear combination of all admitted translational and scaling Lie point symmetries has been used to obtain the system invariants and general forms of the velocity, temperature, and concentration at the stretching surface. The deduced invariants provide a new generalized class of similarity transformations that convert the governing boundary layer equations into a system of non-linear ODEs. Analytic series solutions have been obtained for the resulting system of ODEs using Homotopy Analysis Method (HAM) and the effect of different parameters such as unsteadiness, magnetic parameter, Prandtl number, Schmidt number, and coefficients of the Lie point symmetries has been depicted graphically. It has been found that coefficients of the translational symmetries do not play any role in the solution while coefficients of the scaling symmetries can control the temperature and concentration fields. Secondly, a 1-dimensional optimal system of this flow is obtained which provides 22 new classes of similarity transformations that reduce the governing boundary layer equations into 22 news classes of ODEs, thus providing multiple new solutions of heat and mass transfer.

Similarly, the hydrodynamics and thermal characteristics of the flow induced by the unsteady stretching of a sheet in the presence of thermocapillarity, internal heat source or sink, and variable magnetic field are investigated using Lie point analysis. The linear combinations of Lie point symmetries is again a Lie point symmetry. It is admitted by all boundary conditions while leave the stretching sheet velocity and temperature as a function of both distance and time. We utilize such a linear combination to develop Lie transformations that reduce the governing momentum and energy equations into a system of coupled non-linear ODEs. The resulting five-parameter problem namely, unsteadiness term S, magnetic parameter Ma, Prandtl number Pr, temperature-dependent

heat source or sink term G^* and the thermocapillarity parameter M, is solved using Homotopy Perturbation Method (HPM). It has been found that thermocapillary forces drag the free surface of the fluid in the direction of the stretching sheet, due to which a local velocity minimum forms in the fluid. Thermocapillarity thickens the fluid film resulting in the increase of free surface velocity, temperature, and heat flux from the sheet while reducing the friction between the sheet and the fluid film. The temperature-dependent heat source or sink term and the magnetic parameter greatly affect the variation of the temperature across the fluid and can be useful in speeding up the cooling or heating of the fluid.

Keywords: *Lie point symmetry, Translational symmetries, Scaling symmetries, Thermocapillarity, Homotopy Analysis Method (HAM), Homotopy Perturbation Method (HPM).*

Acknowledgments

I would like to begin by acknowledging the grace and mercy of ALLAH, without whom none of this would have been possible. I am grateful for His guidance, blessings, and protection throughout this academic journey.

I would also like to express my deepest gratitude to my parents for their unwavering support. Their love, encouragement, and sacrifices have been my guiding light and motivation. I am immensely blessed to have them as my parents.

I am deeply indebted to my advisor, Muhammad Safdar, for his invaluable guidance, encouragement, and feedback. His expertise, patience, and commitment to excellence have been instrumental in shaping this thesis. His insightful feedback, constructive criticism, and expert guidance have helped me grow both as a researcher and as a person.

I am fortunate to have such an amazing mentor who has not only supported me throughout the research process but also challenged me to push the boundaries of my knowledge and skills. His mentorship has been transformative and has inspired me to pursue excellence in all aspects of my life.

I am extremely thankful to the members of Guidance and Examination Committee (GEC), Dr. Amir Mubashar, Dr. Emad Uddin, and Dr. Zeeshan Saeed their invaluable contributions in the form of instructive guidance, beneficial suggestions, and enlightening remarks. Lastly, I would like to extend my heartfelt appreciation to all my friends and colleagues for their support, motivation, and inspiration. Your presence in my life has been a tremendous blessing.

Thank you all, and may God bless you abundantly.

Ghani Khan

Contents

Table of Contents

List of Figures

List of Figures

List of Figures

List of Figures

List of Tables

List of Abbreviations and Symbols

Abbreviations

HAM	Homotopy Analysis Method
HPM	Homotopy Perturbation Method
PDEs	Partial Differential Equations
ODEs	Ordinary Differential Equations
S	Unsteadiness Parameter
Pr	Prandtl Number
Ma	Magnetic Parameter
$G^{*}{}^{*}$	Heat generation/absorption coefficient
β	Dimensionless Film Thickness
σ_e	Electrical Conductivity
ν	Kinematic viscosity
κ	Thermal diffusivity
M	Thermocapillarity Parameter

Chapter 1

1. Introduction

In this research flow, heat, and mass transfer in a liquid film over an unsteady stretching surface in the presence variable magnetic field has been analyzed using Lie point symmetry analysis. The objectives of this research are as follows:

- To develop general similarity transformations for hydrodynamics, heat, and mass transfer in a thin film over an unsteady stretching surface in the presence variable magnetic field using a general linear combination of admitted Lie point symmetries.
- To develop a 1-dimensional optimal system of Lie sub-algebra for heat and mass transfer in a thin film over an unsteady stretching surface in the presence of variable magnetic field.
- To analyze the combined effect of thermocapillarity, internal heat source or sink, and a variable magnetic field on the flow and heat transfer in a thin film over an unsteady stretching surface using Lie symmetry analysis.

1.1 Background, Scope and Motivation

Flow-induced by a stretching surface is a fascinating and complex phenomenon that has captivated the attention of researchers and engineers for decades. It is encountered in many industrial applications, including coating, painting, melt-spinning process, polymer processing, glass manufacturing, and metal production. In these processes, a thin sheet or film of material is continuously stretched into a fluid at rest. Due to the stretching action, the fluid starts flowing. The flow behavior in this scenario is complex and depends on the properties of both the material and the fluid. Understanding this phenomenon is essential to optimize these processes.

Polymer processing is one of the most common applications of flow over an unsteady stretching

surface. In this process, molten polymer is extruded through a die, which creates a thin sheet that is then continuously stretched into a fluid for cooling. Similarly, glass manufacturing is another application of flow induced by an unsteady stretching surface. In this process, glass is melted and then drawn out into a thin sheet that is continuously stretched. The stretching motion induces hydrodynamic and thermal boundary layers. Understanding the behavior of these boundary layers is critical for optimizing the manufacturing process and ensuring the quality of the final product.

In all of these applications, the flow behavior is influenced by a wide range of factors, including the material properties, the stretching rate, and the fluid properties. Due to the variable conditions at the boundary (stretching sheet), experimental and numerical techniques are difficult to employ in this case. The similarity solutions prove to be a very handy tool in this case and are used by many researchers to obtain solutions for the hydrodynamic and thermal boundary layers of flow induced by the stretching surface.

Sakaidis [1] was the first to study the boundary layer behavior on a continuous flat surface issuing with a constant velocity from a slit in a stationary fluid. The governing equations were solved by two methods. One method involved the numerical solution of the governing equations reduced to a system of ordinary differential equations, while the other is the integral method based on the assumed velocity profile. A good agreement between the methods was reported. It was also observed that the drag force experienced by the sheet is much larger than the flat plate of finite length. As an extension to this work, Crane [2] made a pioneering contribution by presenting an exact steady-state solution for the flow past a stretching surface with a velocity that varies in proportion to the distance from the slit. Vleggaar [3] presented a comprehensive study on the behavior of laminar boundary-layer on continuous, accelerating surfaces. The conservation equations (momentum and energy) were solved in two reference frames i.e. rectangular and cylindrical with the help of similarity transformations. The obtained numerical results were also applied to two applications i.e. cooling of the sheet and monofilament. Motivated by the situation that often arises in the polymer processing industry, Gupta et al. [4] modified Crane's problem to include the effect of suction or blowing in the stretching sheet and obtain a similarity solution. In Crane's study, it was assumed that the temperature of the sheet is constant along its length which is not the case in real applications. So, Carragher et al. [5] reconsidered Crane's study and provided a similarity solution for the heat transfer at moderate and high Prandtl numbers in a stretching sheet whose temperature difference with the surroundings is proportional to a power of the distance

from the slit. Grubka et al. [6] also studied the effect of power-law surface temperature variation on heat transfer by obtaining a series solution to the energy equation in terms of Kummer's functions. Dutta et al. [7] obtained a temperature field for a linearly-stretching sheet with uniform heat flux for different values of Prandtl number and found that the temperature at a given point decreases with an increase in Prandtl number. Jeng et al. [8] carried out a comprehensive analysis of momentum and heat transfer in a stretching sheet with an arbitrary surface velocity and non-uniform surface temperature. Solutions for both, isothermal and non-isothermal surfaces were obtained in this study. In addition to this, numerical examples for a power-law surface velocity and a linearly-stretching surface velocity with non-zero slit velocity were presented for the case of an isothermal surface. Kumeri et al. [9] expanded the study by exploring the effect of electrical conducting fluid on the heat transfer of the stretching sheet with a magnetic field (MHD flow) for both non-isothermal surface temperature and constant heat flux conditions. It was observed that the magnetic field enhanced the rate of heat transfer for prescribed surface temperature while for constant heat flux condition, the surface temperature reduced with increase in magnetic field.

In 1990, Wang [10] made significant strides in the study of flow on a stretching surface by successfully deriving an exact similarity solution for the unsteady Navier-Stokes equation that characterizes such flow. To accomplish this, Wang utilized a similarity transformation to convert the unsteady Navier-Stokes equation into a system of non-linear ordinary differential equations that is governed by a non-dimensional unsteady parameter, $S \in [0,2]$. Wang was able to obtain Crane's steady-state solution at $S = 0$ while no similarity solution existed for $S > 2$. The solution for thermal part of unsteady stretching was obtained by Andersson et al. [11] for different values of the unsteady parameter. It was observed that the heat transfer from the stretching sheet decreases with S for the lower Prandtl number while it increases with the unsteady parameter for the Prandtl number greater than unity. Later on, Liu et al. [12] generalized this study by providing solutions for the arbitrary powers of time and distance in the surface temperature expression. Dandapat et al. [13] observed that due to the variation of temperature along the free surface of the fluid, the effect of thermocapillarity becomes prominent and causes the motion of the free surface. They found that the similarity transformations used before (in the absence of thermocapillarity) could be used to explain the influence of the thermocapillarity on the flow and heat transfer. In 2006, Wang reconsidered his previous study of unsteady stretching [10] and provided an analytical solution using Homotopy Analysis Method (HAM) [14]. Abel et al. [15] considered the MHD flow

for the unsteady stretching case and studied the effect of viscous dissipations in the presence of a variable magnetic field while Noor et al [16] reported the effect of thermocapillarity in the presence of an external magnetic field. Aziz et al. [17] examined the effect of viscous dissipation for a general surface temperature. Similarly, Aziz et al. [18] investigated the influence of internal heating on the heat transfer in a thin film on an unsteady stretching sheet, whereas Hashim et al. [19] combined the impact of the thermocapillarity and thermal radiation on the hydrodynamics and thermal characteristics of the flow induced by an unsteady stretching sheet. Zhang et al. [20] extended the work [13] to include the effect of concentration variation on the surface tension along with the thermal variation thus, coupling the momentum, energy and concentration equation.

The literature mentioned so far used Newtonian fluids. A significant number of studies have also been conducted on the flow behavior of non-Newtonian fluids on unsteady stretching surfaces. Among these studies, the most commonly used models to describe the rheology of non-Newtonian fluids include the power-law, Casson, Maxwell, Herschel-Bulkley, and Carreau models. These studies can be found in [21-37].

In all of the above-mentioned studies, a similar class of similarity transformations was used to map the conservation equations to a system of non-linear ordinary differential equations. For the steady stretching sheet case, the velocity of the stretching was only a function of distance from the slit, while the surface temperature was either a constant or a function of the distance with a power whereas, for the unsteady stretching case, the velocity of the sheet depended on both, the distance from the slit and the time, while the surface temperature depended on the distance from the slit, time, and the sheet velocity.

Lie point symmetry analysis tells us that if a differential equation possesses a Lie point symmetry, then we can use it to find new solutions to the equation from known solutions. Safdar et al. [38] used this concept to derive six new classes of similarity transformations for the flow and heat transfer on an unsteady stretching surface. Using these transformations, the governing partial differential equations were reduced to a system of non-linear ordinary differential equations which were solved using the Homotopy Analysis Method (HAM). Taj et al. [39] derived two new classes of transformations for flow and heat transfer over an unsteady stretching sheet with viscous dissipation and external magnetic field while Safdar et al. [40] constructed five new classes of transformations for MHD flow leading to three different solutions of the governing equations. Similarly, Bilal et al. [41, 42] performed the Lie symmetry analysis of the flow and heat transfer

on an unsteady stretching surface in the presence of internal heating and thermal radiations, thus providing new solutions for the governing equations. A single or a linear combination of two Lie symmetries were used to derive these transformations.

In the current study, a Lie algebra is developed that is spanned by 8 Lie point symmetries for the system describing flow, heat, and mass transfer in a liquid film on an unsteady stretching surface in the presence of an external, variable magnetic field. Using a generalized linear combination of all admitted translational and scaling Lie point symmetries, the system invariants are derived. These invariants reduce the number of independent variables in the system and finally map the system of PDEs to the system of ODEs which are solved using the Homotopy Analysis Method (HAM). The deduced invariants also provide a generalized form of similarity transformations from which different classes of similarity transformations can be obtained. The linear combination of the Lie symmetries also provides a general specific form of stretching velocity, surface temperature, and film thickness when operated on the boundary conditions.

Moreover, in the present study, a one-dimensional optimal system of sub-algebras has been developed to analyze the flow on an unsteady stretching sheet in the presence of a variable magnetic field. This optimal system of sub-algebras serves as a valuable tool for identifying distinct classes of invariant solutions for differential equations. By identifying these non-equivalent classes, the task of constructing a comprehensive set of invariant solutions for a given differential equation can be streamlined. Upon establishment of the optimal system, any associated differential equation and its solutions can be effectively mapped into one of the classes offered by the optimal system. In essence, all invariant solutions for a given differential equation (or system of differential equations) can be obtained by deducing a single solution for each component of the optimal system of sub-algebras. Furthermore, when two sub-algebras share the same class during a symmetry transformation, the invariant solutions associated with these sub-algebras can be mutually converted under the identical transformation.

The effect of thermocapillarity, variable magnetic field, and an internal heat source or sink on the hydrodynamics and heat transfer in a thin liquid film on an unsteady stretching surface has also been investigated in this study using Lie symmetry analysis. Dandapat et al. [13], in their study of the effect of thermocapillarity on the flow of thin film over an unsteady stretching surface found that transformations used in the absence of thermocapillary effect were also applicable. In the current study, a Lie algebra spanned by 6 dimensional Lie point symmetries is used to construct

new similarity transformations through system invariants that reduces the governing PDEs to a system of non-linear ODEs. The resulting system of equations is solved using the Homotopy Perturbation Method (HPM).

The thesis is organized as following. The problem formulation is presented in chapter 2. Chapter 3 deals with the construction of Lie symmetries and double reductions of the governing PDEs for all three cases. Chapter 4 introduces the solution methods used to develop the solutions for the reduced system of ODEs. In Chapter 5, the results are presented and discussed to analyze the effect of different parameters. Chapter 6 concludes the research.

Chapter 2

2. Problem Formulation

In this research, two different problems are discussed. The mathematical formulation of each problem is given in the following subsections.

2.1 Unsteady Flow over a Stretching Surface in the Presence of Variable Magnetic Field

Consider a thin elastic sheet issuing from a narrow slit. The origin of the reference coordinate system is fixed at the slit with an x-axis parallel to the continuous sheet. The sheet is stretched with the velocity $U_s(x,t)$ in the y = 0 plane. The sheet temperature $T_s(x,t)$ and sheet concentration $C_s(x,t)$ are assumed to be the function of both distance and time. A variable magnetic field $B = \frac{B_0}{\sqrt{1-\alpha t}}$ is set up normal to the stretching sheet. Here B_0 is initial magnetic field strength and α is the arbitrary constant of dimension $time^{-1}$. The governing mass, momentum, energy, and concentration equations are given by

$$u_x + u_y = 0\,, \tag{2.1}$$

$$u_t + uu_x + vu_y = \nu u_{yy} - \frac{\sigma_e B^2}{\rho} u\,, \tag{2.2}$$

$$T_t + uT_x + vT_y = \kappa T_{yy}\,, \tag{2.3}$$

$$C_t + uC_x + vC_y = DC_{yy}\,, \tag{2.4}$$

where u and v represent velocity components in the x and y direction respectively. $\nu = \frac{\mu}{\rho}$ is the kinematic viscosity, ρ is the fluid density, μ is the dynamic viscosity, σ_e is the electrical conductivity, $\kappa = \frac{\mathrm{k}}{\rho C_p}$ is the thermal diffusivity, k is the thermal conductivity, C_p is the specific

heat capacity at constant pressure, D is the mass diffusivity, T is the temperature of the fluid and C is the concentration. The subscripts $t, x,$ and y denote the derivatives with respect to these variables.

The boundary conditions for the above boundary layer equations are

$$u = U_s(x,t), \quad v = 0, \quad T = T_s(x,t), \quad C = C_s(x,t) \quad \text{at } y = 0\,, \tag{2.5}$$

and

$$u_y = 0, \quad T_y = 0, \quad C_y = 0, \quad v = \frac{dh}{dt}, \quad \text{at } y = h(t)\,, \tag{2.6}$$

where $h(t)$ is the elevation of film free surface i.e. the film thickness. It is assumed that $h(t)$ is uniform and only a function of time. $u_y = 0$ points out that the effect of surface tension has been neglected and fluid moves purely due to the viscous shear that arises from the stretching of the sheet. $T_y = 0$ suggests that the free surface of the liquid film is adiabatic while the last boundary condition is a kinematic free surface condition.

From the scaling analysis, it can be found that $u \sim U_\infty$ and $v \sim U_\infty \frac{h}{L}$, where U_∞ is free stream velocity, h is boundary thickness and L is the characteristic length of the sheet. This implies that $\frac{v}{u} \sim \frac{h}{L} \ll 1$. Based upon this reasoning, the boundary-layer equations in the y direction are neglected. Similarly, diffusion along streamlines $u_{xx} \sim \frac{{U_\infty}^2}{L^2}$ is much smaller than the diffusion across lines $u_{yy} \sim \frac{{U_\infty}^2}{h^2}$ and hence, being neglected. The pressure term also does not appear in the above equations which is the consequence of the boundary layer theory assumptions.

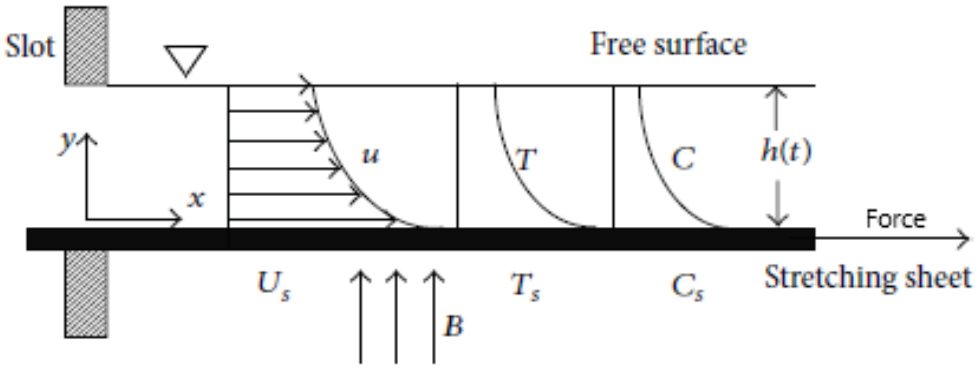

Figure 1: Physical representation of the problem

To reduce the governing equations (4.26-2.6) to a system of non-linear ODEs, Zhang et al. [20] used

$$\eta = \sqrt{\frac{b}{\nu(1-\alpha t)}}\,\frac{y}{\beta}\,, \tag{2.7}$$

$$u = \frac{bx}{1-\alpha t} f'(\eta)\,, \tag{2.8}$$

$$v = -\beta\sqrt{\frac{\nu b}{1-\alpha t}}\, f(\eta)\,, \tag{2.9}$$

$$T = T_0 - T_{ref}\frac{bx^2}{2\nu(1-\alpha t)^{\frac{3}{2}}}\theta(\eta)\,, \tag{2.10}$$

$$C = C_0 - C_{ref}\frac{bx^2}{2\nu(1-\alpha t)^{\frac{3}{2}}}\phi(\eta)\,, \tag{2.11}$$

with the stretching surface velocity, temperature, and concentration

$$U_s = \frac{bx}{1-\alpha t}\,, \tag{2.12}$$

$$T_s = T_0 - T_{ref}\frac{bx^2}{2\nu(1-\alpha t)^{\frac{3}{2}}}\,, \tag{2.13}$$

$$C_s = C_0 - C_{ref}\frac{bx^2}{2\nu(1-\alpha t)^{\frac{3}{2}}}\,, \tag{2.14}$$

respectively. Here, T_0 is the temperature at the slit and T_{ref} is the reference temperature for all $t < \frac{1}{\alpha}$. Similarly, C_0 is the concentration at the slit and C_{ref} is the reference concentration. Like α, b is the constant with the dimension $time^{-1}$. The specific forms of stretching velocity, temperature, and concentration are chosen so that transformations (2.7 - 2.11) map the governing equations (2.1 - 2.6) to

$$f''' + \gamma\left(ff'' - f'^2 - (Ma + S)f' - \frac{\eta S}{2}f''\right) = 0\,, \tag{2.15}$$

$$\theta'' + \gamma Pr\left(f\theta' - \frac{\eta S}{2}\theta' - 2f'\theta - \frac{3}{2}S\theta\right) = 0\,, \tag{2.16}$$

$$\phi'' + \gamma Sc\left(f\phi' - \frac{\eta S}{2}\phi' - 2f'\phi - \frac{3}{2}S\phi\right) = 0\,, \tag{2.17}$$

and boundary conditions (2.5 - 2.6) to

$$f(0) = 0,\ f'(0) = 1,\ \theta(0) = 1,\ \phi(0) = 1\ \ at\ \ \eta = 0\,, \tag{2.18}$$

and

$$f(1) = \frac{S}{2},\ f''(1) = 0,\ \theta'(1) = 0,\ \phi'(1) = 0\ \ at\ \ \eta = 1\,, \tag{2.19}$$

where $'$ represents differentiation w.r.t η. $\gamma = \beta^2$ is the dimensionless film thickness, $Ma = \frac{\sigma_e B_0}{b\rho}$ is the magnetic parameter, $S = \frac{\alpha}{b}$ is the measure of unsteadiness, $Pr = \frac{\nu}{\kappa}$ is the Prandtl number and $Sc = \frac{\nu}{D}$ is the Schmidt number. The transformations (2.7 - 2.11) satisfy the continuity equation (2.1) and setting $\eta = 1$ in eq (2.7) reveals the specific form of dimensionless film thickness $h(t)$

$$h(t) = \beta\sqrt{\frac{\nu(1-\alpha t)}{b}}\,. \tag{2.20}$$

In the next chapter, Lie symmetry analysis is performed to find new similarity solutions of the type (2.7 - 2.11) different from them.

2.2 Unsteady Flow over a Stretching Surface in the Presence of Thermocapillarity, Internal Heat Source/Sink Variable Magnetic Field

Consider an incompressible, conducting Newtonian fluid over a thin elastic sheet that is being pulled out of a narrow slit. The coordinate system has its origin at the slit, with the x-axis running parallel to the sheet. The sheet is being pulled in the horizontal direction in the plane $y = 0$ as shown in the figure.

The sheet velocity $U_s(x,t)$ and temperature $T_s(x,t)$ are assumed to be the arbitrary functions of distance and time. Additionally, a variable magnetic field $B = \frac{B_0}{\sqrt{1-\alpha t}}$ is being set up normal to the

stretching sheet. Here, B_0 is initial magnetic field strength and α is the arbitrary constant of dimension $time^{-1}$. The governing time-dependent boundary layer equations for mass, momentum, and energy equations in the presence of a uniform heat source or sink are given by

$$u_x + u_y = 0\,, \tag{2.21}$$

$$u_t + uu_x + vu_y = \nu u_{yy} - \frac{\sigma_e B^2}{\rho} u\,, \tag{2.22}$$

$$T_t + uT_x + vT_y = \kappa(T_{yy} + Q)\,, \tag{2.23}$$

where, u and v represent the velocity components in x and y direction respectively, whereas T is the temperature of the fluid. $\nu = \frac{\mu}{\rho}$ is the kinematic viscosity, ρ is the fluid density, μ is the dynamic viscosity, σ_e is the electrical conductivity, $\kappa = \frac{k}{\rho C_p}$ is the thermal diffusivity, k is the thermal conductivity, C_p is the specific heat capacity at a constant pressure. The subscripts $t, x,$ and y denote the derivatives with respect to these variables. Q represents the internal heat source or sink and is defined as

$$Q = \left(\frac{U_s\,\Delta T}{\nu x}\right) G^*\,, \tag{2.24}$$

where ΔT represents the temperature of fluid with respect to some fixed point usually the slit, with the temperature T_o and G^* is the temperature-dependent absorption or generation. G^* is positive when heat is generated by the elastic sheet and is negative when heat is being sucked by the stretching sheet from the fluid.

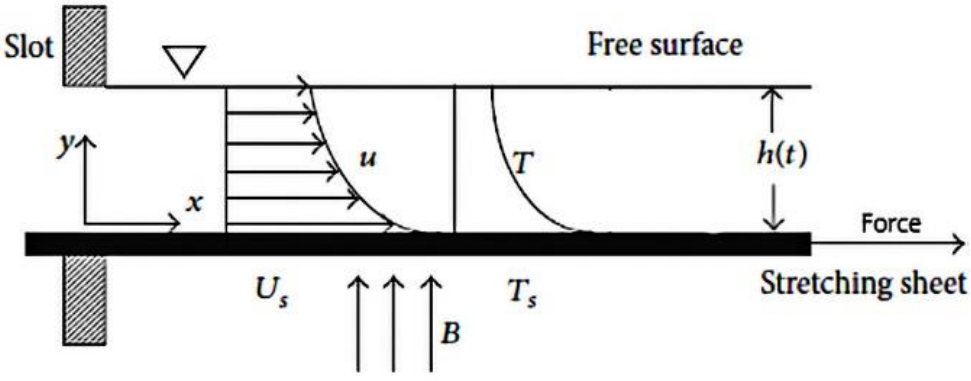

Figure 2: Physical representation of the problem

The scaling analysis of eqs (2.21 - 2.23) which can be found in [43] suggests the magnitude of

velocity in the primary flow direction is $\frac{\delta}{L}$ times larger than magnitude of velocity normal to the flow where, δ is the boundary layer thickness and L is the characteristic length of the sheet. Likewise, the magnitude of cross-diffusion is $\frac{L^2}{h^2}$ times greater than the diffusion along the streamlines. Due to this reasoning, the diffusion term in the momentum and energy has been disregarded. The absence of the pressure term in the aforementioned equation is a direct outcome of the assumptions made in the boundary layer theory [43].

The effect of buoyancy has been neglected in the governing equations since the liquid layer is thin. Also, the volatility of the Newtonian liquid is negligible, so the evaporation from the stretching can be disregarded. All fluid properties in this research are treated as constant except the surface tension σ which varies linearly with the temperature.

$$\sigma = \sigma_o[1 - \Gamma(T - T_0)]\,, \tag{2.25}$$

where σ denotes the surface tension and σ_o is the surface tension at the origin, whereas Γ is a positive fluid property. It is worth-mentioning that surface tension does not induce any type of interfacial motion, but the variation of surface tension along the interface (liquid and ambient gas interface) may induce the interfacial motion due to the temperature variation.

The associated boundary conditions are:

At $y = 0$,

$$u = U_s(x,t),\ v = 0,\ T = T_s(x,t)\,. \tag{2.26}$$

At $y = h(t)$,

$$\mu\frac{\partial \mathrm{u}}{\partial \mathrm{y}} = \frac{\partial \sigma}{\partial \mathrm{x}}\,, \tag{2.27}$$

$$T_y = 0\,, \tag{2.28}$$

$$v = \frac{dh}{dt}\,. \tag{2.29}$$

Here, $h(t)$ denotes the uniform film thickness. This suggests that the free surface of the film is smooth and free of any waves.

The boundary condition (2.27) states that the variation of the surface tension along the interface produces a net force that is balanced by the shear stress at the interface. The boundary condition

(2.27) indicates that heat transfer at the free surface is zero whereas, the boundary condition (2.28) imposes a kinematic constraint on the fluid motion.

The transformations (2.7 - 2.10) map the governing equations (2.21 - 2.23) to

$$f''' + \gamma\left(ff'' - f'^{2} - (Ma + S)f' - \frac{\eta S}{2}f''\right) = 0\,, \tag{2.30}$$

$$\theta'' + \gamma Pr\left(f\theta' - \frac{\eta S}{2}\theta' - 2f'\theta - \frac{3}{2}S\theta + \frac{G^{*}}{Pr}\theta\right) = 0\,, \tag{2.31}$$

and boundary conditions (2.26 - 2.29) to

$$f(0) = 0,\ f'(0) = 1,\ \theta(0) = 1\ \ at\ \ \eta = 0\,, \tag{2.32}$$

and

$$f(1) = \frac{S}{2},\ f''(1) = \mathrm{M}\,\theta(1),\ \theta'(1) = 0,\quad at\ \ \eta = 1\,. \tag{2.33}$$

Here, $\mathrm{M} = \frac{\sigma_o \gamma T_{ref} \beta}{\mu\sqrt{b\boldsymbol{\nu}}}$ is the thermocapillarity parameter which appears in the thermocapillarity driven flows.

In the next section, Lie point analysis is used to derive the new similarity solutions for the governing equation (2.21 - 2.23) into a form that can be easily solved using numerical or analytical techniques.

Chapter 3

3. Lie Symmetry Invariants, Similarity Transformations and Double Reduction

In this chapter Lie point analysis is used to derive new similarity transformations for the two cases given in Chapter 2. These transformations reduce the governing equations to a system of ODEs which are then solved using numerical or analytical techniques.

3.1 Lie Symmetry Analysis of Unsteady Flow over a Stretching Surface in the Presence of Variable Magnetic Field

The Lie point symmetry generator for eqs (2.1 - 2.4) is a vector field defined by

$$\boldsymbol{X} = \xi_t(t,x,y,u,v,T,C)\frac{\partial}{\partial t} + \xi_x(t,x,y,u,v,T,C)\frac{\partial}{\partial x} + \xi_y(t,x,y,u,v,T,C)\frac{\partial}{\partial y} + \eta_u(t,x,y,u,v,T,C)\frac{\partial}{\partial u} + \eta_v(t,x,y,u,v,T,C)\frac{\partial}{\partial v} + \eta_T(t,x,y,u,v,T,C)\frac{\partial}{\partial T} + \eta_C(t,x,y,u,v,T,C)\frac{\partial}{\partial C}, \quad 3.1$$

where ξ and η are called infinitesimal coordinates and are the function of both independent and dependent variables. These coordinates are determined using the algorithm outlined in [38]. The following Lie point symmetries which span 8-dimensional Lie algebra, are obtained.

$$\boldsymbol{X}_1 = \frac{\partial}{\partial x}, \quad 3.2$$

$$\boldsymbol{X}_2 = \frac{\partial}{\partial T}, \quad 3.3$$

$$\boldsymbol{X}_3 = \frac{\partial}{\partial C}, \quad 3.4$$

$$\boldsymbol{X}_4 = T\frac{\partial}{\partial T}, \quad 3.5$$

$$\boldsymbol{X}_5 = C\frac{\partial}{\partial C}, \tag{3.6}$$

$$\boldsymbol{X}_6 = x\frac{\partial}{\partial x} + u\frac{\partial}{\partial u}, \tag{3.7}$$

$$\boldsymbol{X}_7 = t\frac{\partial}{\partial t} + \frac{y}{2}\frac{\partial}{\partial y} - u\frac{\partial}{\partial u} - \frac{v}{2}\frac{\partial}{\partial v}, \tag{3.8}$$

$$\boldsymbol{X}_8 = t^{1-\frac{\sigma_e {B_o}^2}{\alpha\rho}}\frac{\partial}{\partial x} + \left(\frac{\alpha\rho - \sigma_e {B_o}^2}{\alpha t\rho}\right)t^{1-\frac{\sigma_e {B_o}^2}{\alpha\rho}}\frac{\partial}{\partial u}. \tag{3.9}$$

Let

$$\boldsymbol{Z} = k_1\boldsymbol{X}_1 + k_2\boldsymbol{X}_2 + k_3\boldsymbol{X}_3 + k_4\boldsymbol{X}_4 + k_5\boldsymbol{X}_5 + k_6\boldsymbol{X}_6 + k_7\boldsymbol{X}_7 \tag{3.10}$$

Here, a linear combination of all translational and scaling symmetries is considered. $\boldsymbol{X}_8$ is neither translational nor scaling symmetry. That's why it is omitted. $k_1, k_2, k_3, k_4, k_5, k_6$ and k_7 are the constants that belong to the set of real numbers.

To check the invariance of the boundary conditions, **Z** is applied to boundary conditions (2.25 - 2.26). It leaves all the boundary conditions invariant while for $u = U_s(x,t), T = T_s(x,t),\ C = C_s(x,t)$ and $y = h(t)$, it yields

$$k_7 t\frac{\partial U_s}{\partial t} + (k_6 x + k_1)\frac{\partial U_s}{\partial x} - u(k_6 - k_7) = 0, \tag{3.11}$$

$$k_7 t\frac{\partial T_s}{\partial t} + (k_6 x + k_1)\frac{\partial T_s}{\partial x} - k_4 T - k_2 = 0, \tag{3.12}$$

$$k_7 t\frac{\partial T_s}{\partial t} + (k_6 x + k_1)\frac{\partial C_s}{\partial x} - k_5 C - k_3 = 0, \tag{3.13}$$

$$k_7 t\frac{\partial h}{\partial t} - \frac{k_7 y}{2} = 0. \tag{3.14}$$

Solving these linear partial differential equations reveals the specific forms of $U_s(x,t)$, $T_s(x,t)$, $C_s(x,t)$ and $h(t)$ as follow

$$U_s(x,t) = t^{\frac{k_6}{k_7}-1}F_1\left(\frac{(k_6 x + k_1)t^{-\frac{k_6}{k_7}}}{k_6}\right), \tag{3.15}$$

$$T_s(x,t) = t^{\frac{k_4}{k_7}}F_2\left(\frac{(k_6 x + k_1)t^{-\frac{k_6}{k_7}}}{k_6}\right) - \frac{k_2}{k_4}, \tag{3.16}$$

$$C_s(x,t) = t^{\frac{k_5}{k_7}}F_3\left(\frac{(k_6 x + k_1)t^{-\frac{k_6}{k_7}}}{k_6}\right) - \frac{k_3}{k_5}, \tag{3.17}$$

$$h(t) = C_1\sqrt{t}\,, \tag{3.18}$$

where C_1 is a constant of integration.

For the construction of the similarity transformations, system invariants are required. Zeroth-order invariants associated with the Lie algebra spanned by $\boldsymbol{X_i}, i = 1 \ldots 8$ is a function of independent and dependent variables of the system (2.1 - 2.4). The invariants associated with **Z** are obtained through the criterion

$$\boldsymbol{Z}J(t, x, y, T, C, u, v) = 0\,. \tag{3.19}$$

This leads to a linear partial equation given by

$$k_7 t\frac{\partial J}{\partial t} + (k_6 x + k_1)\frac{\partial J}{\partial x} + (k_5 C + k_3)\frac{\partial J}{\partial C} + (k_4 T + k_2)\frac{\partial J}{\partial T} + (k_6 - k_7)u\frac{\partial J}{\partial C} - \frac{k_7 v}{2}\frac{\partial J}{\partial v} = 0. \tag{3.20}$$

Solving (3.20) generates the system invariants $\{\frac{(k_6 x+k_1)t^{-\frac{k_6}{k_7}}}{k_6}, \frac{y}{\sqrt{t}}, \frac{(k_5 C+k_3)t^{-\frac{k_5}{k_7}}}{k_5}, \frac{(k_4 T+k_2)t^{-\frac{k_4}{k_7}}}{k_4}, ut^{\frac{k_6}{k_7}-1}, v\sqrt{t}\ \}$.

Let

$$z_1 = \frac{(k_6 x+k_1)t^{-\frac{k_6}{k_7}}}{k_6}\,, \tag{3.21}$$

$$z_2 = \frac{y}{\sqrt{t}}\,, \tag{3.22}$$

$$P = \frac{(k_5 C+k_3)t^{-\frac{k_5}{k_7}}}{k_5}\,, \tag{3.23}$$

$$Q = \frac{(k_4 T+k_2)t^{-\frac{k_4}{k_7}}}{k_4}\,, \tag{3.24}$$

$$R = ut^{\frac{k_6}{k_7}-1}\,, \tag{3.25}$$

$$W = v\sqrt{t}\,. \tag{3.26}$$

z_1 and z_2 are the new independent variables while $P, Q, R,$ and W are the new dependent variables. These transformations (3.21 - 3.26) map eqs (2.1 - 2.4) to

$$R_{z_1} + W_{z_2} = 0\,, \tag{3.27}$$

$$-\frac{k_6}{k_7}z_1 R_{z_1} - \frac{1}{2}z_2 R_{z_2} + \frac{k_6-k_7}{k_7}R + RR_{z_1} + WR_{z_2} - \boldsymbol{\nu}R_{z_2 z_2} + \frac{\sigma_e {B_o}^2}{\alpha\rho}R = 0\,, \tag{3.28}$$

$$-\frac{k_6}{k_7}z_1 Q_{z_1} - \frac{1}{2}z_2 Q_{z_2} + \frac{k_4}{k_7}Q + RQ_{z_1} + WQ_{z_2} - \kappa Q_{z_2 z_2} = 0\,, \tag{3.29}$$

$$-\frac{k_6}{k_7}z_1P_{z_1}-\frac{1}{2}z_2P_{z_2}+\frac{k_5}{k_7}P\ +RP_{z_1}+WP_{z_2}-DP_{z_2z_2}=0\ . \tag{3.30}$$

while boundary conditions (2.5 - 2.6) map to

$$R=\ F_1(z_1),\ W=0,\ Q=\ F_2(z_1),\ P=\ F_3(z_1)\quad at\ z_2=0 \tag{3.31}$$

$$R_{z_2}=Q_{z_2}=P_{z_2}=0,\ W=\frac{C_1}{2}\quad at\ z_2=C_1\ , \tag{3.32}$$

where C_1 is a constant of integration. Eqs (3.27 - 3.30) have two independent and four dependent variables. Thus, with the help of transformations (3.21 - 3.26) we are able to reduce one independent variable in eqs (2.1 - 2.4). To obtain a system of ODEs, one more such reduction is required. This is obtainable from the Lie algebra associated with (3.27 - 3.32).

The system (3.27 - 3.32) admits three-dimensional symmetry algebra spanned by the symmetry generators

$$\boldsymbol{Y}_1=\ Q\frac{\partial}{\partial Q}, \tag{3.33}$$

$$\boldsymbol{Y}_2=\ P\frac{\partial}{\partial P}, \tag{3.34}$$

$$\boldsymbol{Y}_3=\ z_1\frac{\partial}{\partial z_1}+R\frac{\partial}{\partial R}\ . \tag{3.35}$$

Let $\boldsymbol{Y}=\ \boldsymbol{Y}_1+\boldsymbol{Y}_2+\boldsymbol{Y}_3$. The boundary condition (3.31 - 3.32) remains invariant with respect to $\boldsymbol{Y}$ if

$$F_1(z_1)=C_2z_1\ , \tag{3.36}$$

$$F_2(z_1)=C_3z_1\ , \tag{3.37}$$

$$F_3(z_1)=C_4z_1\ . \tag{3.38}$$

Like C_1, C_2, C_3 and C_4 are also constant of integration. To obtain the invariants of the reduced system, $\boldsymbol{Y}$ is applied on a function $G(z_1, z_2, P, Q, R, W)$ which yields the invariants $\{z_2, \frac{P}{z_1}, \frac{Q}{z_1}, \frac{R}{z_1}, W\}$. Now let

$$\chi=z_2\ ,\qquad g_1=\frac{P}{z_1}\ ,\qquad g_2=\frac{Q}{z_1}\ ,\qquad g_3=\frac{R}{z_1}\ ,\qquad g_3=W\ . \tag{3.39}$$

These transformations reduce (3.27 - 3.32) to

$$g_3 + g_4{}' = 0\,, \tag{3.40}$$

$$-\frac{k_6}{k_7} g_3 - \frac{1}{2} z_2 g_3{}' + \frac{k_6 - k_7}{k_7} g_3 + {g_3}^2 + g_4 g_3{}' - \boldsymbol{\nu} g_3{}'' + \frac{\sigma_e {B_o}^2}{\alpha \rho} g_3 = 0\,, \tag{3.41}$$

$$-\frac{k_6}{k_7} g_2 - \frac{1}{2} z_2 g_2{}' + \frac{k_4}{k_7} g_2 + g_3 g_2 + g_4 g_2{}' - \kappa g_2{}'' = 0\,, \tag{3.42}$$

$$-\frac{k_6}{k_7} g_1 - \frac{1}{2} z_2 g_1{}' + \frac{k_5}{k_7} g_1 + g_3 g_1 + g_4 g_1{}' - D g_1{}'' = 0\,, \tag{3.43}$$

subject to

$$g_3 = C_2,\ g_4 = 0,\ g_2 = C_3,\ g_1 = C_4 \quad at\ \chi = 0\,, \tag{3.44}$$

and

$$g_3{}' = g_2{}' = g_1{}' = 0,\ g_4 = \frac{C_1}{2} \quad at\ \chi = C_1\ , \tag{3.45}$$

where $'$ represents differentiation w.r.t χ.

Eqs (3.40 - 3.45) is the system of ODEs with χ as the independent variable. This is achieved with the help of transformations (3.21 - 3.26) and (3.39) in two steps. To obtain the similarity transformations that directly reduce (2.1 - 2.6) to a system of ODEs, let

$$\beta\sqrt{\frac{\alpha\nu}{b}}\eta = \chi\,,\ -\frac{b}{\alpha} f' = g_3\,,\ \beta\sqrt{\frac{\nu b}{\alpha}} f = g_4\,,\ \theta = g_2\,,\ \phi = g_1 \tag{3.46}$$

This leads to

$$y = \beta\sqrt{\frac{\alpha\nu t}{b}}\eta\,,\ u = \frac{-b\left(x + \frac{k_1}{k_6}\right)}{\alpha t} f'(\eta)\,,\ v = \beta\sqrt{\frac{\nu b}{\alpha t}} f(\eta)\,,\ T = \frac{x + \frac{k_1}{k_6}}{t^{\frac{k_6 - k_4}{k_7}}}\theta(\eta) - \frac{k_2}{k_4}\,,\ C = \frac{x + \frac{k_1}{k_6}}{t^{\frac{k_6 - k_5}{k_7}}}\phi(\eta) - \frac{k_3}{k_5}\,. \tag{3.47}$$

where $f(\eta), \theta(\eta),$ and $\phi(\eta)$ are new dimensionless variables while η is the similarity variable. T and C represent the temperature and concentration difference respectively i.e. $T_0 - T(x,t)$ and $C_0 - C(x,t)$, where T_0 and C_0 is the temperature and concentration of the sheet at the slit. These similarity transformations automatically satisfy the continuity equation and transform the momentum, energy, and concentration equation to

$$f''' + \gamma\left(-ff'' + f'^2 - (Ma - S)f' + \frac{\eta S}{2}f''\right) = 0\,, \tag{3.48}$$

$$Pr^{-1}\theta'' + \gamma\left(-f\theta' + \frac{\eta S}{2}\theta' + \left(f' - \frac{k_4 - k_6}{k_7}S\right)\theta\right) = 0\,, \tag{3.49}$$

$$Sc^{-1}\phi'' + \gamma\left(-f\phi' + \frac{\eta S}{2}\phi' + \left(f' - \frac{k_5 - k_6}{k_7}S\right)\phi\right) = 0\,, \tag{3.50}$$

where $'$ now represents differentiation w.r.t η. $\gamma = \beta^2$ is the dimensionless film thickness, $Ma = \frac{\sigma_e {B_o}^2}{b\rho}$ is the magnetic parameter, $S = \frac{\alpha}{b}$ is the measure of unsteadiness, $Pr = \frac{\boldsymbol{\nu}}{\kappa}$ is the Prandtl number and $Sc = \frac{\boldsymbol{\nu}}{D}$ is the Schmidt number.

The boundary conditions (2.5 - 2.6) transform to

$$f(0) = 0,\ f'(0) = 1,\ \theta(0) = 1,\ \phi(0) = 1\ \ at\ \ \eta = 0\,, \tag{3.51}$$

and

$$f(1) = \frac{S}{2},\ f''(1) = 0,\ \theta'(1) = 0,\ \phi'(1) = 0\ \ at\ \ \eta = 1\,. \tag{3.52}$$

under the transformations (3.47) by assuming the following values of the arbitrary constants C_1, C_2, C_3, and C_4.

$$C_1 = \beta\sqrt{\frac{\alpha\nu}{b}},\ \ C_2 = -\frac{b}{\alpha},\ \ C_3 = 1,\ C_4 = 1 \tag{3.53}$$

It should be noted that $\eta = 1$ represents the free surface. If we put $\eta = 1$ in (3.47), we get

$$h(t) = \beta\sqrt{\frac{\alpha\nu t}{b}} \tag{3.54}$$

It should be noted that film thickness is only a function of time, not space which is one of our assumptions while writing boundary layer equations.

(3.15 - 3.17) and (3.36 - 3.38) tell us about the specific forms of $U_s(x,t)$, $T_s(x,t)$, and $C_s(x,t)$. By combining these equations, we have

$$U_s(x,t) = -\frac{\left(x + \frac{k_1}{k_6}\right)b}{\alpha t}\,, \tag{3.55}$$

$$T_s(x,t) = t^{\frac{k_4-k_6}{k_7}}\left(x+\frac{k_1}{k_6}\right)-\frac{k_2}{k_4}, \tag{3.56}$$

$$C_s(x,t) = t^{\frac{k_5-k_6}{k_7}}\left(x+\frac{k_1}{k_6}\right)-\frac{k_3}{k_5}. \tag{3.57}$$

The negative sign in $U_s(x,t)$ is telling about the velocity direction and can be ignored. It should be noted that $k_1, k_2,$ and k_3 does not appear in eqs (3.48 - 3.50). So, they can be taken as zero. This leads to

$$U_s(x,t) = \frac{xb}{\alpha t}, \tag{3.58}$$

$$T_s(x,t) = t^{\frac{k_4-k_6}{k_7}}x, \tag{3.59}$$

$$C_s(x,t) = t^{\frac{k_5-k_6}{k_7}}x. \tag{3.60}$$

Here, $T_s(x,t)$ and $C_s(x,t)$ represents temperature and concentration difference respectively i.e. $T_0 - T_s(x,t)$ and $C_0 - C_s(x,t)$. As we move from the slit the temperature and concentration of the sheet decrease. This behavior is also similar for time if the ratio $\frac{k_5-k_6}{k_7}$ is positive.

For practical purposes, we need drag force, heat transfer, and mass transfer which can be computed from the skin friction coefficient, Nusselt number, and Sherwood number.

$$C_f = \frac{\mu\left(\frac{\partial u}{\partial y}\right)_{y=0}}{\frac{\rho {U_s}^2}{2}}, \tag{3.61}$$

$$Nu_x = \frac{k\left(\frac{\partial T}{\partial y}\right)_{y=0}}{\frac{kT_0}{x}}, \tag{3.62}$$

$$Sh_x = \frac{D\left(\frac{\partial C}{\partial y}\right)_{y=0}}{\frac{DC_0}{x}}, \tag{3.63}$$

where k is the thermal conductivity of the fluid. The knowledge of $f(\eta)$ and $\theta(\eta)$ allows us to calculate these parameters.

$$C_f = \frac{2}{\beta\, {Re_x}^{\frac{1}{2}}} f''(0), \tag{3.64}$$

$$Nu_x = \frac{Re_x^{\frac{3}{2}}}{2\beta\alpha t}\,\theta'(0)\,, \tag{3.65}$$

$$Sh_x = \frac{Re_x^{\frac{3}{2}}}{2\beta\alpha t}\,\phi'(0)\,, \tag{3.66}$$

where $Re_x = \frac{U_s x}{\nu}$ is the local Reynold's number.

3.2 1-Dimensional Optimal System for Unsteady Flow over a Stretching Surface in the presence of Variable Magnetic Field

In this section, a 1–dimensional optimal system of the momentum, heat, and mass transfer in a liquid film over an unsteady stretching in the presence of a variable magnetic field is developed. The motive of using a general linear combination of all translational and scaling symmetries was to develop generalized similarity transformations from which we can derive all invariants solutions, as infinite sub-algebra always exists, but it did not work as the arbitrary coefficients of the linear combination appear only in the power of variable time t. So, our next resort is to develop a 1-dimensional optimal system of the governing equations (2.1 - 2.6).

This optimal system of sub-algebras serves as a valuable tool for identifying distinct classes of invariant solutions for differential equations. By identifying these non-equivalent classes, the task of constructing a comprehensive set of invariant solutions for a given differential equation can be streamlined.

The established optimal system allows for the transformation of any relevant differential equation and its corresponding solutions into one of the classes provided by the system. Consequently, by deriving a singlw solution for every element within the optimal system of sub-algebras, one can effectively obtain all invariant solutions for a given differential equation (or system of differential equations). Notably, when two sub-algebras share the same class during a symmetry transformation, the invariant solutions associated with these sub-algebras can be mutually converted under the identical transformation.

In the previous section, an 8-dimensional Lie algebra for the PDEs (2.1 - 2.6) is considered, where a linear combination of all translational and scaling symmetries is employed to derive a general

similarity transformation. Here, we develop a 1-dimensional optimal system of the Lie sub-algebras. Any linear combination of Lie point symmetries is again a Lie point symmetry, Consequently, every sub-algebra included in the obtained optimal system can be identified as a Lie symmetry for the associated system of differential equations. For every individual component within the derived optimal system, there exists a similarity transformation comprising the system invariants that transform the governing equations with three independent variables into a system with two independent variables. To obtain a system of ODEs (one independent variable) one more such reduction is performed through the symmetries and invariants of the once-reduced system. Here, all classes of ODEs are obtained through similarity transformations facilitated by each component of the optimal system through the two invariants extracted from the governing PDEs and the once-reduced PDEs.

The 1-dimensional optimal system of the governing PDEs (2.1 - 2.6) derived through the Maple algorithm developed by Zhang et al. [44], reveals 22 linear combinations of Lie symmetry generator. These generators generate 22 unique classes of a system of ODEs upon double reduction describing the dynamics of flow, heat, and mass transfer. A system of ODEs generated by any other linear combination of Lie symmetry generators will belong to one of the 22 classes. Thus the optimal system provides us with all the existent invariants solutions. The linear combinations of Lie symmetry generators developed by the optimal theory are given in Table 1. The corresponding invariants and similarity transformations are given in Table 2. The reduced systems corresponding to each class of symmetries are given in Table 3. The nomenclature used for the reduction of the optimal system is the same as used in the previous section.

Table 1: Lie symmetry generators of optimal system

S. No	Lie Symmetry Generators	S. No	Lie Symmetry Generators
1	$\boldsymbol{X_4 + k_5 X_5 + k_6 X_6 + k_7 X_7}$	12	$\boldsymbol{X_5 + k_1 X_1 + k_2 X_2 + k_8 X_8}$
2	$\boldsymbol{X_4 + k_5 X_5 + k_6 X_6}$	13	$\boldsymbol{X_7 + k_6 X_6 + k_2 X_2 + k_3 X_3}$
3	$\boldsymbol{X_4 + k_1 X_1 + k_5 X_5 + k_7 X_7}$	14	$\boldsymbol{X_6 + k_2 X_2 + k_3 X_3}$
4	$\boldsymbol{X_4 + k_1 X_1 + k_5 X_5 + k_8 X_8}$	15	$\boldsymbol{X_7 + k_1 X_1 + k_2 X_2 + k_3 X_3}$
5	$\boldsymbol{X_4 + k_3 X_3 + k_6 X_6 + k_7 X_7}$	16	$\boldsymbol{X_3 + k_1 X_1 + k_2 X_2 + k_8 X_8}$

6	$\boldsymbol{X_4 + k_3 X_3 + k_6 X_6}$	17	$\boldsymbol{X_4 + k_6 X_6 + k_7 X_7}$
7	$\boldsymbol{X_4 + k_1 X_1 + k_3 X_3 + k_7 X_7}$	18	$\boldsymbol{X_3 + k_4 X_4 + k_6 X_6}$
8	$\boldsymbol{X_4 + k_1 X_1 + k_3 X_3 + k_8 X_8}$	19	$\boldsymbol{X_2 + k_5 X_5 + k_6 X_6 + k_7 X_7}$
9	$\boldsymbol{X_5 + k_2 X_2 + k_6 X_6 + k_7 X_7}$	20	$\boldsymbol{X_2 + k_5 X_5 + k_6 X_6}$
10	$\boldsymbol{X_5 + k_2 X_2 + k_6 X_6}$	21	$\boldsymbol{X_2 + k_3 X_3 + k_6 X_6 + k_7 X_7}$
11	$\boldsymbol{X_5 + k_1 X_1 + k_2 X_2 + k_7 X_7}$	22	$\boldsymbol{X_2 + k_3 X_3 + k_6 X_6}$

Table 2: Invariants of governing and reduced PDEs and corresponding similarity transformations

Symmetries	Invariants	Transformations
$\boldsymbol{X_4 + k_5 X_5 + k_6 X_6 + k_7 X_7}$	$\left\{xt^{-\frac{k_6}{k_7}}, \frac{y}{\sqrt{t}}, Ct^{-\frac{k_5}{k_7}}, Tt^{-\frac{1}{k_7}}, ut^{-\frac{k_6-k_7}{k_7}}, v\sqrt{t}\right\}$ $\left\{z_2, \frac{P}{z_1}, \frac{Q}{z_1}, \frac{R}{z_1}, W\right\}$	$y = \beta\sqrt{\frac{\alpha v t}{b}}\,\eta,\ u = -\frac{bx}{\alpha t}f',\ v = \beta\sqrt{\frac{vb}{\alpha t}}\,f,$ $T = xt^{\frac{1-k_6}{k_7}}\theta\,, C = xt^{\frac{k_5-k_6}{k_7}}\phi$
$\boldsymbol{X_4 + k_5 X_5 + k_6 X_6}$	$\left\{t, y, Cx^{-\frac{k_5}{k_6}}, Tx^{-\frac{1}{k_6}}, \frac{u}{x}, v\right\}$ $\left\{\frac{z_2}{\sqrt{z_1}}, \frac{P}{z_1}, \frac{Q}{z_1}, Rz_1, W\sqrt{z_1}\right\}$	$y = \beta\sqrt{\frac{\alpha v t}{b}}\,\eta,\ u = -\frac{bx}{\alpha t}f',\ v = \beta\sqrt{\frac{vb}{\alpha t}}\,f,$ $T = x^{\frac{1}{k_6}}t\,\theta\,, C = x^{\frac{k_5}{k_6}}t\,\phi$
$\boldsymbol{X_4 + k_1 X_1 + k_5 X_5 + k_7 X_7}$	Does not satisfy continuity equation	
$\boldsymbol{X_4 + k_1 X_1 + k_5 X_5 + k_8 X_8}$	Does not satisfy continuity equation	
$\boldsymbol{X_4 + k_3 X_3 + k_6 X_6 + k_7 X_7}$	$\left\{xt^{-\frac{k_6}{k_7}}, \frac{y}{\sqrt{t}}, ln\left(t^{-\frac{k_3}{k_7}}\right) + C, Tt^{-\frac{1}{k_7}},\right.$ $\left.ut^{-\frac{k_6-k_7}{k_7}}, v\sqrt{t}\right\}$ $\left\{z_2, -\ln(z_1) + P, \frac{Q}{z_1}, \frac{R}{z_1}, W\right\}$	$y = \beta\sqrt{\frac{\alpha v t}{b}}\,\eta,\ u = -\frac{bx}{\alpha t}f',\ v = \beta\sqrt{\frac{vb}{\alpha t}}\,f,$ $T = xt^{\frac{1-k_6}{k_7}}\theta\,, C = \ln(xt^{\frac{k_3-k_6}{k_7}}) + \phi$
$\boldsymbol{X_4 + k_3 X_3 + k_6 X_6}$	$\left\{t, y, C + \ln(x^{-\frac{k_3}{k_6}}), Tx^{-\frac{1}{k_6}}, \frac{u}{x}, v\right\}$ $\left\{\frac{z_2}{\sqrt{z_1}}, P - \ln(z_1), \frac{Q}{z_1}, Rz_1, W\sqrt{z_1}\right\}$	$y = \beta\sqrt{\frac{\alpha v t}{b}}\,\eta,\ u = -\frac{bx}{\alpha t}f',\ v = \beta\sqrt{\frac{vb}{\alpha t}}\,f,$ $T = x^{\frac{1}{k_6}}t\,\theta\,, C = \ln\left(x^{\frac{k_3}{k_6}}t\right) + \phi$
$\boldsymbol{X_4 + k_1 X_1 + k_3 X_3 + k_7 X_7}$	Does not satisfy continuity equation	
$\boldsymbol{X_4 + k_1 X_1 + k_3 X_3 + k_8 X_8}$	Does not satisfy continuity equation	

$\boldsymbol{X_5 + k_2X_2 + k_6X_6 + k_7X_7}$	$\left\{xt^{-\frac{k_6}{k_7}}, \frac{y}{\sqrt{t}}, Ct^{-\frac{1}{k_7}}, \ln\left(t^{-\frac{k_2}{k_7}}\right) + T, ut^{-\frac{k_6-k_7}{k_7}}, v\sqrt{t}\right\}$ $\left\{z_2, \frac{P}{z_1}, -\ln(z_1) + Q, \frac{R}{z_1}, W\right\}$	$y = \beta\sqrt{\frac{\alpha v t}{b}}\,\eta,\ u = -\frac{bx}{\alpha t}f',\ v = \beta\sqrt{\frac{vb}{\alpha t}}\,f,$ $C = xt^{\frac{1-k_6}{k_7}}\phi\,, T = \ln(xt^{\frac{k_2-k_6}{k_7}}) + \theta$
$\boldsymbol{X_5 + k_2X_2 + k_6X_6}$	$\left\{t, y, Cx^{-\frac{1}{k_6}}, \frac{Tk_6 - k_2\ln(x)}{k_6}, \frac{u}{x}, v\right\}$ $\left\{\frac{z_2}{\sqrt{z_1}}, \frac{P}{z_1}, -\ln(z_1) + Q, \frac{R}{z_1}, W\right\}$	$y = \beta\sqrt{\frac{\alpha v t}{b}}\,\eta,\ u = -\frac{bx}{\alpha t}f',\ v = \beta\sqrt{\frac{vb}{\alpha t}}\,f,$ $C = x^{\frac{1}{k_6}}\,t\,\phi\,, T = \ln\left(x^{\frac{k_2}{k_6}}\,t\right) + \theta$
$\boldsymbol{X_5 + k_1X_1 + k_2X_2 + k_7X_7}$	Does not satisfy continuity equation	
$\boldsymbol{X_5 + k_1X_1 + k_2X_2 + k_8X_8}$	Does not satisfy continuity equation	
$\boldsymbol{X_7 + k_6X_6 + k_2X_2 + k_3X_3}$	$\left\{xt^{-k_6}, \frac{y}{\sqrt{t}}, -k_3\ln(t) + C, -k_2\ln(t) + T, ut^{-k_6+1}, v\sqrt{t}\right\}$ $\left\{z_2, -\ln(z_1) + P, -\ln(z_1) + Q, \frac{R}{z_1}, W\right\}$	$y = \beta\sqrt{\frac{\alpha v t}{b}}\,\eta,\ u = -\frac{bx}{\alpha t}f',\ v = \beta\sqrt{\frac{vb}{\alpha t}}\,f,$ $T = \ln\left(xt^{k_2 - k_6}\right) + \theta,\ C = \ln\left(xt^{k_3 - k_6}\right) + \phi$
$\boldsymbol{X_6 + k_2X_2 + k_3X_3}$	$\left\{t, y, -k_3\,ln(x) + C, -k_2\,ln(x) + T, \frac{u}{x}, v\right\}$ $\left\{\frac{z_2}{\sqrt{z_1}}, -\ln(z_1) + P, -\ln(z_1) + Q, Rz_1, W\sqrt{z_1}\right\}$	$y = \beta\sqrt{\frac{\alpha v t}{b}}\,\eta,\ u = -\frac{bx}{\alpha t}f',\ v = \beta\sqrt{\frac{vb}{\alpha t}}\,f,$ $T = \ln\left(x^{k_2}t\right) + \theta,\ C = \ln\left(x^{k_3}t\right) + \phi$
$\boldsymbol{X_7 + k_1X_1 + k_2X_2 + k_3X_3}$	Does not satisfy continuity equation	
$\boldsymbol{X_3 + k_1X_1 + k_2X_2 + k_8X_8}$	Does not satisfy continuity equation	
$\boldsymbol{X_4 + k_6X_6 + k_7X_7}$	$\left\{xt^{-\frac{k_6}{k_7}}, \frac{y}{\sqrt{t}}, C, Tt^{-\frac{1}{k_7}}, ut^{-\frac{k_6-k_7}{k_7}}, v\sqrt{t}\right\}$ $\left\{z_2, \frac{P}{z_1}, \frac{Q}{z_1}, \frac{R}{z_1}, W\right\}$	$y = \beta\sqrt{\frac{\alpha v t}{b}}\,\eta,\ u = -\frac{bx}{\alpha t}f',\ v = \beta\sqrt{\frac{vb}{\alpha t}}\,f,$ $T = xt^{\frac{1-k_6}{k_7}}\theta\,, C = xt^{\frac{-k_6}{k_7}}\phi$
$\boldsymbol{X_3 + k_4X_4 + k_6X_6}$	$\left\{t, y, C - \frac{1}{k_6}\ln(x), Tx^{-\frac{k_4}{k_6}}, \frac{u}{x}, v\right\}$ $\left\{\frac{z_2}{\sqrt{z_1}}, P - \ln(z_1), \frac{Q}{z_1}, Rz_1, W\sqrt{z_1}\right\}$	$y = \beta\sqrt{\frac{\alpha v t}{b}}\,\eta,\ u = -\frac{bx}{\alpha t}f',\ v = \beta\sqrt{\frac{vb}{\alpha t}}\,f,$ $C = x^{\frac{1}{k_6}}\,t + \phi\,, T = x^{\frac{k_4}{k_6}}\,t\,\theta$
$\boldsymbol{X_2 + k_5X_5 + k_6X_6 + k_7X_7}$	$\left\{xt^{-\frac{k_6}{k_7}}, \frac{y}{\sqrt{t}}, Ct^{-\frac{k_5}{k_7}}, \frac{Tk_7 - \ln(t)}{k_7}, ut^{-\frac{k_6-k_7}{k_7}}, v\sqrt{t}\right\}$ $\left\{z_2, \frac{P}{z_1}, Q - \ln(z_1), \frac{R}{z_1}, W\right\}$	$y = \beta\sqrt{\frac{\alpha v t}{b}}\,\eta,\ u = -\frac{bx}{\alpha t}f',\ v = \beta\sqrt{\frac{vb}{\alpha t}}\,f,$ $T = \ln\left(xt^{\frac{1-k_6}{k_7}}\right) + \theta\,, C = xt^{\frac{k_5-k_6}{k_7}}\phi$
	$\left\{t, y, Cx^{-\frac{k_5}{k_6}}, \frac{Tk_6 - \ln(x)}{k_6}, \frac{u}{x}, v\right\}$	$y = \beta\sqrt{\frac{\alpha v t}{b}}\,\eta,\ u = -\frac{bx}{\alpha t}f',\ v = \beta\sqrt{\frac{vb}{\alpha t}}\,f,$

$\boldsymbol{X_2 + k_5X_5 + k_6X_6}$	$\left\{\frac{z_2}{\sqrt{z_1}}, \frac{P}{z_1}, Q - \ln(z_1), Rz_1, W\sqrt{z_1}\right\}$	$T = \ln\left(x^{\frac{1}{k_6}}t\right) + \theta\ , C = x^{\frac{k_5}{k_6}}t\phi$
$\boldsymbol{X_2 + k_3X_3 + k_6X_6 + k_7X_7}$	$\left\{xt^{-\frac{k_6}{k_7}}, \frac{y}{\sqrt{t}}, -\frac{k_3}{k_7}\ln(t) + C, -\frac{1}{k_7}\ln(t) + T, ut^{-\frac{k_6 - k_7}{k_7}}, v\sqrt{t}\right\}$ $\left\{z_2, -\ln(z_1) + P, -\ln(z_1) + Q, \frac{R}{z_1}, W\right\}$	$y = \beta\sqrt{\frac{\alpha\nu t}{b}}\ \eta,\ u = -\frac{bx}{\alpha t}f',\ v = \beta\sqrt{\frac{\nu b}{\alpha t}}\ f,$ $T = \ln\left(xt^{\frac{1-k_6}{k_7}}\right) + \theta,\ C = \ln\left(xt^{\frac{k_3-k_6}{k_7}}\right) + \phi$
$\boldsymbol{X_2 + k_3X_3 + k_6X_6}$	$\left\{t, y, -\frac{k_3}{k_6}\ln(x) + C, -\frac{1}{k_6}\ln(x) + T, \frac{u}{x}, v\right\}$ $\left\{\frac{z_2}{\sqrt{z_1}}, -\ln(z_1) + P, -\ln(z_1) + Q, Rz_1, W\sqrt{z_1}\right\}$	$y = \beta\sqrt{\frac{\alpha\nu t}{b}}\ \eta,\ u = -\frac{bx}{\alpha t}f',\ v = \beta\sqrt{\frac{\nu b}{\alpha t}}\ f,$ $T = \ln\left(x^{\frac{1}{k_6}}\ t\right) + \theta,\ C = \ln\left(x^{\frac{k_3}{k_6}}\ t\right) + \phi$

Table 3: Reduced systems

Symmetries	Reduced System
$\boldsymbol{X_4 + k_5X_5 + k_6X_6 + k_7X_7}$	$f''' + \beta^2\left[-ff'' + f'^2 - (Ma - S)f' + \frac{1}{2}Sf''\right] = 0$ $Pr^{-1}\,\theta'' + \gamma\left(-f\theta' + \frac{\eta S}{2}\theta' + f'\theta + \frac{k_6 - 1}{k_7}S\theta\right) = 0$ $Sc^{-1}\,\phi'' + \gamma\left(-f\phi' + \frac{\eta S}{2}\phi' + f'\phi\ -\ \frac{k_5 - k_6}{k_7}S\phi\right) = 0$ **B.C:** $f(0) = 0,\ f'(0) = 1,\ \theta(0) = 1,\ \phi(0) = 1\ at\ \eta = 0$ $f(1) = \frac{S}{2},\ f''(1) = 0,\ \theta'(1) = 0,\ \phi'(1) = 0\ at\ \eta = 1$
$\boldsymbol{X_4 + k_5X_5 + k_6X_6}$	$f''' + \beta^2\left[-ff'' + f'^2 - (Ma - S)f' + \frac{1}{2}Sf''\right] = 0$ $Pr^{-1}\,\theta'' + \gamma\left(-f\theta' + \frac{\eta S}{2}\theta' + \frac{1}{k_6}f'\theta - S\theta\right) = 0$ $Sc^{-1}\,\phi'' + \gamma\left(-f\phi' + \frac{\eta S}{2}\phi' + \frac{k_5}{k_6}f'\phi\ -\ S\phi\right) = 0$ **B.C:** $f(0) = 0,\ f'(0) = 1,\ \theta(0) = 1,\ \phi(0) = 1\ at\ \eta = 0$ $f(1) = \frac{S}{2},\ f''(1) = 0,\ \theta'(1) = 0,\ \phi'(1) = 0\ at\ \eta = 1$
$\boldsymbol{X_4 + k_1X_1 + k_5X_5 + k_7X_7}$	Does not satisfy continuity equation
$\boldsymbol{X_4 + k_1X_1 + k_5X_5 + k_8X_8}$	Does not satisfy continuity equation
$\boldsymbol{X_4 + k_3X_3 + k_6X_6 + k_7X_7}$	$f''' + \beta^2\left[-ff'' + f'^2 - (Ma - S)f' + \frac{1}{2}Sf''\right] = 0$ $Pr^{-1}\,\theta'' + \gamma\left(-f\theta' + \frac{\eta S}{2}\theta' + f'\theta + \frac{k_6 - 1}{k_7}S\theta\right) = 0$

	$Sc^{-1}\,\phi'' + \gamma\left(-f\phi' + \frac{\eta S}{2}\phi' + f' + \frac{k_6 - k_3}{k_7}S\right) = 0$ **B.C:** $f(0) = 0,\ f'(0) = 1,\ \theta(0) = 1,\ \phi(0) = 1\ at\ \eta = 0$ $f(1) = \frac{S}{2},\ f''(1) = 0,\ \theta'(1) = 0,\ \phi'(1) = 0\ at\ \eta = 1$
$\boldsymbol{X_4 + k_3 X_3 + k_6 X_6}$	$f''' + \beta^2\left[-ff'' + f'^2 - (Ma - S)f' + \frac{1}{2}Sf''\right] = 0$ $Pr^{-1}\,\theta'' + \gamma\left(-f\theta' + \frac{\eta S}{2}\theta' + \frac{1}{k_6}f'\theta - S\theta\right) = 0$ $Sc^{-1}\,\phi'' + \gamma\left(-f\phi' + \frac{\eta S}{2}\phi' + \frac{k_3}{k_6}f' - S\right) = 0$ **B.C:** $f(0) = 0,\ f'(0) = 1,\ \theta(0) = 1,\ \phi(0) = 1\ at\ \eta = 0$ $f(1) = \frac{S}{2},\ f''(1) = 0,\ \theta'(1) = 0,\ \phi'(1) = 0\ at\ \eta = 1$
$\boldsymbol{X_4 + k_1 X_1 + k_3 X_3 + k_7 X_7}$	Does not satisfy continuity equation
$\boldsymbol{X_4 + k_1 X_1 + k_3 X_3 + k_8 X_8}$	Does not satisfy continuity equation
$\boldsymbol{X_5 + k_2 X_2 + k_6 X_6 + k_7 X_7}$	$f''' + \beta^2\left[-ff'' + f'^2 - (Ma - S)f' + \frac{1}{2}Sf''\right] = 0$ $Pr^{-1}\,\theta'' + \gamma\left(-f\theta' + \frac{\eta S}{2}\theta' + f' - \frac{k_2 - k_6}{k_7}S\right) = 0$ $Sc^{-1}\,\phi'' + \gamma\left(-f\phi' + \frac{\eta S}{2}\phi' + f'\phi + \frac{k_6 - 1}{k_7}S\phi\right) = 0$ **B.C:** $f(0) = 0,\ f'(0) = 1,\ \theta(0) = 1,\ \phi(0) = 1\ at\ \eta = 0$ $f(1) = \frac{S}{2},\ f''(1) = 0,\ \theta'(1) = 0,\ \phi'(1) = 0\ at\ \eta = 1$
$\boldsymbol{X_5 + k_2 X_2 + k_6 X_6}$	$f''' + \beta^2\left[-ff'' + f'^2 - (Ma - S)f' + \frac{1}{2}Sf''\right] = 0$ $Pr^{-1}\,\theta'' + \gamma\left(-f\theta' + \frac{\eta S}{2}\theta' + \frac{k_2}{k_6}f' - S\right) = 0$ $Sc^{-1}\,\phi'' + \gamma\left(-f\phi' + \frac{\eta S}{2}\phi' + \frac{1}{k_6}f'\phi - S\phi\right) = 0$ **B.C:** $f(0) = 0,\ f'(0) = 1,\ \theta(0) = 1,\ \phi(0) = 1\ at\ \eta = 0$ $f(1) = \frac{S}{2},\ f''(1) = 0,\ \theta'(1) = 0,\ \phi'(1) = 0\ at\ \eta = 1$
$\boldsymbol{X_5 + k_1 X_1 + k_2 X_2 + k_7 X_7}$	Does not satisfy continuity equation
$\boldsymbol{X_5 + k_1 X_1 + k_2 X_2 + k_8 X_8}$	Does not satisfy continuity equation
$\boldsymbol{X_7 + k_6 X_6 + k_2 X_2 + k_3 X_3}$	$f''' + \beta^2\left[-ff'' + f'^2 - (Ma - S)f' + \frac{1}{2}Sf''\right] = 0$ $Pr^{-1}\,\theta'' + \gamma\left(-f\theta' + \frac{\eta S}{2}\theta' + f' + (k_6 - k_2)S\right) = 0$ $Sc^{-1}\,\phi'' + \gamma\left(-f\phi' + \frac{\eta S}{2}\phi' + f' + (k_6 - k_3)S\right) = 0$ **B.C:** $f(0) = 0,\ f'(0) = 1,\ \theta(0) = 1,\ \phi(0) = 1\ at\ \eta = 0$

	$f(1)=\frac{S}{2},\ f''(1)=0,\ \theta'(1)=0,\ \phi'(1)=0\ \ at\ \ \eta=1$
$\boldsymbol{X_6+k_2X_2+k_3X_3}$	$f'''+\beta^2\left[-ff''+f'^2-(Ma-S)f'+\frac{1}{2}Sf''\right]=0$ $Pr^{-1}\,\theta''+\gamma\left(-f\theta'+\frac{\eta S}{2}\theta'+\ k_2f'-S\ \right)=0$ $Sc^{-1}\,\phi''+\gamma\left(-f\phi'+\frac{\eta S}{2}\phi'+\ k_3f'-S\ \right)=0$ **B.C:** $f(0)=0,\ f'(0)=1,\ \theta(0)=1,\ \phi(0)=1\ \ at\ \ \eta=0$ $f(1)=\frac{S}{2},\ f''(1)=0,\ \theta'(1)=0,\ \phi'(1)=0\ \ at\ \ \eta=1$
$\boldsymbol{X_7+k_1X_1+k_2X_2+k_3X_3}$	Does not satisfy the continuity equation
$\boldsymbol{X_3+k_1X_1+k_2X_2+k_8X_8}$	Does not satisfy the continuity equation
$\boldsymbol{X_4+k_6X_6+k_7X_7}$	$f'''+\beta^2\left[-ff''+f'^2-(Ma-S)f'+\frac{1}{2}Sf''\right]=0$ $Pr^{-1}\,\theta''+\gamma\left(-f\theta'+\frac{\eta S}{2}\theta'+f'\theta+\ \frac{k_6-1}{k_7}S\theta\ \right)=0$ $Sc^{-1}\,\phi''+\gamma\left(-f\phi'+\frac{\eta S}{2}\phi'+f'\phi+\ \frac{k_6}{k_7}S\phi\ \right)=0$ **B.C:** $f(0)=0,\ f'(0)=1,\ \theta(0)=1,\ \phi(0)=1\ \ at\ \ \eta=0$ $f(1)=\frac{S}{2},\ f''(1)=0,\ \theta'(1)=0,\ \phi'(1)=0\ \ at\ \ \eta=1$
$\boldsymbol{X_3+k_4X_4+k_6X_6}$	$f'''+\beta^2\left[-ff''+f'^2-(Ma-S)f'+\frac{1}{2}Sf''\right]=0$ $Pr^{-1}\,\theta''+\gamma\left(-f\theta'+\frac{\eta S}{2}\theta'+\frac{k_4}{k_6}f'\theta-\ S\theta\ \right)=0$ $Sc^{-1}\,\phi''+\gamma\left(-f\phi'+\frac{\eta S}{2}\phi'+\frac{1}{k_6}f'-S\ \right)=0$ **B.C:** $f(0)=0,\ f'(0)=1,\ \theta(0)=1,\ \phi(0)=1\ \ at\ \ \eta=0$ $f(1)=\frac{S}{2},\ f''(1)=0,\ \theta'(1)=0,\ \phi'(1)=0\ \ at\ \ \eta=1$
$\boldsymbol{X_2+k_5X_5+k_6X_6+k_7X_7}$	$f'''+\beta^2\left[-ff''+f'^2-(Ma-S)f'+\frac{1}{2}Sf''\right]=0$ $Pr^{-1}\,\theta''+\gamma\left(-f\theta'+\frac{\eta S}{2}\theta'+f'+\ \frac{k_6-1}{k_7}S\ \right)=0$ $Sc^{-1}\,\phi''+\gamma\left(-f\phi'+\frac{\eta S}{2}\phi'+f'\phi+\ \frac{k_6-k_5}{k_7}S\phi\ \right)=0$ **B.C:** $f(0)=0,\ f'(0)=1,\ \theta(0)=1,\ \phi(0)=1\ \ at\ \ \eta=0$ $f(1)=\frac{S}{2},\ f''(1)=0,\ \theta'(1)=0,\ \phi'(1)=0\ \ at\ \ \eta=1$
$\boldsymbol{X_2+k_5X_5+k_6X_6}$	$f'''+\beta^2\left[-ff''+f'^2-(Ma-S)f'+\frac{1}{2}Sf''\right]=0$ $Pr^{-1}\,\theta''+\gamma\left(-f\theta'+\frac{\eta S}{2}\theta'+\frac{1}{k_6}f'-\ S\ \right)=0$ $Sc^{-1}\,\phi''+\gamma\left(-f\phi'+\frac{\eta S}{2}\phi'+\frac{k_5}{k_6}f'\phi-\ S\phi\ \right)=0$ **B.C:** $f(0)=0,\ f'(0)=1,\ \theta(0)=1,\ \phi(0)=1\ \ at\ \ \eta=0$

	$f(1)=\frac{S}{2},\ f''(1)=0,\ \theta'(1)=0,\ \phi'(1)=0\ \ at\ \ \eta=1$
$\boldsymbol{X_2+k_3X_3+k_6X_6+k_7X_7}$	$f'''+\beta^2\left[-ff''+f'^2-(Ma-S)f'+\frac{1}{2}Sf''\right]=0$ $Pr^{-1}\,\theta''+\gamma\left(-f\theta'+\frac{\eta S}{2}\theta'+f'+\frac{k_6-1}{k_7}S\right)=0$ $Sc^{-1}\,\phi''+\gamma\left(-f\phi'+\frac{\eta S}{2}\phi'+f'+\frac{k_6-k_3}{k_7}S\right)=0$ **B.C:** $f(0)=0,\ f'(0)=1,\ \theta(0)=1,\ \phi(0)=1\ \ at\ \ \eta=0$ $f(1)=\frac{S}{2},\ f''(1)=0,\ \theta'(1)=0,\ \phi'(1)=0\ \ at\ \ \eta=1$
$\boldsymbol{X_2+k_3X_3+k_6X_6}$	$f'''+\beta^2\left[-ff''+f'^2-(Ma-S)f'+\frac{1}{2}Sf''\right]=0$ $Pr^{-1}\,\theta''+\gamma\left(-f\theta'+\frac{\eta S}{2}\theta'+\frac{1}{k_6}f'-S\right)=0$ $Sc^{-1}\,\phi''+\gamma\left(-f\phi'+\frac{\eta S}{2}\phi'+\frac{k_3}{k_6}f'-S\right)=0$ **B.C:** $f(0)=0,\ f'(0)=1,\ \theta(0)=1,\ \phi(0)=1\ \ at\ \ \eta=0$ $f(1)=\frac{S}{2},\ f''(1)=0,\ \theta'(1)=0,\ \phi'(1)=0\ \ at\ \ \eta=1$

Observations about the optimal system:

- The momentum equation is the same for all linear combinations of the Lie symmetries, and hence the transformation of u.
- In the energy and concentration equation, only the velocity and unsteadiness terms i.e. $f'\theta$ and $S\theta$ get affected by the linear combination of the Lie symmetries.
- In the transformation of T and C, either time t has the coefficient of symmetries in power or distance x, but never the both e.g. $T=xt^{\frac{1}{k_6}}\,\theta$ or $T=x^{\frac{1}{k_6}}\,t\,\theta$.
- When the symmetries X_6 and X_7 are used in the linear combination, the coefficients of the symmetries appear in the power of t and affect the unsteadiness term $S\theta$.
- When only X_6 is used in the linear combination, the coefficients of the symmetries appear in the power of x and affect the velocity term $f'\theta$.
- When only X_7 is used, the transformations do not satisfy the continuity equations.
- When the scaling symmetries of T and C are used, the velocity and the unsteadiness term have

the dependent variable $(\theta,\ \phi)$ e.g. $f'\theta$ and $S\theta$.

- When the translating symmetries of C & T are used, the velocity and the unsteadiness terms do not have the dependent variable $(\theta,\ \phi)$ e.g. f' and S.
- Based on these observations, the above optimal system can be divided into the following categories.
    - Linearly-space dependent Symmetries (transformations has x with power 1)
    - Linearly-time dependent Symmetries (transformations has t with power 1)

- *Linearly-space dependent symmetries:*

The general form of this group can be expressed as

$$A_iX_i + A_jX_j + A_6X_6 + A_7X_7\ , \tag{3.67}$$

where $i \in \{2,4\}$ & $j \in \{3,5\}$. A represents the coefficients of the symmetry.
This group leads to the reduction of energy and concentration equations which have the following forms

$$Pr^{-1}\,\theta'' + \gamma\left(-f\theta' + \frac{\eta S}{2}\theta' + f'\theta + \frac{A_6 - A_i}{A_7}S\theta\right) = 0 \quad if\ i = 4\ , \tag{3.68}$$

$$Sc^{-1}\,\phi'' + \gamma\left(-f\phi' + \frac{\eta S}{2}\phi' + f'\phi + \frac{A_6 - A_j}{A_7}S\phi\right) = 0, \quad if\ j = 5\ , \tag{3.69}$$

If $i = 2$ or $j = 3$ (means translational symmetries of T and C), then velocity and unsteadiness terms do not have the dependent variables. i.e.

$$Pr^{-1}\,\theta'' + \gamma\left(-f\theta' + \frac{\eta S}{2}\theta' + f' + \frac{A_6 - A_i}{A_7}S\right) = 0, \quad if\ i = 2 \tag{3.70}$$

$$Sc^{-1}\,\phi'' + \gamma\left(-f\phi' + \frac{\eta S}{2}\phi' + f' + \frac{A_6 - A_j}{A_7}S\right), \quad if\ j = 3 \tag{3.71}$$

- *Linearly-time dependent symmetries:*

The general form of this group can be expressed as

$$A_i X_i + A_j X_j + A_6 X_6 \,, \tag{3.72}$$

where $i \in \{2,4\}$ & $j \in \{3,5\}$.
This group leads to the reduction of energy and concentration equations which have the following forms

$$Pr^{-1}\,\theta'' + \gamma\left(-f\theta' + \frac{\eta S}{2}\theta' + \frac{A_i}{A_6}f'\theta - S\theta\right) = 0 \quad if\ i = 4\,, \tag{3.73}$$

$$Sc^{-1}\,\phi'' + \gamma\left(-f\phi' + \frac{\eta S}{2}\phi' + \frac{A_j}{A_6}f'\phi - S\phi\right) = 0 \quad if\ j = 5\ . \tag{3.74}$$

If $i = 2$ or $j = 3$ (means translational symmetries of T and C), then velocity and unsteadiness terms do not have the dependent variables. i.e.

$$Pr^{-1}\,\theta'' + \gamma\left(-f\theta' + \frac{\eta S}{2}\theta' + \frac{A_i}{A_6}f' - S\right) = 0 \quad if\ i = 2\,, \tag{3.75}$$

$$Sc^{-1}\,\phi'' + \gamma\left(-f\phi' + \frac{\eta S}{2}\phi' + \frac{A_j}{A_6}f' - S\right) = 0,\ \ if\ j = 3\,. \tag{3.76}$$

3.3 Lie Symmetry Analysis of Unsteady Flow over a Stretching Surface in the Presence of Thermocapillarity, Internal Heat Source/Sink Variable Magnetic Field

Lie point symmetry generators along with their first extensions for the governing equations (2.21 - 2.23) while considering the form of Q given in eq (2.24) and $U_s = \frac{bx}{\alpha t}$ are,

$$\boldsymbol{X_1} = \frac{\partial}{\partial x}\,, \tag{3.77}$$

$$\boldsymbol{X}_2 = x\frac{\partial}{\partial x} + u\frac{\partial}{\partial u} + u_t\frac{\partial}{\partial u_t} - T_x\frac{\partial}{\partial T_x} - v_x\frac{\partial}{\partial v_x} + u_y\frac{\partial}{\partial u_y}, \quad 3.78$$

$$\boldsymbol{X}_3 = T\frac{\partial}{\partial T} + T_t\frac{\partial}{\partial T_t} + T_x\frac{\partial}{\partial T_x} + T_y\frac{\partial}{\partial T_y}, \quad 3.79$$

$$\boldsymbol{X}_4 = t\frac{\partial}{\partial t} + \frac{y}{2}\frac{\partial}{\partial y} - u\frac{\partial}{\partial u} - \frac{v}{2}\frac{\partial}{\partial v} - T_t\frac{\partial}{\partial T_t} - 2u_t\frac{\partial}{\partial u_t} - \frac{3}{2}v_t\frac{\partial}{\partial v_t} - u_x\frac{\partial}{\partial u_x} - \frac{1}{2}v_x\frac{\partial}{\partial v_x} - \frac{1}{2}T_y\frac{\partial}{\partial T_y} - \frac{3}{2}u_y\frac{\partial}{\partial u_y} - v_y\frac{\partial}{\partial v_y}, \quad 3.80$$

$$\boldsymbol{X}_5 = t^{\frac{G^*b\kappa}{\alpha\rho}}\frac{\partial}{\partial T} + \frac{t^{\frac{G^*b\kappa}{\alpha\rho}}}{\boldsymbol{\nu}\alpha t}G^*b\kappa\frac{\partial}{\partial T_t}, \quad 3.81$$

$$\boldsymbol{X}_6 = t^{1-\frac{\sigma_e{B_o}^2}{\alpha\rho}}\frac{\partial}{\partial x} + \left(\frac{\alpha\rho-\sigma_e{B_o}^2}{\alpha t\rho}\right)t^{1-\frac{\sigma_e{B_o}^2}{\alpha\rho}}\frac{\partial}{\partial u} - \left(\frac{\alpha\rho-\sigma_e{B_o}^2}{\alpha t\rho}\right)t^{1-\frac{\sigma_e{B_o}^2}{\alpha\rho}}T_x\frac{\partial}{\partial T_t} - \left(\frac{\alpha\rho-\sigma_e{B_o}^2}{\alpha t\rho}\right)\left(\frac{\alpha\rho t u_x+\sigma_e{B_o}^2}{\alpha t\rho}\right)t^{1-\frac{\sigma_e{B_o}^2}{\alpha\rho}}\frac{\partial}{\partial u_t} - \left(\frac{\alpha\rho-\sigma_e{B_o}^2}{\alpha t\rho}\right)t^{1-\frac{\sigma_e{B_o}^2}{\alpha\rho}}v_x\frac{\partial}{\partial v_t}. \quad 3.82$$

Our criterion for deriving the system invariants is to use only those Lie symmetry generators or a linear combination of the generators that leave all the boundary conditions invariant and render U_s and T_s a function of both time and distance. Unlike the previous case, here only the following three linear combinations meet this criterion.

$$\boldsymbol{Y}_1 = \boldsymbol{X}_2 + 2\,\boldsymbol{X}_3\,, \quad 3.83$$

$$\boldsymbol{Y}_2 = \boldsymbol{X}_3 - \frac{2}{3}\,\boldsymbol{X}_4\,, \quad 3.84$$

$$\boldsymbol{Y}_3 = \boldsymbol{X}_2 + \frac{4}{3}\,\boldsymbol{X}_4\,. \quad 3.85$$

Adapting the same procedure used in section (3.1), the generators (3.83 - 3.85) are used to reduce the governing PDEs (2.21 - 2.23) to a system of ODEs. It has been observed that all three generators generate the same similarity transformations and hence, reduce the governing PDEs to the same system of ODEs.

The deduced similarity transformations are,

$$y = \beta\sqrt{\frac{\alpha\boldsymbol{\nu}t}{b}}\eta\,,\ \ u = \frac{-bx}{\alpha t}f'(\eta),\ \ v = \beta\sqrt{\frac{\boldsymbol{\nu}b}{\alpha t}}f(\eta)\,,\ \ T = \frac{x^2}{t^{\frac{3}{2}}}\theta(\eta)\ , \quad 3.86$$

Here, T represents the temperature i.e. $T_o - T$.

The reduced system of ODEs is,

$$f''' + \gamma\left(-ff'' + f'^2 - (Ma - S)f' + \frac{\eta S}{2}f''\right) = 0 \quad 3.87$$

$$\theta'' + \gamma Pr\left(-f\theta' + \frac{\eta S}{2}\theta' + 2f'\theta + \frac{3}{2}S\theta + \frac{G^*}{Pr}\theta\right) = 0 \quad 3.88$$

subject to the boundary conditions

$$f(0) = 0,\ f'(0) = 1,\ \theta(0) = 1\ \ at\ \ \eta = 0\,, \tag{3.89}$$

and

$$f(1) = \frac{S}{2},\ f''(1) = 2S^{3/2}\mathrm{M}\,\theta(1),\ \theta'(1) = 0\ \ \ at\ \ \eta = 1, \tag{3.90}$$

where, $\mathrm{M} = \frac{\sigma_o \beta\sqrt{\nu}}{\mu}$ is the thermocapillarity parameter which appears in the thermocapillarity driven flows. The prime symbol denotes differentiation with respect to the similarity variable η. The equations (3.87 - 3.88) contain several parameters, including the dimensionless film thickness $\gamma = \beta^2$, the magnetic parameter $Ma = \frac{\sigma_e {B_o}^2}{b\rho}$, the unsteadiness measure $S = \frac{\alpha}{b}$, and the Prandtl number $\mathrm{Pr} = \frac{\boldsymbol{\nu}}{\kappa}$.

The specific forms of the stretching surface velocity and temperature are determined to be

$$U_s(x,t) = \frac{xC_1}{t}\,, \tag{3.91}$$

$$T_s(x,t) = T_o - \frac{x^2 C_2}{t^{3/2}}\,, \tag{3.92}$$

whereas the dimensionless film thickness is given by

$$h(t) = C_3\sqrt{t}\,. \tag{3.93}$$

The values of the arbitrary constants are determined to be

$$C_1 = -\frac{b}{\alpha}\,,\ C_2 = 1\,,\ C_3 = \beta\sqrt{\frac{\alpha\nu}{b}}\,. \tag{3.94}$$

The invariants of the governing PDEs are given in Table 4, the reduced PDEs are given in Table 5, while the invariants of the reduced PDEs and double-reduced system are given in Table 6.

Table 4: Invariants of the governing PDEs

Generators	Invariants
$\boldsymbol{Y}_1 = \boldsymbol{X}_2 + 2\,\boldsymbol{X}_3$	$\left\{t, y, \frac{T}{x^2}, \frac{u}{x}, v\right\}$
$\boldsymbol{Y}_2 = \boldsymbol{X}_3 - \frac{2}{3}\,\boldsymbol{X}_4$	$\left\{x, \frac{y}{\sqrt{t}}, Tt^{\frac{3}{2}}, ut, v\sqrt{t}\right\}$
$\boldsymbol{Y}_3 = \boldsymbol{X}_2 + \frac{4}{3}\,\boldsymbol{X}_4$	$\left\{\frac{x}{t^{\frac{3}{4}}}, \frac{y}{\sqrt{t}}, T, ut^{\frac{1}{4}}, v\sqrt{t}\right\}$

Table 5: First reduction of the governing PDEs

Generators	Reduced System
$\boldsymbol{Y}_1 = \boldsymbol{X}_2 + 2\,\boldsymbol{X}_3$	$R + W_{z_2} = 0$, $R_{z_1} + R^2 + WR_{z_2} - \boldsymbol{\nu} R_{z_2 z_2} + \frac{\sigma_e {B_o}^2}{\alpha \rho z_1} R = 0$, $Q_{z_1} + 2RQ + WQ_{z_2} - \kappa Q_{z_2 z_2} - \frac{\kappa b G^*}{\alpha \boldsymbol{\nu} z_1} Q = 0$, *B.C:* $R = U_s(z_1), \quad W = 0, \quad Q = T_s(z_1)$ at $z_2 = 0$, $R_{z_2} = -\frac{2\sigma_o \gamma}{\mu} Q, \quad Q_{z_2} = 0, \quad W = \frac{dh}{dz_1}$ at $z_2 = h(z_1)$.
$\boldsymbol{Y}_2 = \boldsymbol{X}_3 - \frac{2}{3}\,\boldsymbol{X}_4$	$R_{z_1} + W_{z_2} = 0$, $-\frac{z_2}{2} R_{z_2} + RR_{z_1} - R + WR_{z_2} - \boldsymbol{\nu} R_{z_2 z_2} + \frac{\sigma_e {B_o}^2}{\alpha \rho} R = 0$, $-\frac{z_2}{2} Q_{z_2} + RQ_{z_1} - \frac{3}{2} Q + WQ_{z_2} - \kappa Q_{z_2 z_2} - \frac{\kappa b G^*}{\alpha \boldsymbol{\nu}} Q = 0$, *B.C:* $R = F_1(z_1), \quad W = 0, \quad Q = F_2(z_1)$ at $z_2 = 0$, $R_{z_2} = -\frac{\sigma_o \gamma}{\mu} Q_{z_1}, \quad Q_{z_2} = 0, \quad W = \frac{C_3}{2}$ at $z_2 = C_3$.
$\boldsymbol{Y}_3 = \boldsymbol{X}_2 + \frac{4}{3}\,\boldsymbol{X}_4$	$R_{z_1} + W_{z_2} = 0$, $-\frac{z_2}{2} R_{z_2} - \frac{3z_1}{4} R_{z_1} + RR_{z_1} - \frac{R}{4} + WR_{z_2} - \boldsymbol{\nu} R_{z_2 z_2} + \frac{\sigma_e {B_o}^2}{\alpha \rho} R = 0$,

	$-\frac{z_2}{2}Q_{z_2}+RQ_{z_1}-\frac{3}{4}z_1Q_{z_1}+WQ_{z_2}-\kappa Q_{z_2z_2}-\frac{\kappa bG^*}{\alpha\boldsymbol{\nu}}Q=0$, *B.C:* $R=F_1(z_1),\quad W=0,\quad Q=F_2(z_1)$ at $z_2=0$, $R_{z_2}=-\frac{\sigma_o\gamma}{\mu}Q_{z_1},\quad Q_{z_2}=0,\quad W=\frac{C_1}{2}$ at $z_2=C_3$.

Table 6: Invariants of reduced PDEs and double-reduced system

Generators	**Invariants**	**Double-reduced system**
$\boldsymbol{Y}_1=\boldsymbol{X}_2+2\,\boldsymbol{X}_3$	$\left\{\frac{z_2}{\sqrt{z_1}},Qz_1^{\frac{3}{2}},Rz_1,W\sqrt{z_1}\right\}$	$g_2+{g_3}'=0$, $-\frac{\chi}{2}g_2-g_2+{g_2}^2+g_3{g_2}'-\boldsymbol{\nu}{g_2}''+\frac{\sigma_e{B_o}^2}{\alpha\rho}g_2=0$, $-\frac{\chi}{2}g_1-\frac{3}{2}g_1+2g_2g_1+g_3{g_1}'-\kappa{g_1}''-\frac{\kappa bG^*}{\alpha\boldsymbol{\nu}}g_1=0$, **B.C:** $g_2=C_1,\ g_3=0,\ g_1=C_2$ at $\chi=0$, ${g_2}'=-2\frac{\sigma_o\gamma}{\mu}g_1,\ {g_1}'=0,\ g_3=\frac{C_3}{2}$ at $=C_3$.
$\boldsymbol{Y}_2=\boldsymbol{X}_3-\frac{2}{3}\boldsymbol{X}_4$	$\left\{z_2,\frac{Q}{z_1^2},\frac{R}{z_1},W\right\}$	
$\boldsymbol{Y}_3=\boldsymbol{X}_2+\frac{4}{3}\boldsymbol{X}_4$	$\left\{z_2,\frac{Q}{z_1^2},\frac{R}{z_1},W\right\}$	

Chapter 4

4. Solution Methods

In this study, two analytical solution methods are used to obtain the solution i.e. Homotopy Analysis Method (HAM) and Homotopy Perturbation Method (HPM). The solutions for momentum, heat, and mass transfer in the presence of a variable magnetic field are obtained using Homotopy Analysis Method (eqs 3.48 - 3.52 and eqs in Table 3) while the solutions of flow and heat transfer in the presence of thermocapillarity, internal heat source/sink and variable magnetic field (eqs 3.87 - 3.90) are obtained using Homotopy Perturbation Method (HPM).

4.1 Homotopy Analysis Method

Let $f_0(\eta)$, γ_o, $\theta_0(\eta)$ and $\phi_0(\eta)$ denote an initial solution of $f(\eta)$, γ, $\theta(\eta)$ and $\phi(\eta)$ that satisfy the initial conditions and $q \in [0,1]$ denotes the so called embedding parameter. The main idea of HAM is based upon the continuous mapping of $f(\eta) \to F(\eta;q), \acute{\Gamma}(q) \to \gamma,\ \theta(\eta) \to \Theta(\eta;q)$ and $\phi(\eta) \to \varphi(\eta;q)$ such that as q varies from 0 to 1, $F(\eta;q)$, $\acute{\Gamma}(q)$, $\Theta(\eta;q)$ and $\varphi(\eta;q)$ vary from the initial solution $f_0(\eta),\ \gamma_0, \theta_0(\eta)$ and $\phi_0(\eta)$ to the exact solution $f(\eta), \gamma,\ \theta(\eta)$ and $\phi(\eta)$. This is possible by choosing a linear auxiliary operator with the property that

$$\mathcal{L}\, g = 0 \quad when \quad g = 0\,, \tag{4.1}$$

where g is any arbitrary function.

To find the solution of eqs (3.48 - 3.52), HAM defines a family of equations called zero-order

deformation equations, given below

$$(1-q)\mathcal{L}_f[F(\eta;q)-f_0(\eta)] = q\hbar_f H_f(\eta)N_f\left[F(\eta;q),\acute{\Gamma}(q)\right], \quad 4.2$$

$$(1-q)\mathcal{L}_\theta[\Theta(\eta;q)-\theta_0(\eta)] = q\hbar_\theta H_\theta(\eta)N_\theta\left[F(\eta;q),\Theta(\eta;q),\acute{\Gamma}(q)\right], \quad 4.3$$

$$(1-q)\mathcal{L}_\phi[\varphi(\eta;q)-\phi_0(\eta)] = q\hbar_\phi H_\phi(\eta)N_\phi\left[F(\eta;q),\varphi(\eta;q),\acute{\Gamma}(q)\right], \quad 4.4$$

subject to the boundary conditions

$$F(0;q)=0,\ F'(0;q)=1,\ \Theta(0;q)=1,\ \varphi(0;q)=1, \quad 4.5$$

and

$$F(1;q)=\frac{S}{2},\ F''(1;q)=0,\ \Theta'(1;q)=0,\ \varphi'(1;q)=0\ . \quad 4.6$$

where $'$ represents differentiation w.r.t η, $\hbar$ is the non-zero auxiliary parameter, $H(\eta)$ is the non-zero auxiliary function while N denotes the non-linear operator defined as

$$N_f\left[F(\eta;q),\acute{\Gamma}(q)\right] = F''' + \acute{\Gamma}\left(-FF'' + F'^2 - (Ma-S)F' + \frac{\eta S}{2}F''\right) \quad 4.7$$

$$N_\theta\left[F(\eta;q),\Theta(\eta;q),\acute{\Gamma}(q)\right] = Pr^{-1}\Theta'' + \acute{\Gamma}\left(-F\Theta' + \frac{\eta S}{2}\Theta' + \left(F' - \frac{k_4-k_6}{k_7}S\right)\Theta\right) \quad 4.8$$

$$N_\phi\left[F(\eta;q),\varphi(\eta;q),\acute{\Gamma}(q)\right] = Pr^{-1}\varphi'' + \acute{\Gamma}\left(-F\varphi' + \frac{\eta S}{2}\varphi' + \left(F' - \frac{k_4-k_6}{k_7}S\right)\varphi\right) \quad 4.9$$

$F(\eta;q),\Theta(\eta;q),\varphi(\eta;q)$ and $\acute{\Gamma}(q)$ can be expanded into a power series of the embedding parameter q by using Taylor's theorem.

$$F(\eta;q) = F(\eta;0) + \sum_{m=1}^{+\infty}\frac{1}{m!}\frac{\partial^m F(\eta;q)}{\partial q^m}_{q=0} q^m \quad 4.10$$

$$\acute{\Gamma}(q) = \acute{\Gamma}(0) + \sum_{m=1}^{+\infty}\frac{1}{m!}\frac{\partial^m \acute{\Gamma}(q)}{\partial q^m}_{q=0} q^m \quad 4.11$$

$$\Theta(\eta;q) = \Theta(\eta;0) + \sum_{m=1}^{+\infty}\frac{1}{m!}\frac{\partial^m \Theta(\eta;q)}{\partial q^m}_{q=0} q^m \quad 4.12$$

$$\varphi(\eta;q) = \varphi(\eta;0) + \sum_{m=1}^{+\infty}\frac{1}{m!}\frac{\partial^m \varphi(\eta;q)}{\partial q^m}_{q=0} q^m \quad 4.13$$

Let

$$f_m(\eta) = \frac{1}{m!}\left.\frac{\partial^m F(\eta;q)}{\partial q^m}\right|_{q=0}, \quad \gamma_m = \frac{1}{m!}\left.\frac{\partial^m \acute{\Gamma}(q)}{\partial q^m}\right|_{q=0}, \tag{4.14}$$

$$\theta_m(\eta) = \frac{1}{m!}\left.\frac{\partial^m \Theta(\eta;q)}{\partial q^m}\right|_{q=0}, \ \phi_m(\eta) = \frac{1}{m!}\left.\frac{\partial^m \varphi(\eta;q)}{\partial q^m}\right|_{q=0}. \tag{4.15}$$

Thus, eqs (4.10 - 4.13) become

$$F(\eta;q) = f_0(\eta) + \sum_{m=1}^{+\infty} f_m(\eta)\, q^m\,, \tag{4.16}$$

$$\acute{\Gamma}(q) = \gamma_o + \sum_{m=1}^{+\infty} \gamma_m q^m\,, \tag{4.17}$$

$$\Theta(\eta;q) = \theta_0(\eta) + \sum_{m=1}^{+\infty} \theta_m(\eta) q^m\,, \tag{4.18}$$

$$\varphi(\eta;q) = \phi_0(\eta) + \sum_{m=1}^{+\infty} \phi_m(\eta) q^m\,, \tag{4.19}$$

where $F(\eta;0) = f_0(\eta), \acute{\Gamma}(0) = \gamma_o, \Theta(\eta;0) = \theta_0(\eta)$ and $\varphi(\eta;0) = \phi_0(\eta)$. If the auxiliary parameter $\hbar$, the auxiliary function $H(\eta)$, the initial approximation, and the linear operator $\mathcal{L}$ are chosen properly then at $q = 1$, the series (3.26) converges to the exact solutions i.e.

$$F(\eta;1) = f(\eta), \quad \acute{\Gamma}(1) = \gamma, \quad \Theta(\eta;1) = \theta(\eta), \quad \varphi(\eta;1) = \phi(\eta). \tag{4.20}$$

Thus, we obtain

$$f(\eta) = f_0(\eta) + \sum_{m=1}^{+\infty} f_m(\eta)\,, \ \gamma = \gamma_o + \sum_{m=1}^{+\infty} \gamma_m\,, \tag{4.21}$$

$$\theta(\eta) = \theta_0(\eta) + \sum_{m=1}^{+\infty} \theta_m(\eta)\,, \quad \phi(\eta) = \phi_0(\eta) + \sum_{m=1}^{+\infty} \phi_m(\eta) \tag{4.22}$$

In the current study, the power series of η is chosen as a base function to express the solution.

$$\{\eta^m \mid m = 0,1,2 \ldots.\}\,. \tag{4.23}$$

Then,

$$f_0(\eta) = \eta + \tfrac{3S-6}{4}\eta^2 + \tfrac{2-S}{4}\eta^3, \quad \theta_0(\eta) = 1\,, \ \phi_0(\eta) = 1, \tag{4.24}$$

become the obvious choice for the initial solution, obtained by utilizing the boundary conditions

$$f_0(0) = 0, \ f_0'(0) = 1, \ \theta_0(0) = 1, \ \phi_0(0) = 1, \tag{4.25}$$

and

$$f_0(1) = \frac{S}{2},\ f_0''(1) = 0,\ \theta_0'(1) = 0,\ \phi_0'(1) = 0\,. \tag{4.26}$$

$\mathcal{L}_f = \frac{\partial^3}{\partial \eta^3}$, $\mathcal{L}_\theta = \frac{\partial^2}{\partial \eta^2}$ and $\mathcal{L}_\phi = \frac{\partial^2}{\partial \eta^2}$ are chosen as the linear operators. The value of auxiliary function $H(\eta) = 1$ is determined utilizing the rule of solution expression and the rule of coefficient ergodicity [45].

To derive $f_m(\eta)$, differentiate zero-order deformation equation m times with respect to q, then divide by $m!$ and finally set $q = 0$. The generalized higher-order deformation equation can be written as

$$\mathcal{L}_f[f_m(\eta) - x_m f_{m-1}(\eta)] = \hbar_f H_f(\eta) R_{f,m}(\eta)\,, \tag{4.27}$$

$$\mathcal{L}_\theta[\theta_m(\eta) - x_m \theta_{m-1}(\eta)] = \hbar_\theta H_\theta(\eta) R_{\theta,m}(\eta)\,, \tag{4.28}$$

$$\mathcal{L}_\phi[\phi_m(\eta) - x_m \phi_{m-1}(\eta)] = \hbar_\phi H_\phi(\eta) R_{\phi,m}(\eta)\,, \tag{4.29}$$

subjected to the boundary conditions

$$f_m(0) = 0,\ f_m'(0) = 0,\ \theta_m(0) = 0,\ \phi_m(0) = 0, \tag{4.30}$$

and

$$f_m(1) = 0,\ f_m''(1) = 0,\ \theta_m'(1) = 0,\ \phi_m'(1) = 0\,, \tag{4.31}$$

for $m \geq 1$, where

$$R_{f,m}(\eta) = f_m'''(\eta) + \sum_{n=0}^{m-1} \gamma_{m-1-n} \sum_{i=0}^{n} (-f_i f''_{n-i} + f_i' f'_{n-i}) + \sum_{n=0}^{m-1} \gamma_n \left(-(Ma - S) f'_{m-1-n} + \frac{S\eta}{2} f''_{m-1-n}\right), \tag{4.32}$$

$$R_{\theta,m}(\eta) = Pr^{-1} \theta_m''(\eta) + \sum_{n=0}^{m-1} \gamma_{m-1-n} \sum_{i=0}^{n} (-f_i \theta'_{n-i} + f'_{n-i} \theta_i) + \sum_{n=0}^{m-1} \gamma_n \left(-\left(\frac{k_4 - k_6}{k_7}\right) S\theta_{m-1-n} + \frac{S\eta}{2} \theta'_{m-1-n}\right), \tag{4.33}$$

$$R_{\phi,m}(\eta) = Sc^{-1} \phi_m''(\eta) + \sum_{n=0}^{m-1} \gamma_{m-1-n} \sum_{i=0}^{n} (-f_i \phi'_{n-i} + f'_{n-i} \phi_i) + \sum_{n=0}^{m-1} \gamma_n \left(-\left(\frac{k_5 - k_6}{k_7}\right) S\phi_{m-1-n} + \frac{S\eta}{2} \phi'_{m-1-n}\right), \tag{4.34}$$

and

$$x_m = \begin{cases} 1, & m > 1 \\ 0, & m = 1 \end{cases}. \quad 4.35$$

The solution of eqs (4.27 - 4.31) is given by

$$f_m(\eta) = x_m f_{m-1}(\eta) + \int_0^\eta \int_0^\eta \int_0^\eta \hbar_f H_f(\eta) R_{f,m}(\eta)\, d\eta d\eta d\eta + a_1 + a_2\eta + a_3\eta^2, \quad 4.36$$

$$\theta_m(\eta) = x_m \theta_{m-1}(\eta) + \int_0^\eta \int_0^\eta \hbar_\theta H_\theta(\eta) R_{\theta,m}(\eta)\, d\eta d\eta + a_4 + a_5\eta\,, \quad 4.37$$

$$\phi_m(\eta) = x_m \phi_{m-1}(\eta) + \int_0^\eta \int_0^\eta \hbar_\phi H_\phi(\eta) R_{\phi,m}(\eta)\, d\eta d\eta + a_6 + a_7\eta\,, \quad 4.38$$

where a_1, a_2 .. a_7 are the integration constants. It should be noted that $R_{f,m}(\eta)$ contains the unknown γ_{m-1}that must be calculated along with the integration constants using the boundary conditions (4.30 - 4.31).

Simplifying (4.36 - 4.38) for $m = 1,2\ldots\ p$, we obtain an analytical series solution of pth-order for $f(\eta)$, γ, $\theta(\eta)$ and $\phi(\eta)$.

Using a similar procedure, the solutions for the optimal system are obtained. In the current study, solutions with the accuracy of 10^{-9} are obtained.

4.2 Homotopy Perturbation Method

The Homotopy Perturbation Method (HPM) is a powerful mathematical technique used to solve a wide range of linear and nonlinear ordinary/partial differential equations. It combines two mathematical concepts i.e. perturbation and homotopy. Perturbation refers to a technique for solving mathematical problems by introducing small changes to a known solution and then using those changes to derive a new solution while homotopy refers to a continuous transformation between two mathematical functions. Solutions developed with perturbation techniques are so sensitive w.r.t to the small parameter that a minute change in the small parameter alters the results. Moreover, a majority of the nonlinear differential equations do not have small parameters which restricts the application of perturbation techniques.

Homotopy Perturbation Method (HPM) developed by He [46], couples the homotopy and perturbation technique. It eliminates the shortcomings of the perturbation techniques and takes full advantage of the traditional perturbation techniques. The basic idea of the Homotopy Perturbation Method (HPM) is presented below.

Consider a general differential equation

$$A(\varphi) - f(r) = 0, \quad r \in \Omega \tag{4.39}$$

subject to the boundary condition

$$B\left(\varphi, \frac{d\varphi}{dr}\right) = 0, \quad r \in \Gamma \tag{4.40}$$

where A is a general operator, φ is the dependent variable, r is the independent variable, $f(r)$ is the known analytic function, B is the boundary operator and Γ is the boundary of domain Ω.
The general operator can be decomposed into linear and non-linear operators, denoted by $\mathcal{L}$ and N respectively.

$$\mathcal{L}(\varphi) + N(\varphi) - f(r) = 0 \tag{4.41}$$

Using the homotopy technique [45], we construct a homotopy $U(r,p) : \Omega \times [0,1] \to \mathbb{R}$, which satisfies,

$$H(U,p) = (1-p)[\mathcal{L}(U) - \mathcal{L}(\Phi_o)] + p[\mathcal{L}(U) + N(U) - f(r)] = 0, \quad p \in [0,1] \tag{4.42}$$

where p is the embedding parameter (also known as an artificial parameter). Φ_o is the initial approximation of the solution which satisfies the given boundary conditions.
Eq (4.42) can be simplified to the form,

$$H(U,p) = \mathcal{L}(U) - \mathcal{L}(\Phi_o) + p\mathcal{L}(\Phi_o) + p[N(U) - f(r)] = 0, \quad p \in [0,1]\,. \tag{4.43}$$

By substituting $p = 0$ and $p = 1$ in above equation, we get the following equations, respectively.

$$H(U,0) = \mathcal{L}(U - \Phi_o) = 0\,, \tag{4.44}$$

and

$$H(U,1) = A(U) - f(r) = 0\,. \tag{4.45}$$

As p varies from 0 to 1, $U(r,p)$ varies from the initial approximation $\varphi_o(r)$ to the final solution $\varphi(r)$. This means that $\mathcal{L}(U - \Phi_o)$ and $A(U) - f(r)$ are homotopic to each other.
Since p a is a small parameter, so it can be expanded into a power series of p.

$$U = U_o + p^1 U_1 + p^2 U_2 \ldots \tag{4.46}$$

As $p \to 1$, we get an approximate solution for (4.39) i.e.

$$\varphi = U_o + U_1 + U_2 \ldots \quad 4.47$$

In the succeeding text, the above method is employed to find the solution of (3.87 - 3.90).

To this end, we construct homotopy for (3.87) and (3.88) which satisfy the following equations, respectively.

$$(1-p)[F'''(\eta) - f_o'''(\eta)] + p\left[F''' + \gamma\left(-FF'' + F'^2 - (Ma - S)F' + \frac{\eta S}{2}F''\right)\right] = 0 \quad 4.48$$

,

and

$$(1-p)[\vartheta''(\eta) - \theta_o''(\eta)] + p\left[\vartheta'' + \gamma Pr\left(-F\vartheta' + \frac{\eta S}{2}\vartheta' + 2F'\vartheta + \frac{3}{2}S\vartheta + \frac{G^*}{Pr}\vartheta\right)\right] = 0. \quad 4.49$$

Here, $F(\eta)$ and $\vartheta(\eta)$ denotes the approximate solution of $f(\eta)$ and $\theta(\eta)$, respectively. $f_o(\eta)$ and $\theta_o(\eta)$ are the initial approximations for $f(\eta)$ and $\theta(\eta)$, respectively. For this study, $f_o(\eta) = 0$ and $\theta_o(\eta) = 1$.

Now, perturb $F(\eta)$ and $\vartheta(\eta)$ in the power series of p.

$$F(\eta) = \sum_{m=0}^{M} F_m(\eta)\, p^m \ , \ \ \vartheta(\eta) = \sum_{m=0}^{M} \vartheta_m(\eta)\, p^m \quad 4.50$$

Here M represents the order of approximation. Substitute these equations in (4.48 - 4.49) and in the associated boundary conditions (3.88 - 3.89). By equating the terms with the same power of the parameter p, we get a system of linear ODEs.

p^0:

$F_o''' = 0, \quad \vartheta_o'' = 0$

$F_o(0) = 0, \quad F_o'(0) = 1, \quad F_o''(0) = \alpha_1,$

$\vartheta_o(0) = 1, \ \vartheta_o'(0) = \alpha_2$

p^1:

$F_1''' + \gamma\left(-F_0F_0'' + F_0'^2 - (Ma - S)F_0' + \frac{\eta S}{2}F_o''\right) = 0, \quad \vartheta_1'' + \gamma Pr\left(-F_0\,\vartheta_o' + \frac{\eta S}{2}\,\vartheta_o' + 2F_0'\,\vartheta_o + \frac{3}{2}S\,\vartheta_o + \frac{G^*}{Pr}\,\vartheta_o\right) = 0$

$F_1(0) = 0, \quad F_1'(0) = 0, \quad F_1''(0) = 0,$

$\vartheta_1(0) = 0, \quad \vartheta_1'(0) = 0$

p^2:

$F_2''' + \gamma\left(-F_0F_1'' - F_1F_0'' + 2F_0'F_1' - (Ma - S)F_1' + \frac{\eta S}{2}F_1''\right) = 0, \quad \vartheta_2'' + \gamma Pr\left(-F_0\,\vartheta_1' -$

$$F_1\,\vartheta_0{}' + \frac{\eta S}{2}\,\vartheta_1{}' + 2F_1{}'\,\vartheta_o + 2f_0{}'\,\vartheta_1 + \frac{3}{2}S\,\vartheta_1 + \frac{G^*}{Pr}\,\vartheta_1\Big) = 0$$

$$F_2(0) = 0, \quad F_2{}'(0) = 0, \quad F_2{}''(0) = 0,$$

$$\vartheta_2(0) = 0, \quad \vartheta_2{}'(0) = 0$$

and, so on.

By integration these linear differential equations, we get the values of the coefficients in eqs (4.50).

Now, setting $p = 1$ in eqs (4.50) results in the M^{th} order approximate solution for system (3.87 - 3.90), given by

$$f(\eta) = \lim_{p\to 1} F(\eta) = \sum_{m=0}^{M} F_m(\eta), \quad \text{and} \quad \theta(\eta) = \lim_{p\to 1} \vartheta(\eta) = \sum_{m=0}^{M} \vartheta_m(\eta)\,. \tag{4.51}$$

It should be noted that α_1, α_2 and γ are unknowns whose values are yet to be determined. These values can be determined using the outer boundary conditions (3.89) that have not been utilized yet i.e.

$$f(1) = \frac{1}{2}S, \quad f''(1) = 2S^{3/2}\mathrm{M}\theta(1), \quad \theta'(1) = 0. \tag{4.52}$$

In this study, we have obtained 15th-order approximations for both $f(\eta)$ and $\theta(\eta)$, which exhibit an accuracy of up to 10 decimal places.

Chapter 5

5. Results and Discussion

In this chapter, the results for all three cases i.e.

1. Analytic solutions for the system of ODEs comprising to unsteady flow over a stretching surface in the presence of a variable magnetic field. They are obtained from the reduction of flow model through

   - Generalized similarity transformations eqs (3.48 - 3.52)
   - Similarity transformations associated with 1-dimensional optimal system Table (3), and

2. Analytic solutions for the system of ODEs comprising to unsteady flow over a stretching surface in the presence of thermocapillarity, a variable magnetic field, and a heat source or sink eqs (3.87 - 3.90),

are presented and discussed.

5.1 HAM Analytic Solutions for Unsteady Flow over a Stretching Surface in the Presence of Variable Magnetic Field

5.1.1 Case 1 (a): System of ODEs obtained through Generalized Similarity Transformations

The effect of unsteadiness parameter S on the dimensionless film-thickness β, skin friction co-efficient $f''(0)$, Nusselt number $\theta'(0)$, Sherwood number $\phi'(0)$, dimensionless free-surface velocity $f''(1)$, temperature $\theta(1)$ and concentration $\phi(1)$ is presented in Table 7. It shows that as the unsteadiness term S increases the dimensionless film thickness β decreases which is in agreement with the result obtained in [10]. At the low stretching rate (higher values of S), the skin friction coefficient increases whereas the local Nusselt number and the Sherwood number both decrease. Due to this, the temperature and concentration of the free surface are low at the higher values of S.

Table 7: Variation of $\beta, f'(1), \theta(1), \phi(1), f''(0), \theta'(0)\ and\ \phi'(0)$ with S

S	β	$f'(1)$	$\theta(1)$	$\phi(1)$	$-f''(0)$	$-\theta'(0)$	$-\phi'(0)$
0.8	1.93005806	0.15059272	0.829934419	0.829934419	2.204067862	0.252026157	0.262509614
1	1.59899637	0.272005949	0.864342477	0.864342477	1.666681269	0.219440864	0.228570149
1.2	1.38487105	0.407844998	0.884523598	0.879716133	1.256078993	0.199529366	0.207844404

The lateral velocity $f'(\eta)$ profiles are presented in Figure 3 for the different values of S. At the sheet $\eta = 0$, the lateral velocity of the fluid is the same as that of the sheet U_s but it decreases as we move away from the sheet due to the viscous shearing. This reduction decreases for the higher values of the S because the skin friction coefficient decreases with the increase in S. The dimensionless temperature $\theta(\eta)$ profiles for different S are depicted in Figure 4 which shows that $\theta(\eta)$ starts from unity at the sheet ($\eta = 0$) and decreases monotonically with η. This implies that temperature T increases as we move away from the sheet. The behavior of $\phi(\eta)$ is similar, shown in Figure 5.

Figure 6 demonstrates the effect of the magnetic parameter Ma on the lateral velocity $f'(\eta)$. Increasing the value of the magnetic parameter Ma increases the hindrance to the lateral velocity near the sheet but as we move away from the sheet its effect is overcome by the momentum of the fluid in the lateral direction. The effect of Ma is more pronounced on the temperature $\theta(\eta)$ and concentration $\phi(\eta)$ field shown in Figure 7 and Figure 8 respectively. $\theta(\eta)$ and $\phi(\eta)$ approach towards unity as the magnetic parameter Ma increases which means that the temperature T and the concentration C approach T_s and C_s at the higher Ma values. This fact is also evident from the decreasing values of the gradients $\theta'(0)$ and $\phi'(0)$ shown in table 8. The table also shows that the

film thickness decreases with increasing the value Ma.

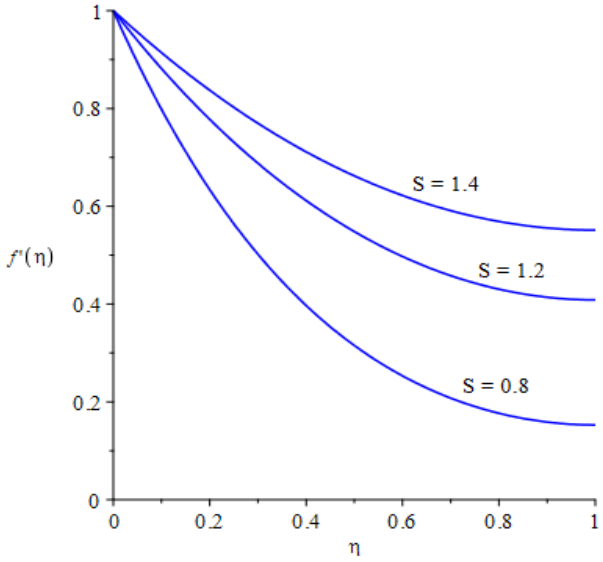

Figure 3: Variation of lateral velocity $f'(\eta)$ with S at Ma = 3 and $\hbar_f = -0.1$

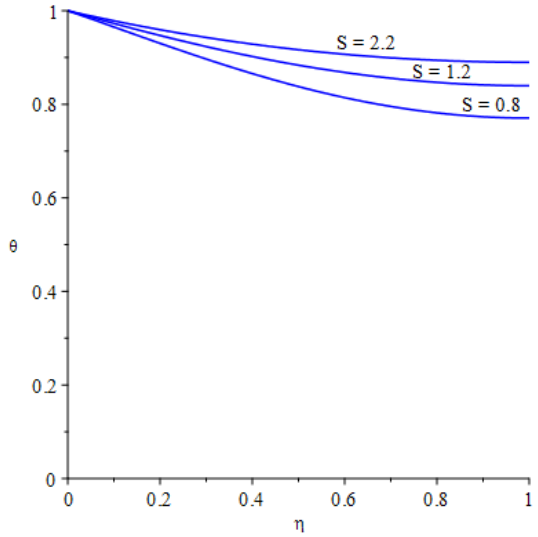

Figure 4: Variation of dimensionless temperature $\theta(\eta)$ with S at Ma = 3, Pr = 1, $k_4 = k_7 = 1$, $k_6 = 0$ and $\hbar_\theta = -0.01$

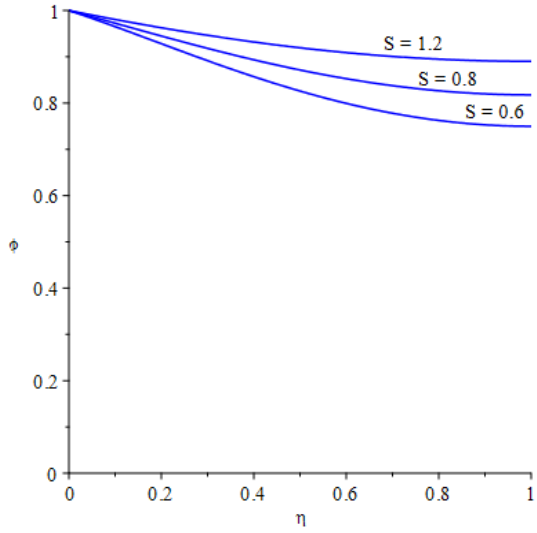

Figure 5: Variation of dimensionless $\phi(\eta)$ with S at Ma = 3, Sc = 4, $k_5 = k_7 = 1$, $k_6 = 0$ and $\hbar_\phi = -0.01$

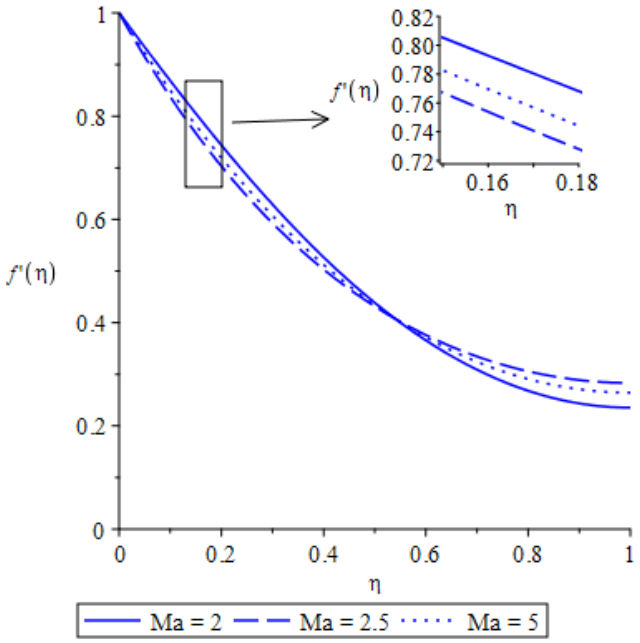

Figure 6: Variation of lateral velocity $f'(\eta)$ with Ma at S = 1 and $\hbar_f = -0.1$

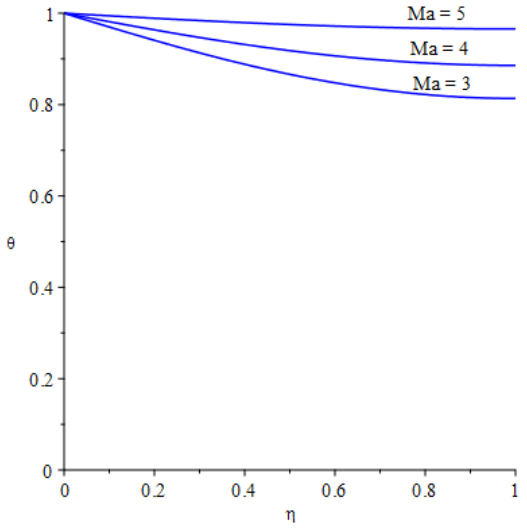

Figure 7: Variation of dimensionless temperature $\theta(\eta)$ with Ma at S = 1, Pr = 1, $k_4 = k_7 = 1$, $k_6 = 0$ and $\hbar_\theta = -0.01$

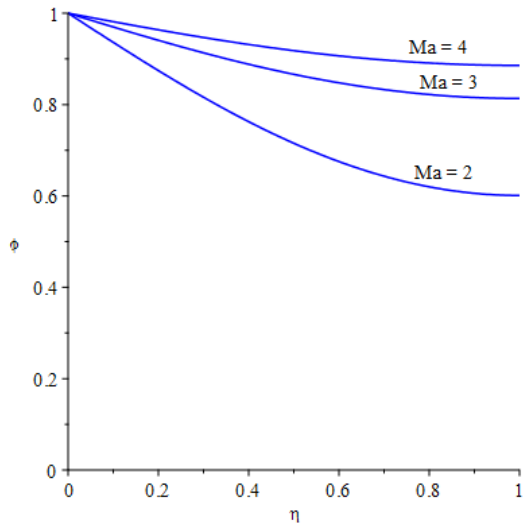

Figure 8: Variation of dimensionless concentration $\phi(\eta)$ with Ma at Sc = 1, S = 1, $k_5 = k_7 = 1$, $k_6 = 0$ and $\hbar_\phi = -0.01$

Table 8: Variation of $\beta, f'(1), \theta(1), \phi(1), f''(0), \theta'(0)\ and\ \phi'(0)$ with Ma

Ma	β	$f'(1)$	$\theta(1)$	$\phi(1)$	$-f''(0)$	$-\theta'(0)$	$-\phi'(0)$
3	1.59899637	0.272005949	0.864342477	0.867392281	1.666681269	0.219440864	0.214513338
4	1.22656552	0.277653682	0.918037288	0.919896934	1.722338532	0.132717235	0.129712335
5	0.65952873	0.283288639	0.975674594	0.976231306	1.779031686	0.039425895	0.038526279

Table 9: Variation of $\theta(1), \phi(1), \theta'(0)\ and\ \phi'(0)$ with Pr and S

Pr	Sc	$\theta(1)$	$\phi(1)$	$-\theta'(0)$	$-\phi'(0)$
0.001	0.001	0.99708223	0.99708223	0.004622006	0.004622006
0.01	0.01	0.971536493	0.971536493	0.045123974	0.045123974
0.1	0.1	0.78630659	0.78630659	0.340693651	0.340693651
1	1	0.585736625	0.585736625	0.662483622	0.662483622
10	10	0	0	1.774155458	1.774155458

Figure 9 presents the effect of the Prandtl number Pr on the dimensionless temperature $\theta(\eta)$. At the smaller Prandtl number $Pr \ll 1$, $\theta(\eta)$ varies marginally across the film thickness and approaches unity in the limiting case of $Pr \to 0$. This signifies that at the lower Pr (high thermal diffusion), the temperature T is fairly uniform (equal to T_s) in the vertical direction and $\theta'(0)$ is negligible. Heat transfer is dominated by thermal diffusion. At the higher Prandtl number, the thermal boundary layer develops which reduces with the $Pr > 1$. In this case, the heat transfer is dominated by the advection. The values of $\theta'(0)$ at different Prandtl numbers are given in table 9. The role of the Sherwood number (Sc) in the concentration equation is similar to the Prandtl number in the energy equation.

The influence of the constants k_4, k_5, k_6 and k_7 on the solutions is shown in Figure 11-Figure 16. At smaller $\frac{k_4 - k_6}{k_7}$ and $\frac{k_5 - k_6}{k_7}$ ratios, $\theta(\eta)$ and $\phi(\eta)$ vary marginally with the η but as the ratios increase the decay of the temperature T and the concentration C becomes more pronounced and eventually reaches T_0 and C_0. So, these constants give us the liberty to control $\theta(\eta)$ and $\phi(\eta)$ which is very important for the better quality of the products. It should be noted that not every value of the constants (k_4, k_5, k_6 and k_7) generates a realistic solution. For $S = 1,\ Pr = 1, Sc = 1$ and $Ma = 2$, realistic solutions exist if $0.5 \leq \frac{k_4 - k_6}{k_7} \leq 2.7$ and $0.5 \leq \frac{k_5 - k_6}{k_7} \leq 2.7$. Some non-realistic solutions are given in Figure 17 and Figure 18.

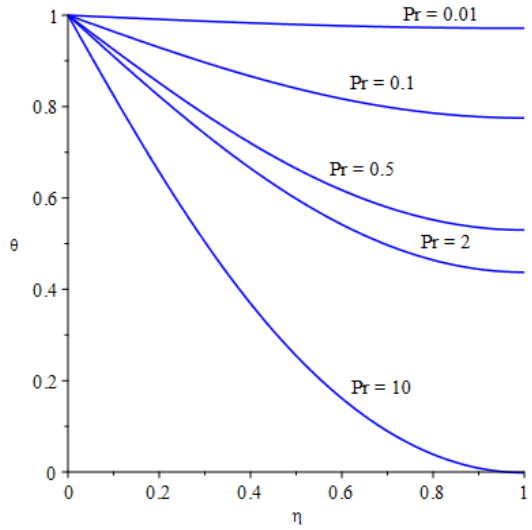

Figure 9: Variation of $\theta(\eta)$ with Pr at S = 1, Ma =2, $k_4 = k_7 = 1,\ k_6 = 0$ and $\hbar_\theta = -0.01$

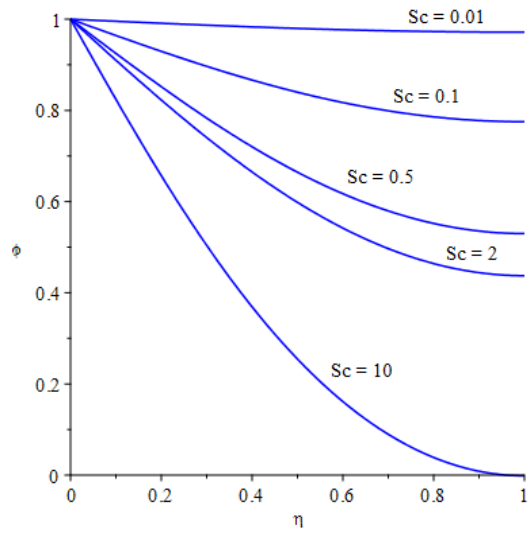

Figure 10: Variation of $\phi(\eta)$ with Sc at Ma = 2, S = 1, $k_5 = k_7 = 1,\ k_6 = 0$ and $\hbar_\phi = -0.01$

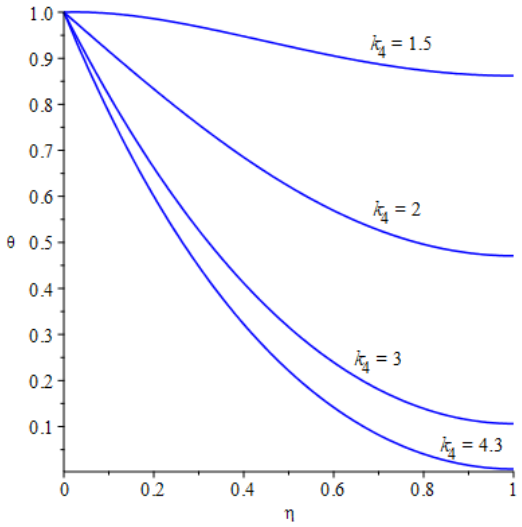

Figure 11: Effect of k_4 on $\theta(\eta)$ with $k_6 = k_7 = 1$

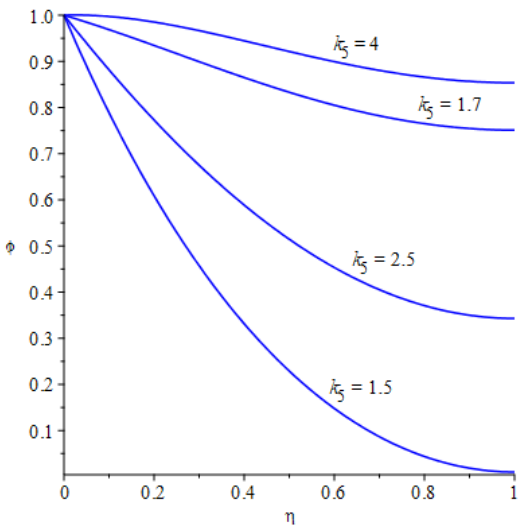

Figure 12: Effect of k_5 on $\phi(\eta)$ with $k_6 = k_7 = 1$

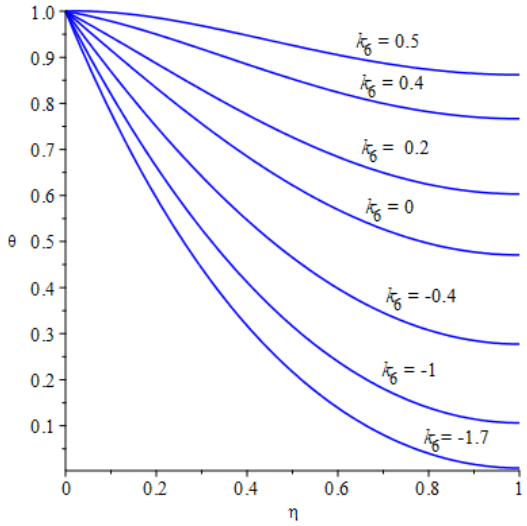

Figure 13: Effect of k_6 on $\theta(\eta)$ with $k_4 = k_7 = 1$

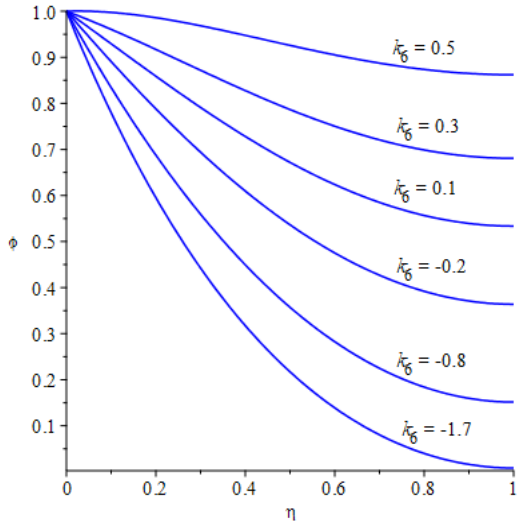

Figure 14: Effect of k_6 on $\phi(\eta)$ with $k_5 = k_7 = 1$

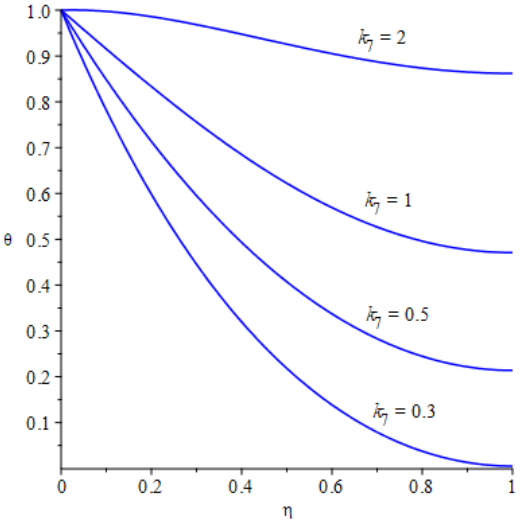

Figure 15: Effect of k_7 on $\theta(\eta)$ with $k_4 = k_6 = 1$

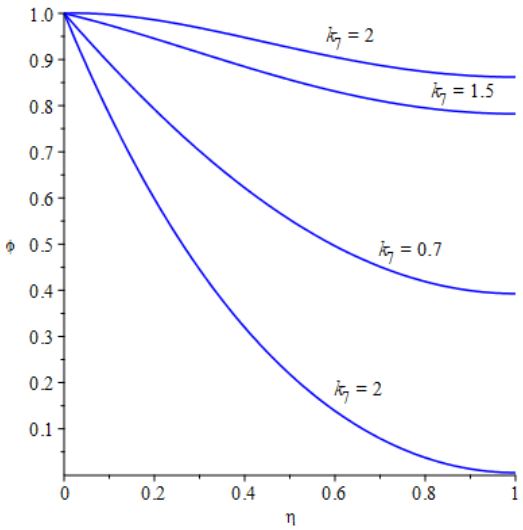

Figure 16: Effect of k_7 on $\phi(\eta)$ with $k_5 = k_6 = 1$

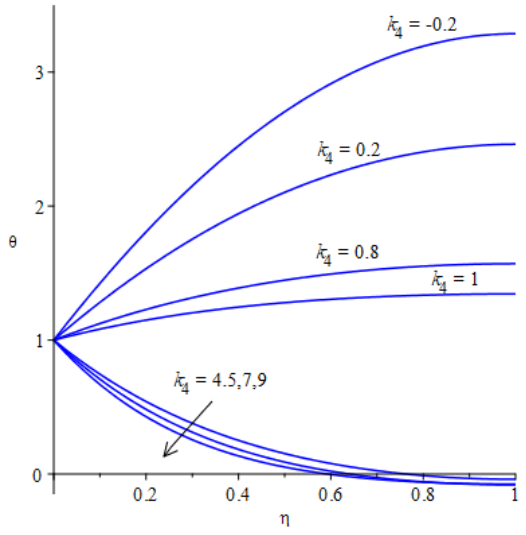

Figure 17:Non-realistic solutions for $\theta(\eta)$

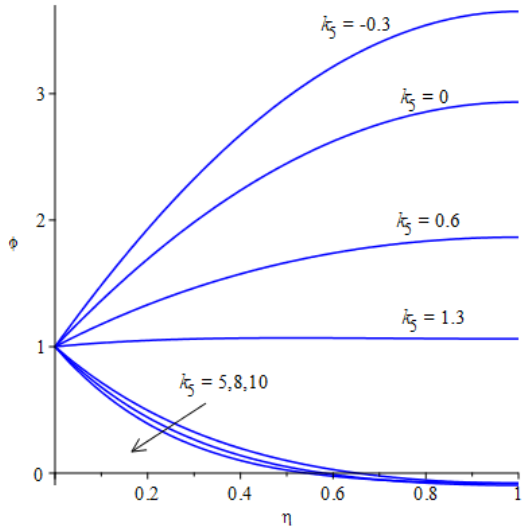

Figure 18: Non-realistic solutions for $\phi(\eta)$

5.1.2 Case 1 (b): System of ODEs obtained through Similarity Transformations associated with 1-Dimensional Optimal System

In Chapter 3, we divided the 1-dimensional optimal system for unsteady flow over a stretching surface in the presence of a variable magnetic field into two groups i.e. linearly-space dependent symmetries group (3.68 -3.71) and linearly-time dependent symmetries group (3.73 - 3.76). Their solutions are given below.

- *Linearly-space Dependent Symmetries*

When the scaling symmetries are used in this group, the governing equations (3.68 - 3.69) are the same as equations (3.49 - 3.50) which are the governing equations obtained when the linear combinations of all scaling and translational symmetries were used. So, the solutions obtained in the previous subsection (5.1), are also the solutions of equations (3.68 - 3.69). The dimensionless temperature $\theta(\eta)$ and concentration $\phi(\eta)$ profiles for different ratios of the constants $\frac{A_6-A_4}{A_7}$ and $\frac{A_6-A_5}{A_7}$ denoted by λ, are given in Figure 19 and Figure 20. It has been observed that the realistic solutions of $\theta(\eta)$ only exist for the range $0.5 \leq \lambda \leq 60$ while the realistic solutions of $\phi(\eta)$ exist

for the range $0.5 \leq \lambda \leq 80$. It is important to mention that these ranges are calculated for $S = 1, Pr = 1,\ Sc = 0.5\ and\ Ma = 10$. For different values of these parameters, the ranges of the realistic solutions will change.

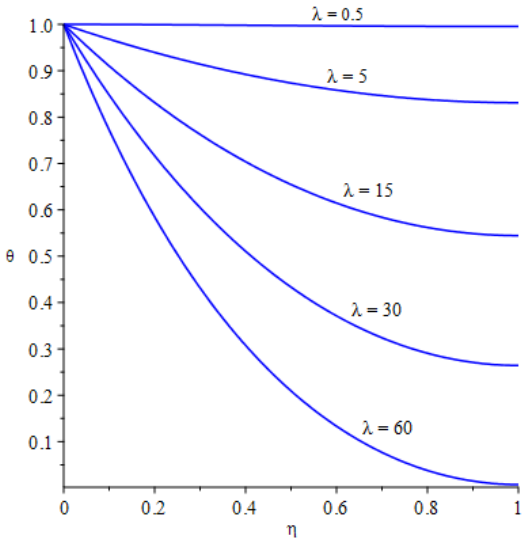

Figure 19: Dimensionless temperature $\theta(\eta)$ profiles for different ratios of the constants

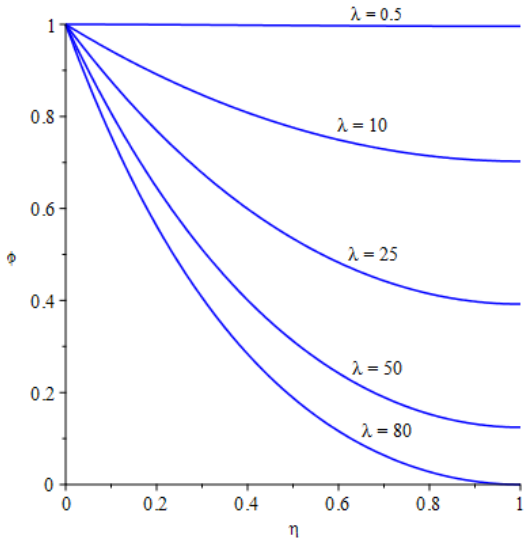

Figure 20: Dimensionless temperature $\phi(\eta)$ profiles for different ratios of the constants

The solutions of the equations (3.70 - 3.71), when the translational symmetries are used in this group are given in Figure (21-28). It can be seen that results follow the same trend as discussed previously. The only observable change is the sensitivity of the dependent variables $\theta(\eta)$ and $\phi(\eta)$ with respect to the parameters S, Pr, Sc and Ma. Contrary to the previous case, the effect of these parameters is relatively more pronounced on the $\theta(\eta)$ and $\phi(\eta)$. Due to this reason, the operating range of these parameters is small for these symmetries. The realistic solutions of $\theta(\eta)$ only exist in the range $0.5 \leq \lambda \leq 2.7$ while the realistic solutions of $\phi(\eta)$ exist in the range $0.5 \leq \lambda \leq 2.8$, for $S = 1, Pr = 1,\ Sc = 0.5\ and\ Ma = 10$.

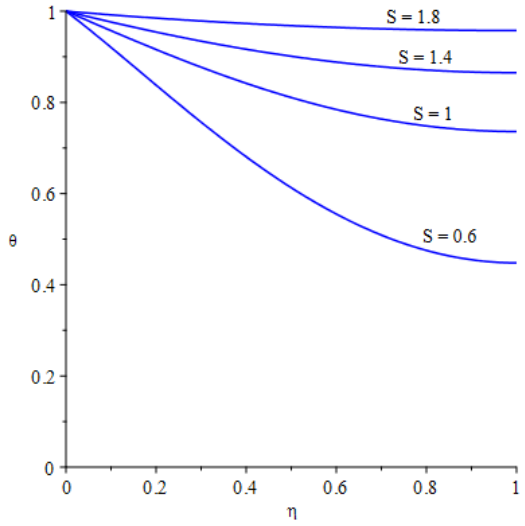

Figure 21: Variation of dimensionless temperature $\theta(\eta)$ with S at Ma = 10, Pr = 1, $A_2 = A_7 = 1$, $A_6 = 0$ and $\hbar_\theta = -0.01$

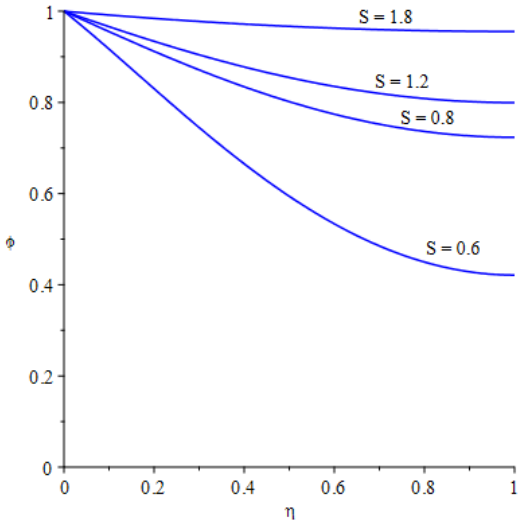

Figure 22: Variation of dimensionless concentration $\phi(\eta)$ with S at $Ma = 10$, $Sc = 4, A_3 = A_7 = 1$, $A_6 = 0$ and $\hbar_\phi = -0.01$

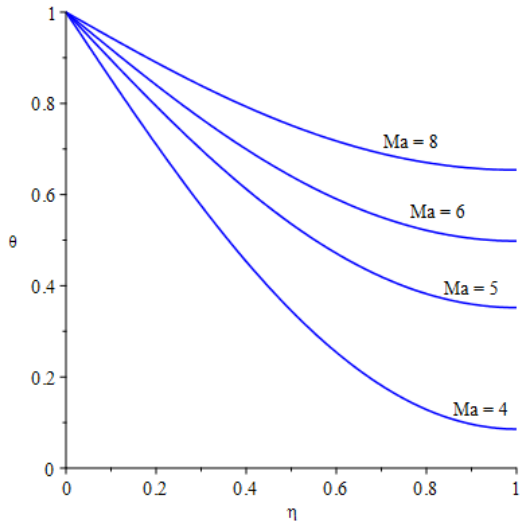

Figure 23: Variation of dimensionless temperature $\theta(\eta)$ with Ma at S = 1, Pr = 1, $A_2 = A_7 = 1$, $A_6 = 0$ and $\hbar_\theta = -0.01$

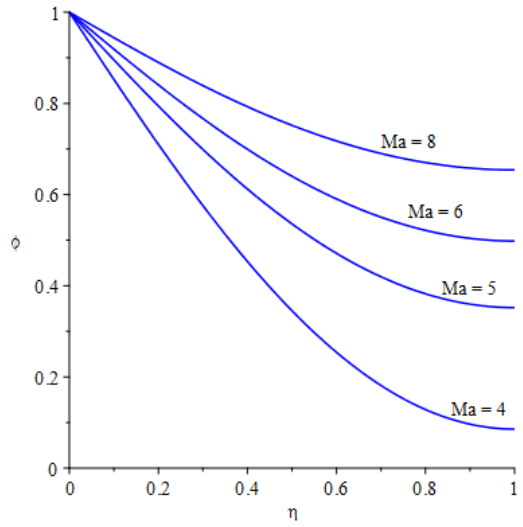

Figure 24: Variation of dimensionless concentration $\phi(\eta)$ with Ma at $S = 1, Sc = 4$, $A_3 = A_7 = 1$, $A_6 = 0$ and $\hbar_\phi = -0.01$

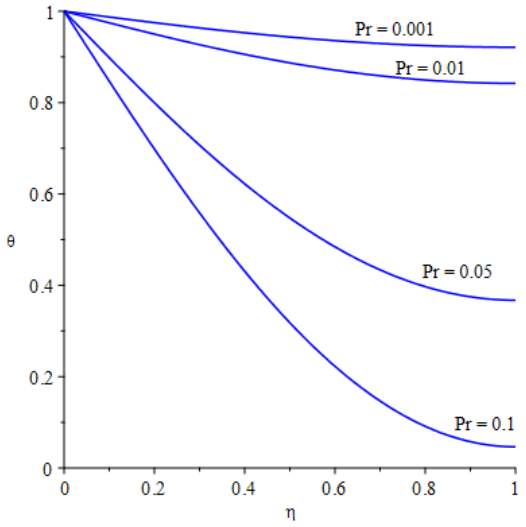

Figure 25: Variation of dimensionless temperature $\theta(\eta)$ with Pr at Ma = 10, S = 1, $A_2 = A_7 = 1$, $A_6 = 0$ and $\hbar_\theta = -0.01$

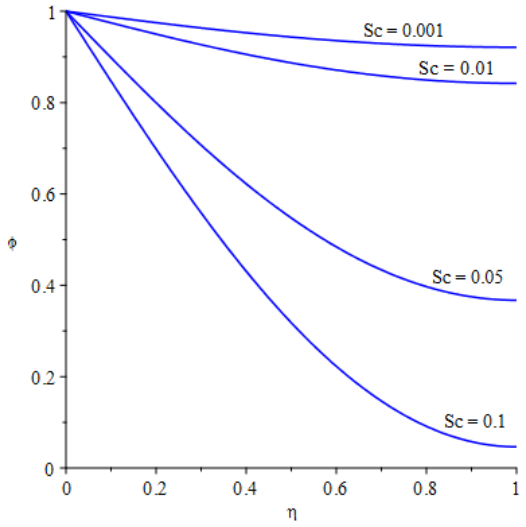

Figure 26: Variation of dimensionless concentration $\phi(\eta)$ with Sc at Ma = 10, S = 1, $A_3 = A_7 = 1$, $A_6 = 0$ and $\hbar_\theta = -0.01$

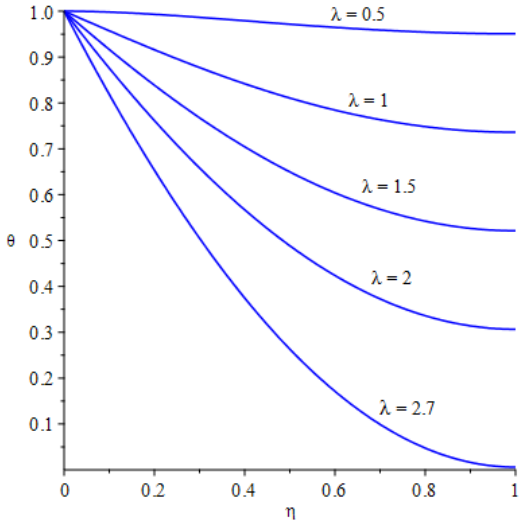

Figure 27: Dimensionless temperature $\theta(\eta)$ profiles for different ratios of the constants

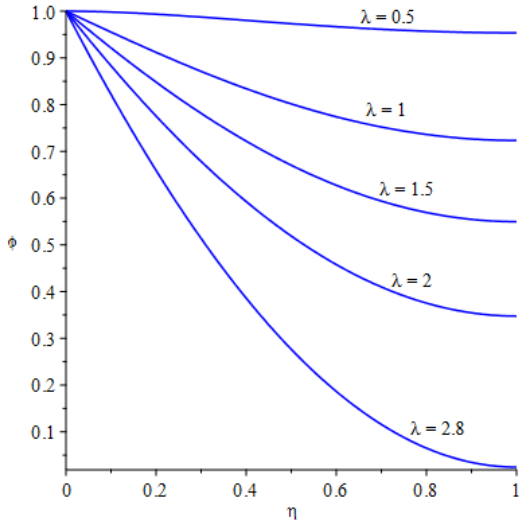

Figure 28: Dimensionless concentration $\phi(\eta)$ profiles for different ratios of the constants

- *Linearly-time Dependent Symmetries*

The solutions of the equations (3.73 and 3.74), obtained when the scaling symmetries are used in this group are given in Figure 29 – 36. Figure 29 and Figure 30 show the effect of the unsteadiness parameter S on the dimensionless temperature $\theta(\eta)$ and concentration $\phi(\eta)$ respectively. It can be observed the effect of S on $\theta(\eta)$ and $\phi(\eta)$ is relatively smaller as compared to the previous

group. This effect further diminishes at the higher values of S. The behavior of $\theta(\eta)$ and $\phi(\eta)$ at different values of magnetic parameter Ma, given in Figure 31 and Figure 32 is same as discussed earlier. $\theta(\eta)$ and $\phi(\eta)$ exhibit the strange behavior at different values of Prandtl number and Schmidt number, respectively given in Figure 33 and Figure 34. Their variation against η increases with the increase in Pr and Sc upto certain point. After that, $\theta(\eta)$ and $\phi(\eta)$ become almost independent of Pr and Sc, respectively.

For this group, the dimensionless temperature $\theta(\eta)$ and concentration $\phi(\eta)$ profiles for different ratios of the constants $\frac{A_4}{A_6}$ and $\frac{A_5}{A_6}$ denoted by ω, are given Figure 35 and Figure 36. The realistic solutions of $\theta(\eta)$ only exist in the range $-140 \leq \omega \leq 2$ while the realistic solutions of $\phi(\eta)$ exist in the range $-160 \leq \omega \leq 0.5$ for $S = 1, Pr = 1,\ Sc = 0.5\ and\ Ma = 10$.

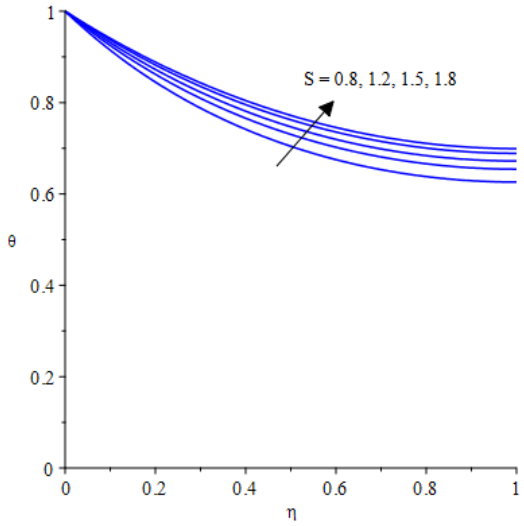

Figure 29: Variation of dimensionless temperature $\theta(\eta)$ with S at Ma = 3, Pr = 1, $A_4 = -2$, $A_6 = 1$ and $\hbar_\theta = -0.01$

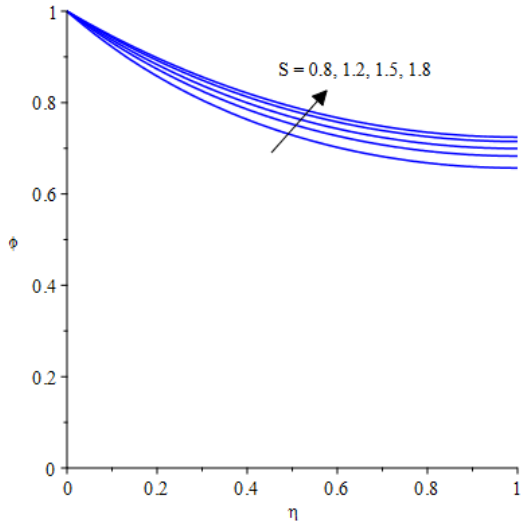

Figure 30: Variation of dimensionless concentration $\phi(\eta)$ with S at Ma = 3, Sc = 0.5, $A_5 = -2$, $A_6 = 1$ and $\hbar_\phi = -0.01$

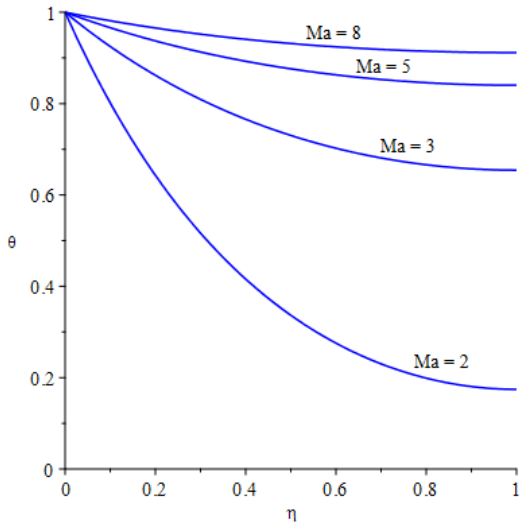

Figure 31: Variation of dimensionless temperature $\theta(\eta)$ with Ma at S = 1, Pr = 1, $A_4 = -2$, $A_6 = 1$ and $\hbar_\theta = -0.01$

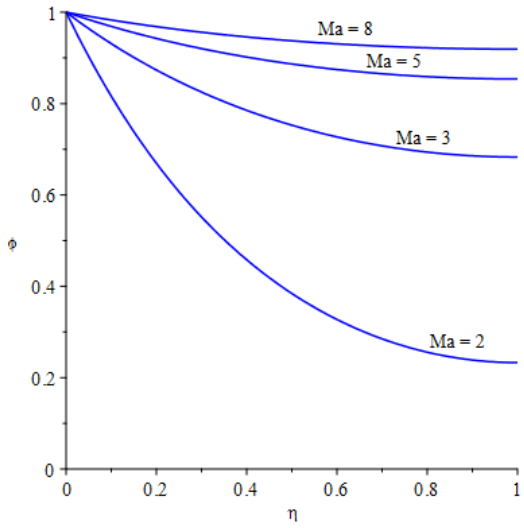

Figure 32: Variation of dimensionless concentration $\phi(\eta)$ with Ma at S = 1, Sc = 0.5, $A_5 = -2$, $A_6 = 1$ and $\hbar_\phi = -0.01$

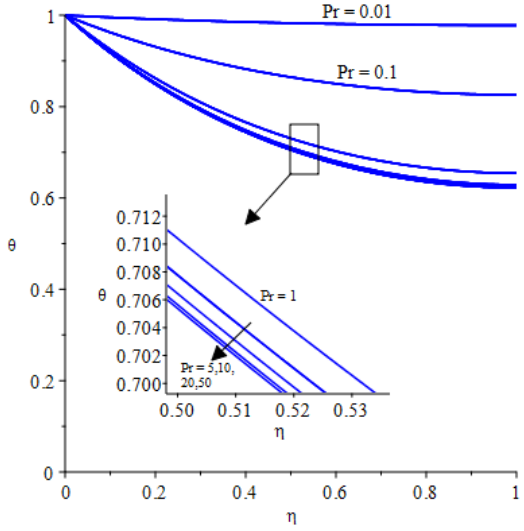

Figure 33: Variation of dimensionless temperature $\theta(\eta)$ with Pr at S = 1, Ma = 3, $A_4 = -2$, $A_6 = 1$ and $\hbar_\theta = -0.01$

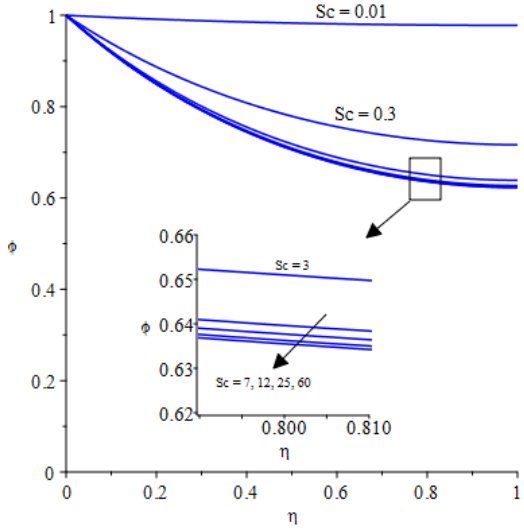

Figure 34: Variation of dimensionless concentration $\phi(\eta)$ with Sc at S = 1, Ma = 3, $A_5 = -2$, $A_6 = 1$ and $\hbar_\phi = -0.01$

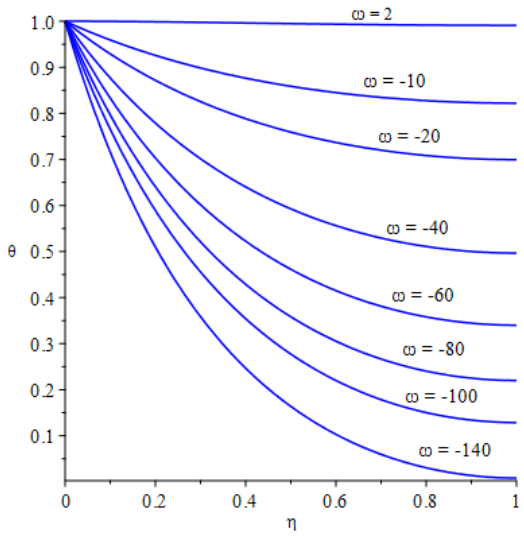

Figure 35: Dimensionless temperature $\theta(\eta)$ profiles for different ratios of the constants

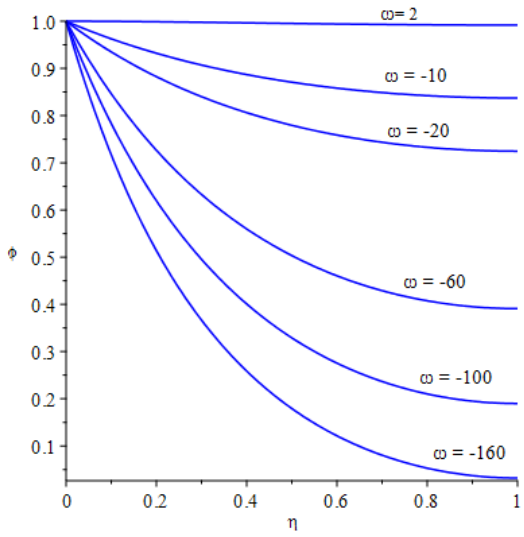

Figure 36: Dimensionless concentration $\phi(\eta)$ profiles for different ratios of the constants

The solutions of the equations (3.75 and 3.76), obtained when the translational symmetries are used in this group are given in Figure 37 – 44. Like in the previous group when the scaling symmetries are used, here too the operating range of the parameters $S, Ma,$ Pr and Sc due to the increased sensitivity of $\theta(\eta)$ and $\phi(\eta)$ against these parameters. The operating ranges of the ratios of constants $\frac{A_2}{A_6}$ and $\frac{A_3}{A_6}$ denoted by ω, are $-3.4 \leq \omega \leq 1$ and $-3.8 \leq \omega \leq 1$, respectively at $S = 1, Pr = 1,\ Sc = 0.5\ and\ Ma = 10.$

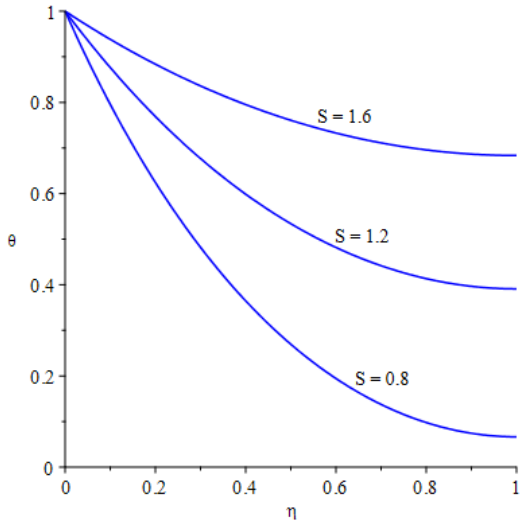

Figure 37: Variation of dimensionless temperature $\theta(\eta)$ with S at Ma = 10, Pr = 1, $A_2 = -2$, $A_6 = 1$ and $\hbar_\theta = -0.01$

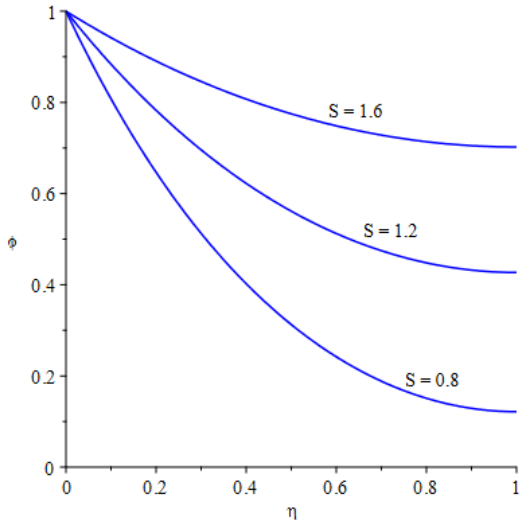

Figure 38: Variation of dimensionless concentration $\phi(\eta)$ with S at Ma = 10, Pr = 1, $A_3 = -2$, $A_6 = 1$ and $\hbar_\phi = -0.01$

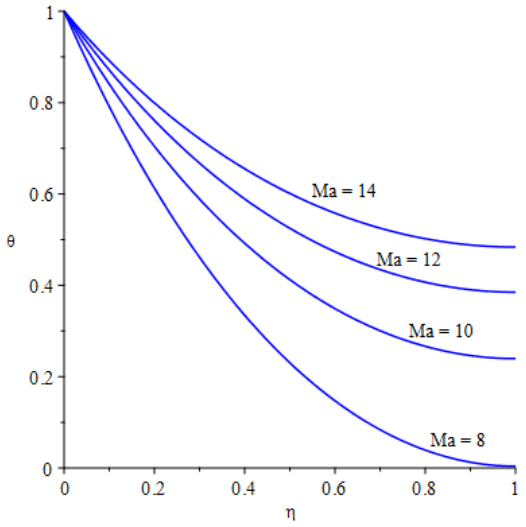

Figure 39: Variation of dimensionless temperature $\theta(\eta)$ with Ma at S = 1, Pr = 1, $A_2 = -2$, $A_6 = 1$ and $\hbar_\theta = -0.01$

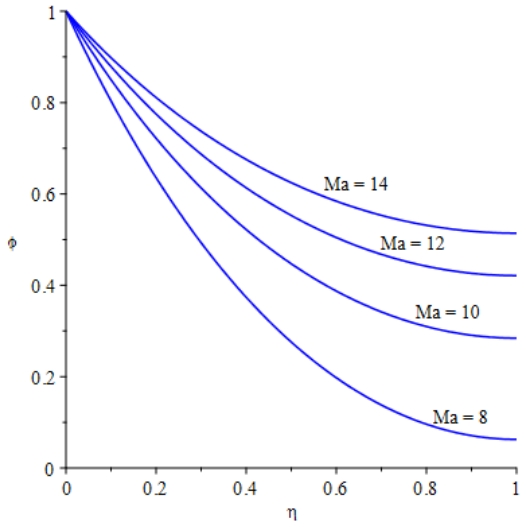

Figure 40: Variation of dimensionless concentration $\phi(\eta)$ with Ma at S = 1, Sc = 0.5, $A_3 = -2$, $A_6 = 1$ and $\hbar_\phi = -0.01$

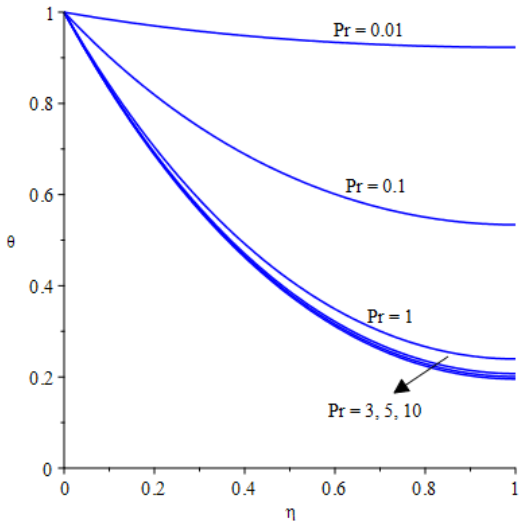

Figure 41: Variation of dimensionless temperature $\theta(\eta)$ with Pr at S = 1, Ma = 10, $A_2 = -2$, $A_6 = 1$ and $\hbar_\theta = -0.01$

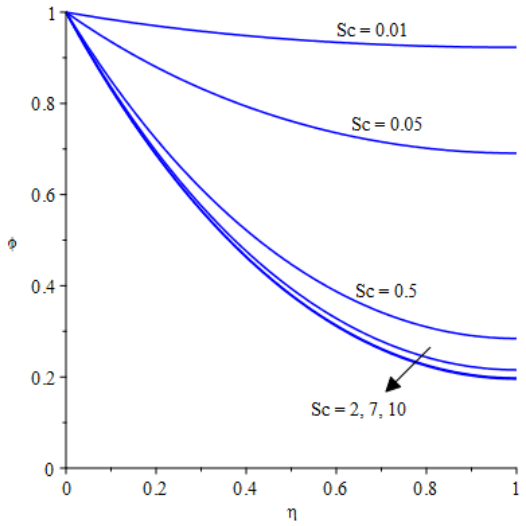

Figure 42: Variation of dimensionless concentration $\phi(\eta)$ with Sc at S = 1, Ma = 10, $A_3 = -2$, $A_6 = 1$ and $\hbar_\phi = -0.01$

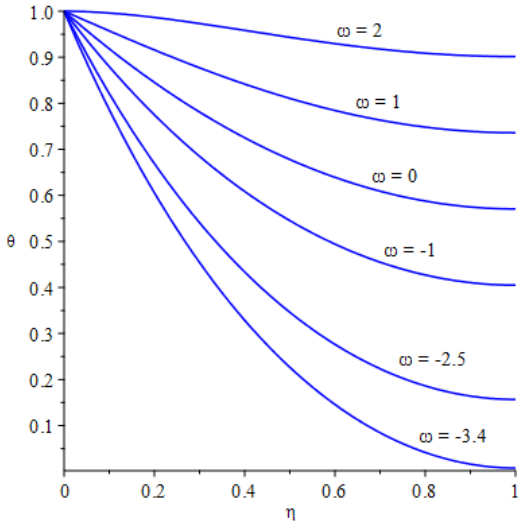

Figure 43: Dimensionless temperature $\theta(\eta)$ profiles for different ratios of the constants

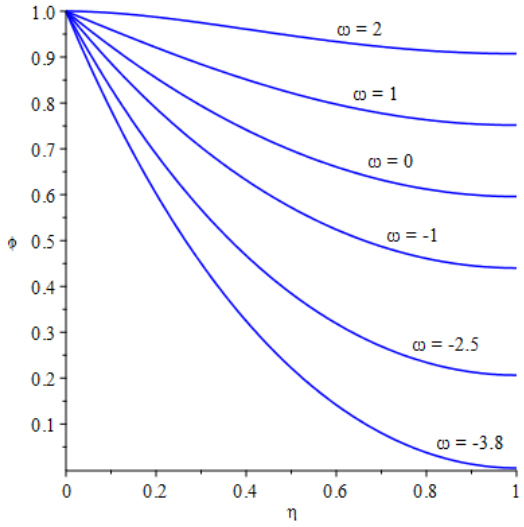

Figure 44: Dimensionless concentration $\phi(\eta)$ profiles for different ratios of the constants

5.2 HPM Analytic Solutions for Unsteady Flow over a Stretching Surface in the Presence of Thermocapillarity, Internal Heat Source/Sink and Variable Magnetic Field

The temperature $\theta(\eta)$ and velocity $f'(\eta)$ profiles for the different values of thermocapillarity parameter M are given in Figure 45 and Figure 46 respectively, which show that M significantly affects the behavior of temperature and velocity in the fluid film. Figure 45 shows that the dimensionless temperature $\theta(\eta)$ decreases monotonically with η which suggests that temperature of fluid increases as we move from the stretching sheet towards the free surface. It should also be noted from this graph that $\theta(1)$ decreases with increasing the value of M, meaning that thermocapillarity increases the free surface temperature of the fluid. Since the temperature reduces proportional to x^2 (given in Eq (3.92)) as we move away from the slit which implies that the surface tension increases with the distance from the slit. Hence, the top layer of the fluid experiences a net surface tension force which causes it to flow in the x-direction. The top layer of the fluid in turn dragged the layer below the free surface with itself due to the viscosity and so on. The two effects i.e. the motion caused by the stretching sheet and the motion caused by the thermocapillarity meet in the interior of the film where a local velocity minimum forms. It can be seen in Figure 46. The motion caused by the thermocapillarity increases with M and may outrun the motion caused by the stretching of the sheet at the higher M values.

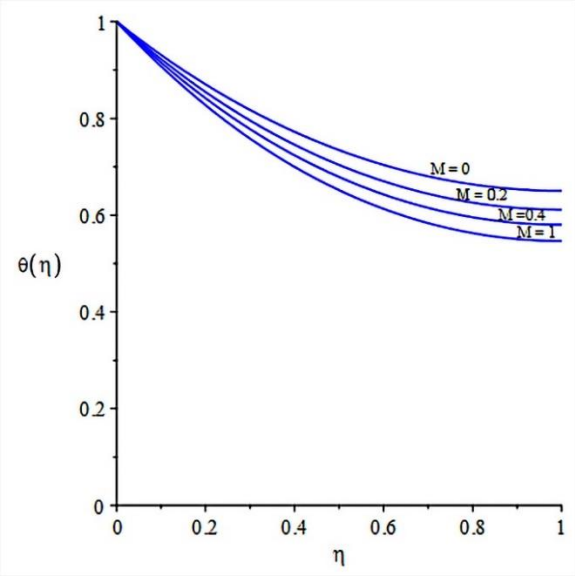

Figure 45: Dimensionless temperature profiles at S = 1, Ma = 25, G^*= -10, and Pr = 1 for different values of thermocapillarity parameter M.

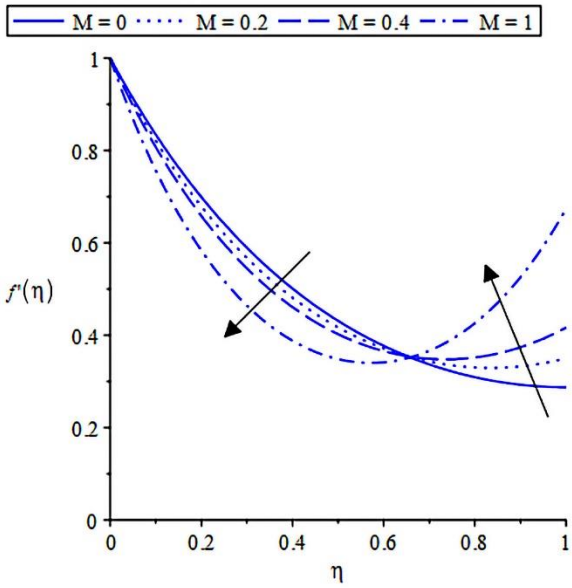

Figure 46: Lateral velocity profiles at S = 1, Ma = 25, and Pr = 1 for different values of thermocapillarity parameter M

The effect of thermocapillarity on the dimensionless film thickness β is given in Figure 47. It can be observed that the film thickness increases with M for a given value of unsteadiness parameter S. Wang [10] reported that at $S = 0$, the film becomes infinitely thick while at $S = 2$, it becomes infinitely thin, suggesting that solution only exists for $S \in [0, 2]$. With the thermocapillarity effect, a modest increase in the outer limit of S is observed which magnifies with the increase in the value

M. This signifies that fluid film becomes infinitely thin at the comparatively smaller stretching rate (higher value of S) in the presence of thermocapillarity.

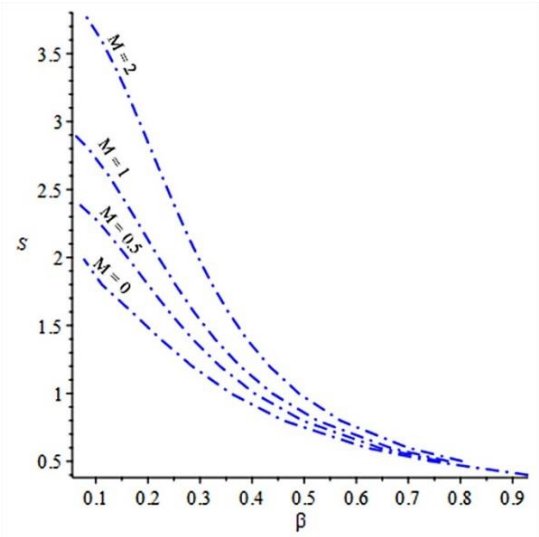

Figure 47: Unsteadiness parameter versus film thickness Ma = 30, Pr = 1, and G^*= -10 at different values of thermocapillarity parameter M.

Figure 48 depicts the free surface velocity $f'(1)$ profile against the unsteadiness parameter S for different values of M. $f'(1)$ demonstrates linear-like behavior and does not exceed unity i.e. U_s in the absence of thermocapillarity. As the thermocapillarity is taken into account, $f'(1)$ exceeds 1. The observed excess in the free surface velocity is certainly due to the thermocapillary forces.

The effect of thermocapillarity on the friction between the sheet and fluid is given in Figure 49. An increase in friction is observed with an increment in M at a given value of S due to the fact that thermocapillarity thickens the fluid film. The negative sign of $f''(0)$ calls attention to the resistive nature of the friction.

The behavior of $f'(\eta)$ at different values of unsteadiness parameter S is shown in Figure 50. The lateral velocity $f'(\eta)$ at the given height from the stretching sheet (fixed value of η) decreases as the stretching rate increases because at lower values of S, the fluid film becomes comparatively thick, and thus, the motion caused by the stretching sheet does not arrive at the given height that much effectively. Figure 51 shows that the magnetic field minutely influences the lateral velocity $f'(\eta)$. $f'(\eta)$ reduces marginally with the increase in the magnetic parameter Ma, as the transverse magnetic field offers resistive drag force to the flow. But its effect is overcome by the thermocapillarity as we move towards the free surface.

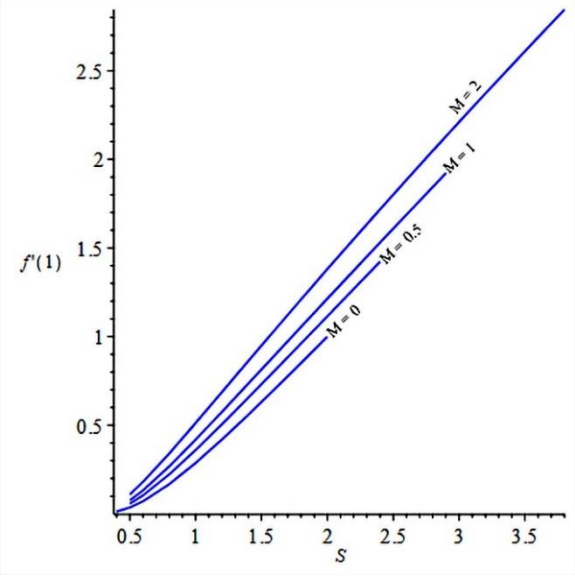

Figure 48: Free surface velocity versus unsteadiness parameter for Ma = 30, Pr = 1, and G^*= -10 at different values of thermocapillarity parameter M.

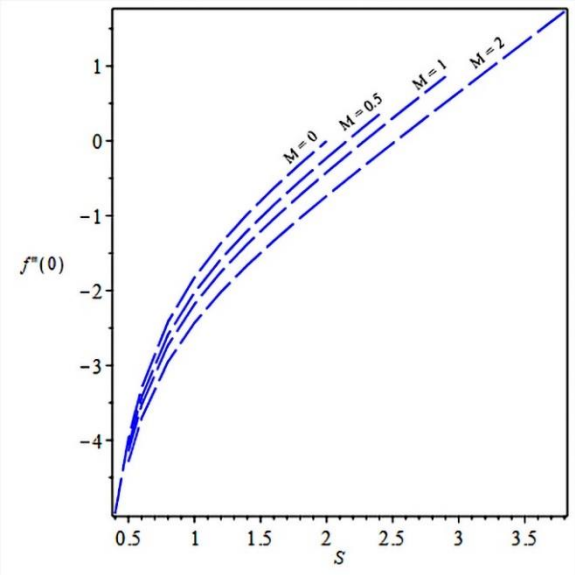

Figure 49: Shear stress versus unsteadiness parameter for Ma = 30, Pr = 1, and G^*= -10 at different values of thermocapillarity parameter M.

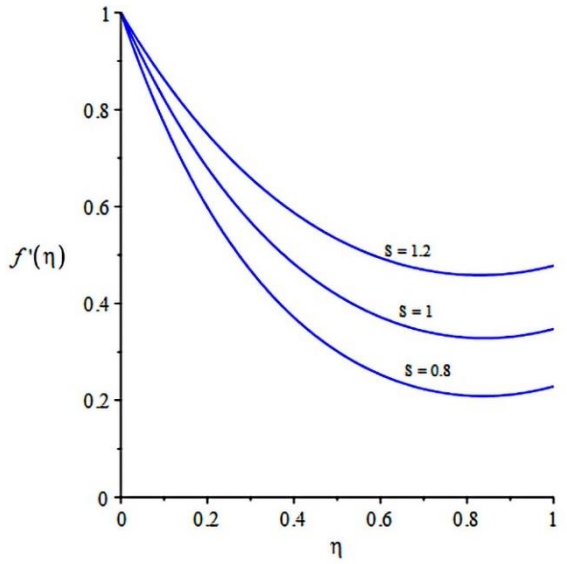

Figure 50: Velocity profile at M = 0.2, Ma = 30, G^*= -10, and Pr = 1 for different values of unsteadiness parameter S.

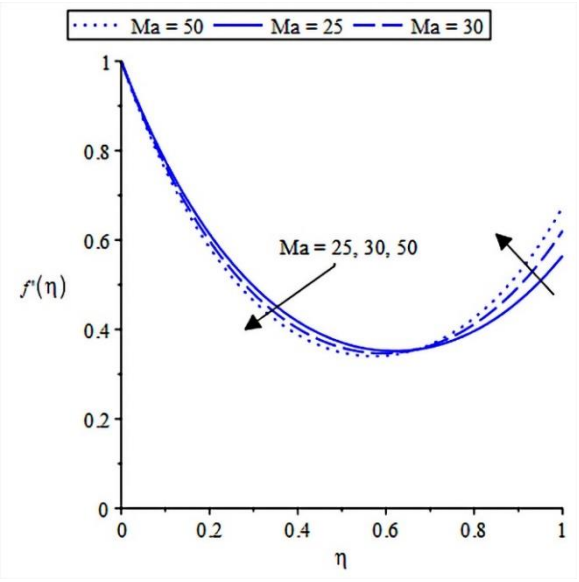

Figure 51: Velocity profile at M = 0.5, S = 1, G^*= 0, and Pr = 1 for different values of unsteadiness parameter S.

Figure 52 illustrates how the dimensionless temperature $\theta(\eta)$ is affected by the magnetic parameter Ma. The influence of Ma on $\theta(\eta)$ is pronounced compared to the influence on $f'(\eta)$. Increasing the magnetic parameter Ma leads to a substantial decline in the variation of dimensionless temperature across the fluid film, indicating that heat transfer from sheet to the fluid decreases. At some value of Ma, the variation of $\theta(\eta)$ will cease to exist. From this point onwards, an increase in Ma results in the heat transfer in the opposite direction i.e. from fluid to the sheet. In Figure 52, $\theta(\eta)$ is calculated at considerably higher values of Ma, which explains why the fluid temperature reduces as we move away from the stretching sheet.

Figure 53 presents the effect of temperature-dependent heat absorption/generation G^* on the dimensionless temperature $\theta(\eta)$. It shows that G^* greatly affects the variation of $\theta(\eta)$ across the fluid film. It can be used to speed up the heating/cooling of the fluid film.

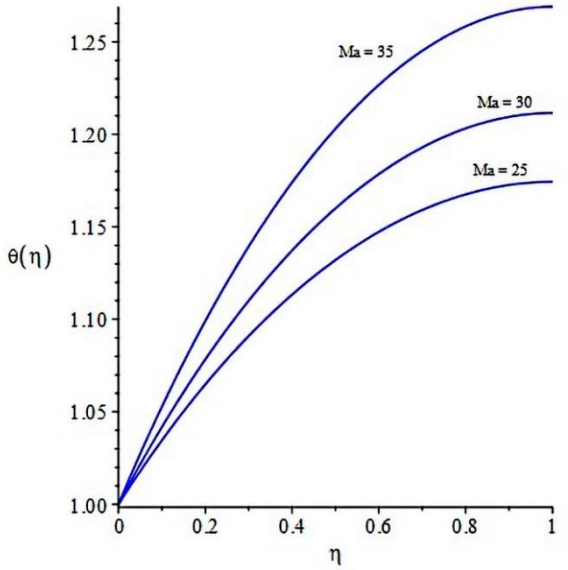

Figure 52: Temperature profile at M = 0.1, S = 1, G^*= 0, and Pr = 1 for different values of magnetic parameter Ma.

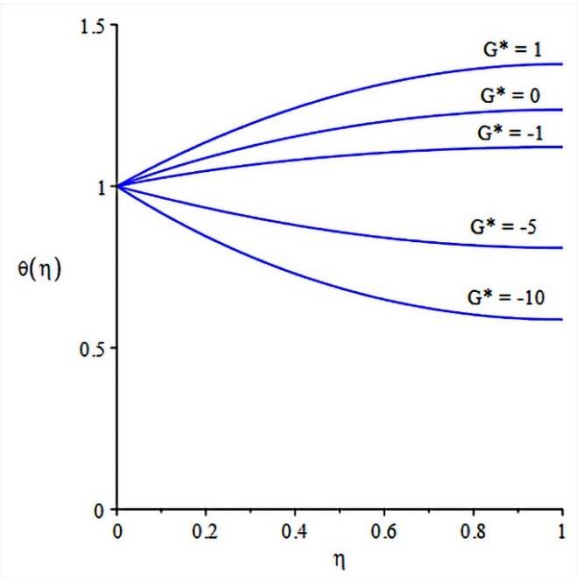

Figure 53: Temperature profile at M = 0.1, S = 1, Ma = 25, and Pr = 1 for different values of temeperature dependent source/sink parameter G^*.

$\theta(1)$ at different values of M against the unsteadiness parameter S is given in Figure 54. As expected, $\theta(1)$ reduces with the increase in M which implies that free surface temperature rises due to the thermocapillarity. Figure 55 demonstrates that heat flux $-\theta'(0)$ decreases monotonically with the increase in the S at the different values of M. The reduction in heat flux with S is due to the inverse relation of film thickness with the S. At the given value of S, heat flux increases with the rise in the thermocapillarity obviously, due to the thickening of the fluid film.

The dimensionless temperature $\theta(\eta)$ at different values of the Prandtl number is given in Figure 56. At high thermal diffusivity (small Pr), the variation of $\theta(\eta)$ across the fluid is negligible and the temperature of the fluid is nearly the same as the stretching surface T_s. At the higher Prandtl numbers, $\theta(\eta)$ varies from 1 to 0 with the thermal boundary layer existing in the small region near the stretching surface where an isothermal condition with the fluid having the temperature T_o.

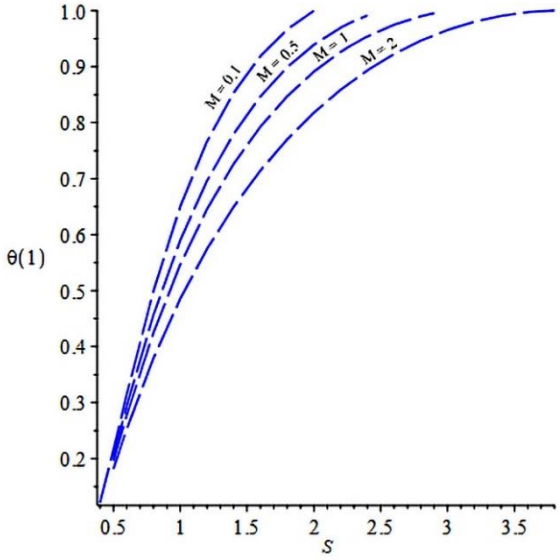

Figure 54: Free surface temperature versus unsteadiness parameter for Ma = 30, Pr = 1, and G^*= -10 at different values of thermocapillarity parameter M.

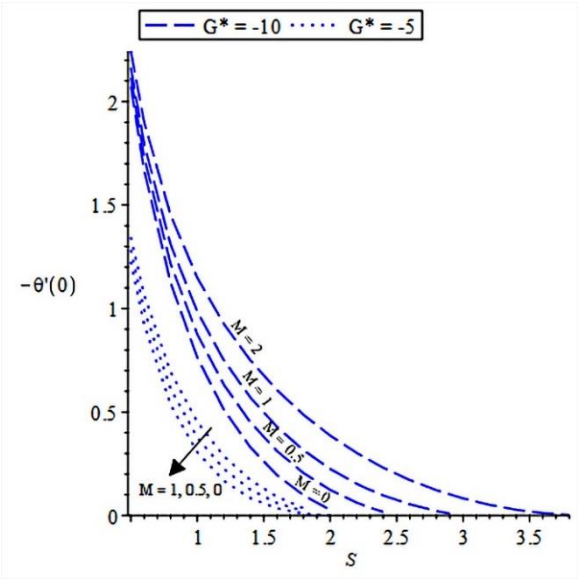

Figure 55: Dimensionless heat flux versus unsteadiness parameter for Ma = 30, and Pr = 1 at different values of thermocapillarity parameter M.

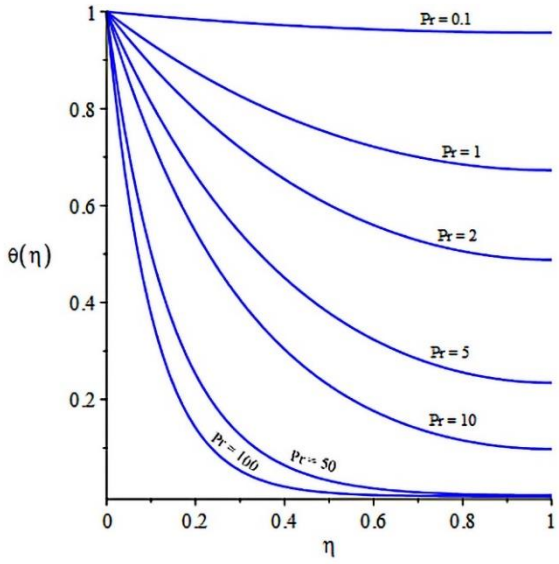

Figure 56: Dimensionless temperature profile at S = 1.8, Ma = 1, M = 0.1, and G^*= 0 for different values Pr.

In this section, we conducted a meticulous analysis of different parameters, including M, Ma, G^*, S and Pr and their impact on the velocity and temperature distribution in a fluid. Our findings indicate that these parameters have a profound influence on the profile of velocity and temperature in the fluid except for Ma, which has a relatively minor effect on fluid velocity. These insights are of paramount importance for manufacturing processes that utilize the mechanism discussed in this paper, as a deep understanding of these variations can enable the production of sheets of higher quality.

Conclusions

In this study, flow over an unsteady stretching surface has been analyzed using Lie point symmetry analysis. The whole study is divided into three parts. In the first part, flow over an unsteady stretching surface in the presence of a variable magnetic field is been analyzed. In the second part, a 1-dimensional optimal system for this flow is obtained. The final part of the study analyzes the combined effect of thermocapillarity, an internal heat source/sink, and a variable magnetic field on the flow and heat transfer in a film on an unsteady stretching surface. The major findings of each part are given below.

- **Unsteady Flow over a Stretching Surface in the Presence of a Variable Magnetic Field**

a) Generalized Similarity Transformations

In this study, Lie symmetry analysis has been used to obtain a generalized solution for a viscous film on an unsteady stretching surface in the presence external magnetic field. A linear combination of all translational and scaling Lie point symmetries has been utilized to obtain a more general variation of the surface velocity, temperature, and concentration. The admitted Lie point symmetries also provide a new class of similarity transformations that converts the governing boundary layer equations into a system of non-linear ODEs. The resulting system of non-linear ODEs has been solved using Homotopy Analysis Method (HAM). The following observations have been made:

1. The film thickness, free surface temperature, and concentration decrease with the increase in the stretching rate whereas the free surface velocity escalates.
2. The temperature and concentration gradient decrease at larger values of the magnetic parameter Ma, whilst the flow obstruction increases.
3. At much smaller Pr and Sc, $\theta'(0)$ and $\phi'(0)$ are negligible and heat and mass transfer are dominated by diffusion while at the higher Pr and Sc, advection dominates the heat and mass transfer.
4. With the help of the constants k_4, k_5, k_6 and k_7 we can control $\theta(\eta)$ and $\phi(\eta)$ and hence, can obtain the desired results.

b) Similarity Transformations associated with 1-Dimensional Optimal system:

In this part, 22 new classes of similarity transformations have been obtained using the optimal theory such that if any linear combination of Lie point symmetries is used, the resulting transformations belongs to the one of 22 classes. Based upon some common features, these 22 classes have been divided into two groups i.e. linearly-space dependent symmetries and linearly-time dependent symmetries.

It has been observed that both groups follow the same general trends at the different values of the parameters except at high values of the unsteadiness parameter and Prandtl number. At these values, the dependent variables of the linearly-time dependent symmetries group become almost independent of these parameters. Also, an increase in the sensitivity of the dependent variables with respect to the parameters has been observed in both groups when translational symmetries are used.

- **Unsteady Flow over a Stretching Surface in the Presence of Thermocapillarity, Internal Heat Source/Sink, and Variable Magnetic Field:**

In this part, Lie point algebra is used to obtain the symmetries of the governing differential equations in the presence of different effects viz. thermocapillarity, variable magnetic field, and heat generation/absorption. These symmetries allow us to identify the transformations that leave the differential equations and associated boundary conditions invariants. These symmetries are then utilized to simplify the governing equations and obtain the solutions. The major findings are;

1. All linear combinations of the admitted Lie symmetries that leave the sheet velocity and temperature as a function of both distance and time, lead to the same Lie transformations irrespective of the fact that they generate different system invariants.
2. The reduction of temperature along the free surface results in the net surface tension force in the direction of flow due to which a local velocity minimum is formed in the interior of the fluid.
3. Thermocapillarity increases the film thickness.
4. Free surface velocity exceeds the velocity of the stretching sheet due to the thermocapillarity.
5. Heat flux and friction between the fluid and sheet increase in the presence of thermocapillarity due to the film thickening.

6. The temperature-dependent heat absorption/generation can speed up the heating and cooling of the fluid.
7. The effect of the magnetic parameter on the velocity is negligible whereas, it has a dominant effect on the variation of dimensionless temperature distribution.
8. The presence of thermocapillarity does not affect the influence of the Prandtl number on the dimensionless temperature.

The current work can be extended to 3-dimensional flow caused by the stretching of the surface in the two lateral directions. The Lie symmetry analysis can be used to reduce the 3 dimensional Navier-Stokes equations into a system of non-linear ordinary differential equations that can be solved using approximate numerical or analytical techniques. The effects of viscous dissipations, internal source or sink, magnetic field, and thermocapillarity will add more complexity to this problem.

In the current study, the solutions are obtained in the laminar regime only. It can be extended to the turbulent regime and accuracy of the similarity solutions can be compared with the solutions obtained through established turbulent models.

References

[1] B. C. Sakiadis, "Boundary-layer behavior on continuous solid surfaces," *A.I.Ch.E. Journal,* pp. 221-225, 1961.

[2] L. J. Crane, "Flow past a stretching plate," *Journal of Applied Mathematics and Physics* pp. 645-647, 1970.

[3] J. Vleggaar, "Laminar boundary-layer behaviour on continuous, accelerating surfaces," *Chemical Engineering Science,* vol. 32, no. 12, pp. 1517-1525, 1977.

[4] P. S. Gupta and A. S. Gupta, "Heat and mass transfer on a stretching sheet with suction or blowing," *The Canadian Journal of Chemical Engineering,* pp. 744-746, 1977.

[5] P. Carragher and L. J. Crane, "Heat Transfer on a continuous stretching sheet," *Journal of Applied Mathematics and Mechanics,* vol. 62, pp. 564-565, 1982.

[6] L. J. Grubka and K. M. Bobba, "Heat transfer characteristics of a continuous, stretching surface with variable temperature," *ASME J. Heat Transfer,* vol. 107, pp. 248-250, 1985.

[7] B. K. Dutta, P. Roy, and A. Gupta, "Temperature field in flow over a stretching sheet with uniform heat flux," *International Communications in Heat and Mass Transfer,* pp. 89-94, 1985.

[8] D. R. Jeng, T. C. A. Chang, and K. J. De Witt, "Momentum and heat transfer on a continuous moving surface " *Journal of Heat Transfer,* vol. 108, no. 32, 1986.

[9] M. Kumari, H. S. Takhar, and G. Nath, "MHD flow and heat transfer over a stretching surface with prescribed wall temperature or heat flux," *Heat and mass transfer* vol. 25, pp. 331–336, 1990.

[10] C. Y. Wang, "Liquid film on an unsteady stretching Surface," *Quarterly of Applied Mathematics,* vol. XLVIII, no. 4, pp. 601-610, 1990.

[11] H. I. Andersson, J. B. Aarsetha, and B. S. Dandapat, "Heat transfer in a liquid on an unsteady stretching," *International Journal of Heat and Mass Transfer* vol. 43, pp. 69-74, 2000.

[12] I. C. Liu and H. I. Andersson, "Heat transfer in a liquid film on an unsteady stretching sheet," *International Journal of Thermal Sciences,* vol. 47, pp. 766-772 2008.

[13] B. S. Dandapat, B. Santra, and H. I. Andersson, "Thermocapillarity in a liquid film on an unsteady stretching surface," *International Journal of Heat and Mass Transfer,* vol. 56, pp. 3009–3015, 2003.

[14] C. Y. Wang, "Analytic solutions for a liquid film on an unsteady stretching surface," *Heat and Mass Transfer,* vol. 42, pp. 759-766, 2006.

[15] M. S. Abel, N. Mahesha, and J. Tawade, "Heat transfer in a liquid film over an unsteady stretching surface with viscous dissipation in presence of external magnetic field," *Applied Mathematical Modelling,* vol. 33, pp. 3430–3441, 2009.

[16] N. F. M. Noor and I. Hashim, "Thermocapillarity and magnetic field effects in a thin liquid film on an unsteady stretching surface," *International in Heat and Mass Transfer,* vol. 53, no. 9-10, pp. 2044-2051, 2010.

[17] R. C. Aziz and I. Hashim, "Liquid film on unsteady stretching sheet with general surface temperature and viscous dissipation," *Chinese Physics Letters,* vol. 27, no. 11, 2010.

[18] R. C. Aziz, I. Hashim, and A. Alomari, "Thin film flow and heat transfer on an unsteady stretching sheet with internal heating," *Meccanica,* vol. 46, no. 2, pp. 349-357, 2011.

[19] R. C. Aziz, I. Hashim, and S. Abbasbandy, "Thermocapillarity and thermal Radiation on flow and heat transfer in a thin liquid film on an unsteady stretching sheet," *Mathematical Problems in Engineering,* vol. 2012, pp. 1-14, 2012.

[20] Y. Zhang, M. Zhang, and S. Qi, "Heat and mass transfer in a thin liquid film over an unsteady stretching surface in the presence of thermosolutal capillarity and variable magnetic field," *Mathematical Problems in Engineering,* vol. 2016, 2016.

[21] H. I. Andersson, J. B. Aarsetha, N. Brauda, and B. S. Dandapat, "Flow of a power-law fluid film on an unsteady stretching surface," *Journal of Non-Newtonian Fluid Mechanics,* vol. 62, no. 1, pp. 1-8, 1996.

[22] K. Prasad, S. Abel, and P. Datti, "Diffusion of chemically reactive species of a non-Newtonian fluid immersed in a porous medium over a stretching sheet," *International Journal of Non-Linear Mechanics,* vol. 38, no. 5, pp. 651-657, 2003.

[23] S. Abel, P. Veena, K. Rajgopal, and V. Pravin, "Non-Newtonian magnetohydrodynamic flow over a stretching surface with heat and mass transfer," *International Journal of Non-*

Linear Mechanics, vol. 39, no. 7, pp. 1067-1078, 2004.

[24] C. Y. Wang and L. Pop, "Analysis of the flow of a power-law fluid film on an unsteady stretching surface by means of homotopy analysis method," *Journal of Non-Newtonian Fluid Mechanics*, vol. 138, no. 2-3, pp. 161-172, 2006.

[25] C. H. Chen, "Effect of viscous dissipation on heat transfer in a non-Newtonian liquid film over an unsteady stretching sheet," *Journal of Non-Newtonian Fluid Mechanics*, vol. 135, no. 2-3, pp. 128-135, 2006.

[26] M. M. Nandeppanavar, M. S. Abel, and M. S. Abel, "Effects of thermal Radiation and non-uniform heat source on MHD flow of viscoelastic fluid and heat transfer over a stretching sheet," *International Journal of Applied Mechanical Engineering*, vol. 14, no. 4, pp. 903-918, 2007.

[27] G. Makanda, S. Shaw, and P. Sibanda, "Diffusion of chemically reactive species in Casson fluid flow over an unsteady stretching surface in porous medium in the presence of a magnetic field," *Mathematical Problems In Engineering*, pp. 1–10, 2015, doi: https://doi.org/10.1155/2015/724596.

[28] K. K. Ali, H. F. Ismael, B. A. Mahmood, and M. A. Yousif, "MHD Casson fluid with heat transfer in a liquid film over unsteady stretching plate," *International journal of advanced and applied sciences*, vol. 4, no. 1, pp. 55–58, 2016, doi: https://doi.org/10.21833/ijaas.2017.01.008.

[29] A. Sojoudi, A. Mazloomi, S. C. Saha, and Y. Gu, "Similarity solutions for flow and heat transfer of non-Newtonian fluid over a stretching surface," *Journal of Applied Mathematics*, pp. 1-8, 2014.

[30] N. Bachok, A. M. Ishak, and R. M. Nazar, "Flow and heat transfer over an unsteady stretching sheet in a micropolar fluid," *Meccanica*, vol. 46, no. 5, pp. 935–942, 2011.

[31] R. C. Aziz, I. Hashim, and S. Abbasbandy, "Flow and heat transfer in a nanofluid thin film over an unsteady stretching sheet," *Sains Malaysiana*, vol. 47, pp. 1599–1605, 2018, doi: https://doi.org/10.17576/jsm-2018-4707-31.

[32] S. E. Waheed, "Flow and heat transfer in a Maxwell liquid film over an unsteady stretching sheet in a porous medium with radiation," *Springerplus*, vol. 5, no. 1, 2016.

[33] M. Raj, A. K. Jha, and A. K. Sharma, "Casson fluid flow over a stretching surface with variable thermal conductivity and partial slip," *International journal of engineering and*

technology, 2017, doi: https://doi.org/10.21817/ijet/2017/v9i1/170902301.

[34] B. M. Rao, M. K. Murthy, N. Sivakumar, B. R. Kumar, and C. S. K. Raju, "Slip effects on MHD three dimensional flow of Casson fluid over an exponentially stretching surface," *Journal of physics*, vol. 1000, pp. 12156–12156, 2018, doi: https://doi.org/10.1088/1742-6596/1000/1/012156.

[35] M. A. El-Aziz and A. A. Afify, "MHD Casson fluid flow over a stretching sheet with entropy generation analysis and hall Influence," *Entropy*, vol. 21, no. 6, pp. 592–592, 2019, doi: https://doi.org/10.3390/e21060592.

[36] M. N. Tufail and F. Zaib, "Symmetry analysis of MHD Casson fluid flow for heat and mass transfer near a stagnation point over a linearly stretching sheet with variable viscosity and thermal conductivity," *Heat Transfer*, vol. 50, no. 6, pp. 5418-5438, 2021, doi: https://doi.org/10.1002/htj.22131.

[37] M. Qayyum *et al.*, "Heat transfer analysis of unsteady MHD Carreau fluid flow over a stretching/shrinking sheet," *Coatings*, vol. 12, 2022, doi: https://doi.org/10.3390/coatings12111661

[38] M. Safdar, M. I. Khan, S. Taj, M. Y. Malik, and Q.-H. Shi, "Construction of similarity transformations and analytic solutions for a liquid film on a unsteady stretching sheet using lie point symmetries," *Choas, Solitons and Fractals*, vol. 150, no. 2021, 2021.

[39] S. Taj, M. I. Khan, M. Safdar, S. Elattar, and A. M. Galal, "Lie symmetry analysis of heat transfer in a liquid film over an unsteady stretching surface with viscous dissipation and external magnetic field " *Waves in Random and Complex Media*, 2022.

[40] M. Safdar *et al.*, "Analytic solutions for the MHD flow and heat transfer in a thin liquid film over an unsteady stretching surface with Lie symmetry and homotopy analysis method," *Waves in Random and Complex Media*, 2022.

[41] M. Bilal, M. Safdar, S. Taj, A. Zafar, M. U. Ali, and S. W. Lee, "Reduce-Order modeling and higher order numerical solutions for unsteady flow and heat transfer in boundary layer with internal heating," *Mathematics*, vol. 10, no. 24, 2022.

[42] M. Bilal, M. Safdar, S. Ahmed, and R. A. Khan, "Analytic similarity solutions for fully resolved unsteady laminar boundary layer flow and heat transfer in the presence of radiation," *Heliyon*, vol. 9, 2023.

[43] H. Schlichting, *Boundary Layer Theory*. McGraw-Hill, 1968.

[44] L. Zhang, Z. Han, and Y. Chen, "A direct algorithm Maple package of one-dimensional optimal system for group invariant solutions," *Communications in Theoretical Physics*, vol. 69, no. 1, 2018.

[45] S. Liao, *Beyound Perturbation - Introduction to the Homotopy Analysis Method*. 2004: CRC Press LLC, Florida.

[46] J.-H. He, "Homotopy perturbation technique," *Computer Method in Applied Mechanics and Engineering*, vol. 178, no. 3-4, pp. 257-262, 1999.